Volume 2

E77-10234
CR-155024

(E77-10234) SEISMOTECTONIC, STRUCTURAL, VOLCANOLOGIC, AND GEOMORPHIC STUDY OF NEW ZEALAND; INDIGENOUS FOREST ASSESSMENT IN NEW ZEALAND; MAPPING, LAND USE, AND (Department of Scientific and Industrial Research)

N77-33565

NC A01/MF A01

G3/43

Unclas
00234

PHYSICS AND ENGINEERING LABORATORY

DSIR

NEW ZEALAND

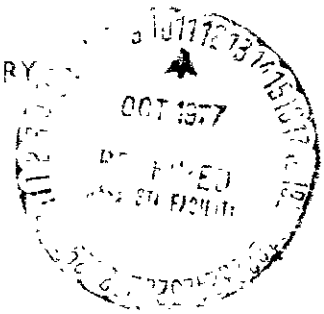

FINAL REPORT

LANDSAT II INVESTIGATION PROGRAMME

No. 28230

VOLUME II

Physics and Engineering Laboratory
Report No. 587 September 1977

Editors: P J Ellis, I L Thomas, M J McDonnell

Principal Investigator:

Dr Mervyn C Probine (Programme No. 28230)

Co-Investigators:

Dr Richard P Suggate (Programme No. 2823A)
Mr Michael G McGreevy (Programme No. 2823B)
Mr Ian F Stirling (Programme No. 2823C)

CHAPTER 7

IMAGE PROCESSING ON A MINICOMPUTER

M. J. McDonnell

ABSTRACT

New Zealand involvement in the LANDSAT II investigation program has led to the rapid development of a digital image processing facility within the Remote Sensing Section of the Physics and Engineering Laboratory of the Department of Scientific and Industrial Research. The quality of images produced by this facility is comparable to that produced by larger overseas laboratories. This paper outlines the present status and forthcoming development of this facility.

7.1 INTRODUCTION

Because of New Zealand's involvement in the LANDSAT II investigation program, the Remote Sensing Section of the Physics and Engineering Laboratory (PEL), DSIR, has, since 1975, been regularly receiving imagery of New Zealand in the form of computer compatible tapes (CCTs). Each CCT set contains a 185 km square digital image taken in each of the four spectral bands of the LANDSAT multispectral scanner (MSS). Each single-band image consists of approximately 2340 x 3264 picture elements or pixels. For each band, each pixel has been assigned a value of from 0 to 127 which is proportional to the radiance within the MSS spectral band of a 79 m square area of the earth's surface. Each CCT image thus contains an enormous amount of digital information (about 30 M bytes)—so much, in fact, that no single 70 mm photographic transparency can adequately display all the information in the CCT image. In addition, each image suffers from a number of radiometric and geometric distortions which it is desirable to remove. Computer processing offers the versatility required to remove these distortions and display LANDSAT imagery to the best advantage. The particular processing required will depend on the application for which the imagery is to be used. In general, optical processing of the LANDSAT negatives available directly from NASA is unsatisfactory, unless the resolution requirements are comparatively low (e.g., 150 m). However, many more applications of LANDSAT imagery are made possible by the improved resolution (e.g., 80 m) and tonal quality that is available through the use of computer processing.

For the above reasons it was decided to develop a computer image processing facility at PEL which would be used to process LANDSAT imagery, aircraft multispectral imagery, and possibly other imagery as the need arose. The aim of this development was to produce a system capable of meeting the needs of user groups within New Zealand for computer-processed LANDSAT imagery, and also to provide a research and development tool for the Remote Sensing Section, PEL. The way in which this facility has been developed over the last year and a half has been determined by a number of factors: the computing facilities available at PEL, the size of images to be processed, the rate at which they would be required, the particular processing involved, available manpower, and available finance.

In view of the limited manpower available and the expected steady demand for colour and to a lesser extent monochrome processed imagery, the overall system has to be as efficient as possible. Initially it was assumed that a suitable device would become available for producing high-quality photographic negatives from image data stored on magnetic tape after computer processing. There is no such device available in New Zealand, but an Optronics C-4300 Colorwrite machine is being purchased by PEL and will form the basis of an operational image processing facility. This machine, which should be installed in November 1977, is capable of producing 25 cm square colour transparencies with a minimum pixel size of 50 microns square. Use of the Colorwrite machine, rather than the corresponding photowrite machine for producing monochrome transparencies will substantially increase efficiency. This is

due to the considerable practical difficulties involved in producing high-quality colour transparencies from monochrome negatives. For monochrome negatives smaller than 7 cm square, colour transparencies can be prepared on our colour additive viewer. However, this typically takes several hours and misregistrations of at least 50 microns between the colour bands are likely to be present in the colour negative as discussed in chapter five. Larger colour transparencies can be produced by punch registering the monochrome transparencies. However, this is even more time consuming.

The major demand for computer processed LANDSAT imagery is expected to be for specially processed small to medium size images. These may cover, for example, an area from eight to eighty kilometres square. The particular processing required will depend on the application but may include some or all of the following standard processing techniques (Andrews 1974, Bernstein et al. 1975): image rectification, enhancement (e.g., by stretching or histogram equalisation), band ratioing, noise reduction (e.g., striping removal), and cluster analysis. It is desirable that the processing system developed at PEL should be primarily designed to meet the above processing demands for up to several small to medium size images every day. Demand for larger images is expected to be mainly for suitably processed whole LANDSAT scenes, and to a lesser extent for mosaics of the whole country or large portions of it. A fast turn-around time is not required for the production of these larger images. The above processing requirements could be easily accomplished on a large time-shared computer system. This has been the approach successfully adopted by a number of large image processing laboratories in America (Carter et al. 1977). However, such a system would be unduly expensive for us, and the turn-around time in producing magnetic tapes for outputting on an off-line colorwrite machine in our laboratory would be excessive. The above processing requirements were, however, considered to be within the capability of a minicomputer equipped with suitable peripheral devices. A number of suitable minicomputers are available at PEL, and sufficient computer time is available on them (particularly at night) to meet our needs. Consequently, operation of a minicomputer system for image processing at PEL is financially feasible. In addition such a system would be convenient and reliable to operate. For these reasons it was decided to develop a digital image processing facility at PEL based on the use of a minicomputer.

The initial development of this system and its present status are described in section 7.2. Forthcoming expansion of the system to include the colorwrite machine is described in section 7.3.

7.2 PRESENT PROCESSING SYSTEM

Three minicomputer systems are available for use by the Remote Sensing Section of PEL for image processing: an HP 2100 and a Varian 620f at PEL, and a PDP 11/20 at the nearby Institute of Nuclear Sciences. Each computer has 32K (16 bit words) of core storage. The Varian 620f is available at all times on a time-shared basis. Its peripherals include a single 800/1600 BPI (bytes/inch) magnetic tape unit and a Varian Statos electrostatic printer. The magnetic tape unit has been useful for checking data

on magnetic tape, and the Statos was used as a monochrome display device for 128 x 128 pixel images. Although the quality of images produced on the Statos was low, it was the best display device available to us in the early stages of this project. The PDP 11/20 is less convenient to use but has the advantage of having two 800/1600 BPI magnetic tape units as peripherals. Up till now this computer has been used to perform straightforward magnetic tape operations such as copying a tape from one packing density to another (e.g., 800 to 1600 BPI).

The HP 2100 computer forms the basis of the present processing system. This computer is available for use by us in the late afternoons and overnight. The system configuration (including only the peripherals which we use) is shown in Fig. 7.1. One 2.5 M byte disk is used to store the operating system, all image processing programs, and a number of small data files (most of which contain 128 x 128 pixel images). The other disk is used as a single data file for temporarily storing large images. Most programs are run interactively from the teletype, which is very convenient for programs which are not too time consuming. Longer programs can be run from paper tape. Digital imagery such as LANDSAT CCTs, previously processed images, or digitised aircraft imagery is initially read from the 800 BPI magnetic tape unit and stored on disk. Alternatively, scanned images produced by the off-line PEL microdensitometer can be read in from paper tape. After whatever processing is required, an image is written back to disk or it is written out to magnetic tape line-by-line. At any time, a 128 pixel wide strip of an image on magnetic tape or disk may be printed out on the lineprinter. Each pixel radiance ranging from 0 to 127 can be displayed as a unique character or as one of sixteen grey levels which are produced by character overprinting.

Initial software development on the HP 2100 was aimed at producing a wide range of programs for processing images of a standard 128 x 128 pixel size. These programs allowed such operations as reading, displaying, scaling, stretching, enhancing, ratioing, adding, subtracting, and simple clustering to be performed interactively from the teletype. They have proved very useful for experimenting with and evaluating different processing techniques. Experience gained in processing small images was then used in the development of programs to perform efficiently the most useful operations on much larger images and to prepare magnetic tapes containing images in a suitable format for outputting on a photowrite machine. Most of this software development has been documented, and references are given at the end of this chapter. We were assisted by Optronics International Sales Corporation, U.S.A., and the Minerals Research Laboratories, CSIRO, Australia, both of whom produced some photowrite negatives for us from our processed tapes.

Because of the single magnetic tape unit and the limited disk storage on the HP 2100, the largest single-band image that can be stored for processing is limited to, for example, 1448 x 1536 pixels. For most of our applications this is not a serious limitation, although it allows only about a quarter of a full LANDSAT scene (typically 2340 x 3264 pixels) to be stored. The actual maximum image size on disk varies with shape. For example,

another maximum image size is 1241 x 1792 pixels, which is large enough to store a full LANDSAT scene if only every second row and column is included. Note that it is the size of the input image not the output image that is limited. The output processed image is calculated one line at a time and written immediately to magnetic tape.

Full evaluation of the best way to apply sophisticated image processing techniques in New Zealand will have to wait until our colorwrite machine has arrived. This is because fair comparison of these techniques requires the use of a quality display device.

An example of such a process is band ratioing in which each pixel of a single-band image is divided by the corresponding pixel from another band of the same image. The resulting image, correctly scaled, should minimise the effect of terrain slope variations.

One processing technique which has been studied in some detail and applied successfully to large portions of LANDSAT images is image enhancement. Some simple enhancement techniques, which can be applied by a table lookup method, are now discussed with respect to Fig. 7.2. Consider an image g which is to be enhanced to produce an image f. Fig. 7.2(a) is a plot of the level occurrence statistics N(g) for g (i.e., the number of times each level of g occurs). Let us suppose that f is to be written to photographic film and that the density of each pixel is linearly related to its radiance from 0 to 127. If g is linearly stretched to give f in Fig. 7.2(b), then the whole dynamic range of the output film is used and the image contrast will be much better than in Fig. 7.2(a). However, some levels in Fig. 7.2(b) are much less likely to occur than others. This means that f, given by Fig. 7.2(b), is inefficient in terms of information transfer. The ideal distribution N(f) is shown in Fig. 7.2(d), and this can be achieved by the nonlinear mapping depicted in Fig. 7.2(c). This process is called histogram equalisation. In practice, N(g) for a typical LANDSAT image is of the form shown in Fig. 7.2 (e) rather than Fig. 7.2(a). The corresponding N(f) is shown in Fig. 7.2(f). In Fig. 7.2(d) every density level is equally likely, whereas in Fig. 7.2(f) the density levels are distributed as evenly as possible. Histogram equalisation improves the contrast of levels that occur often at the expense of those that occur rarely. This results in an image which on general viewing conveys more information to the eye than the corresponding stretched image, so long as the number of radiance levels used in the original image is not too low (e.g., 10 or less). For a particular application, detail of interest can be further enhanced at the expense of detail which is of less interest.

A package of HP 2100 computer programs to rectify geometrically distorted imagery has been developed. This rectification system, which is described in detail in chapter 8 of this report, can produce a LANDSAT image at any desired sampling rate, and any required map projection which is geometrically correct to an r.m.s. accuracy of ±50 m. Aircraft imagery can be rectified also. The size of image which can be rectified is determined by the map projection required. A LANDSAT image of an area 13.7 km square can be produced in the Transverse Mecator projection used in the New Zealand inch to the mile map series. It is assumed that such

an image has its edges parallel to the map grid lines. If, however, the image edges are parallel to a map grid formed by rotating the Transverse Mecator map grid by - 12.5° about its artificial origin, then a much larger scene can be rectified. In fact, a whole LANDSAT scene can be rectified if only even row and column numbers are used.

The resolution obtainable by rectifying a full LANDSAT scene in this way is sufficient for the preparation of large mosaics of LANDSAT imagery. Indeed the preparation of such a computer mosaic of New Zealand has already begun. Each scene to be used in the mosaic will be rectified, band by band, on the HP 2100. Next a set of 1600 BPI master tapes will be created on the Varian magnetic tape unit. Each of these tapes will contain a number of image lines or records each followed by a tapemark. The presence of the tapemark allows image lines to be safely overwritten without affecting the rest of the tape. Initially each master image line will contain zeros. The mosaic is built up by reading each master image line into a computer, merging it with the corresponding line from a rectified image, and rewriting the new master line back to the master tape. This operation must be performed on a computer with two magnetic tape units. Initially it will be carried out on the INS PDP 11/20, but later this year it will be carried out on the Varian computer when a second tape unit has been installed. Finally, the full mosaic will be output on the colorwrite machine. Each full scene rectification takes several hours. This processing is accomplished by running the computer unattended overnight.

Fig. 7.3 is a 120 x 80 km portion of LANDSAT image 2334-21123 taken on 22 December 1975. It depicts Lake Taupo and the Kaingaroa state forest in the centre of the North Island of New Zealand. This image has been enhanced by histogram equalisation on the HP 2100 and written for us by Optronics on a colorwrite machine. The horizontal and vertical sampling distance of 80 m and the image has only been geometrically corrected for the effect of the earth's rotation. Fig. 8 in the next chapter has been enhanced and fully geometrically corrected. These images give a fair indication of our present capability for computer image processing.

7.3 FORTHCOMING DEVELOPMENT

It has been decided that the colorwrite machine will be interfaced to the Varian computer which is being upgraded to a Varian V76 computer with 64K (16 bit words) of core storage. Some imagery will continue to be processed on the HP 2100 but an increasing proportion of the required processing is expected to be accomplished on the upgraded Varian, which will soon have two 800/1600 BPI magnetic tape units as peripherals. Software required for image processing on the Varian will be developed during the coming months. Many of the FORTRAN programs will be minor modifications of those already operating on the HP 2100.

Fig. 7.4 shows the configuration of the image processing system which is being developed. We have a colour TV monitor which is used as a colour isodensitometer for viewing monochrome transparencies.

It is hoped next year to interface this colour TV to the Varian computer and use it to interactively display small colour images (e.g., 128 x 128 pixels initially) which will be stored in a refresh memory.

In addition to the processing outlined in the previous section, it is intended to generate a master set of monochrome and colour negatives for each full LANDSAT scene. These negatives will be written on the colorwrite from a 1600 BPI magnetic tape containing a full reformatted LANDSAT scene generated on the Ministry of Works and Development IBM 370/168 computer as discussed in Chapter 6. This reformatting could be accomplished using the two magnetic tape units to be installed on the V 76 computer, but would be time consuming.

7.4 CONCLUSIONS

New Zealand's involvement in the LANDSAT II investigation program has given impetus to the development of a computer image processing facility at PEL. Considerable experience in this field has been gained as a consequence of this co-operative project. We have demonstrated that our present limited processing facility can process images to a quality comparable to that produced by larger overseas image processing laboratories. We are confident that, with the forthcoming developments of our facility, we will be able to satisfy the demand for computer-processed LANDSAT imagery within New Zealand.

REFERENCES

Andrews, H. C. (1974): Monochrome digital image enhancement, Applied Optics 15(2): 495-503.

Bernstein, R., Ferneyhough, D. G. (1975): Digital image processing, Photographic Engineering and Remote Sensing, 41(12): 1465-1476.

Carter, K., Billingsley, F., Lamar, J. (1977): Summary tables for selected digital image processing systems, United States Dept of the Interior, Geological Survey, Open-File Report 77-414.

McDonnell, M. J. (1976-1977): Computer programs for processing LANDSAT imagery on a HP 2100 computer, parts I-III, PEL, DSIR report nos. 519, 545, 567.

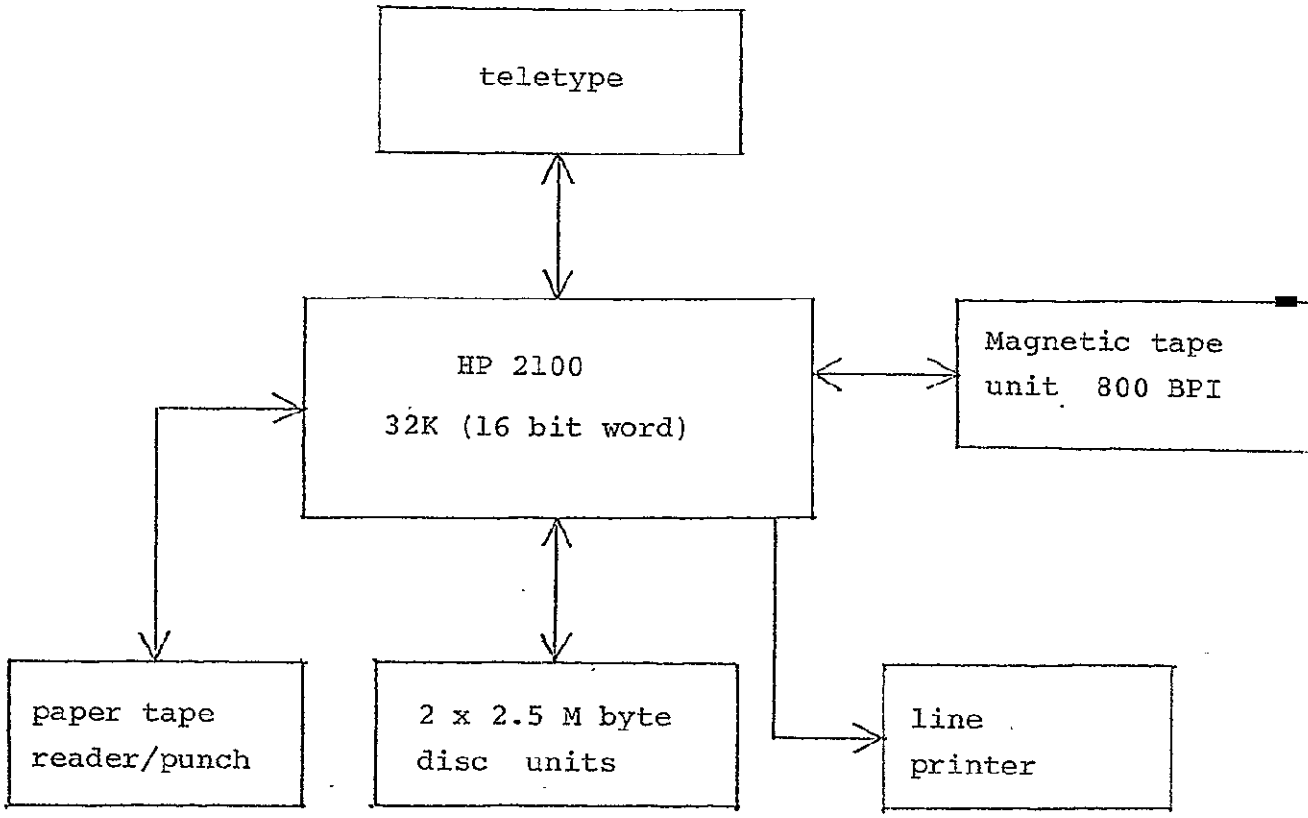

Figure 7.1 System configuration for image processing on the HP 2100 computer.

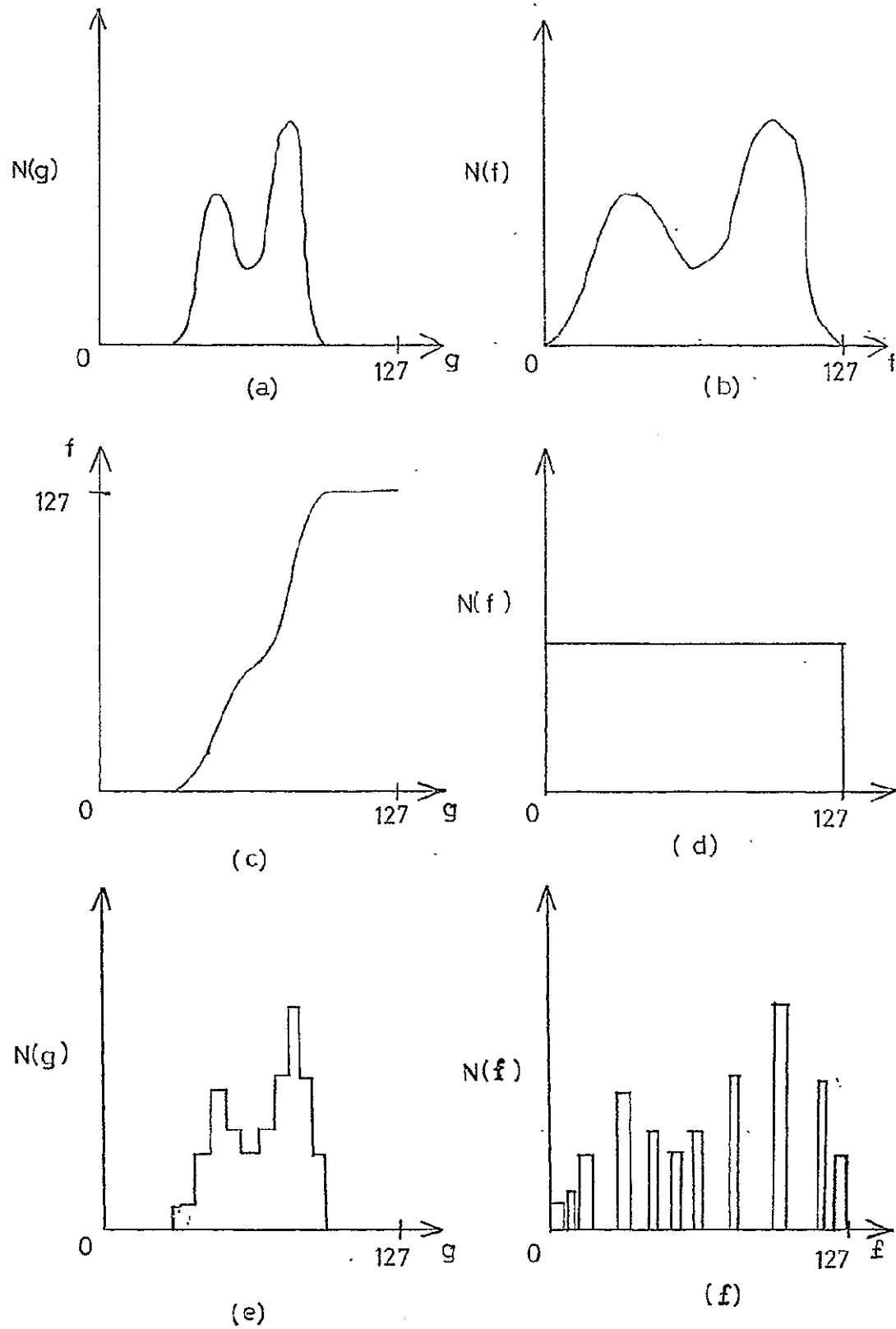

Figure 7.2 (a) level occurrence statistics N(g) for image g,
(b) N(f) for f obtained by linearly stretching g,
(c) nonlinear mapping from g to f,
(d) N(f) for f given by mapping in (c),
(e) typical form for N(g) in practice,
(f) typical N(f) for f obtained by performing histogram equalisation on g in (e).

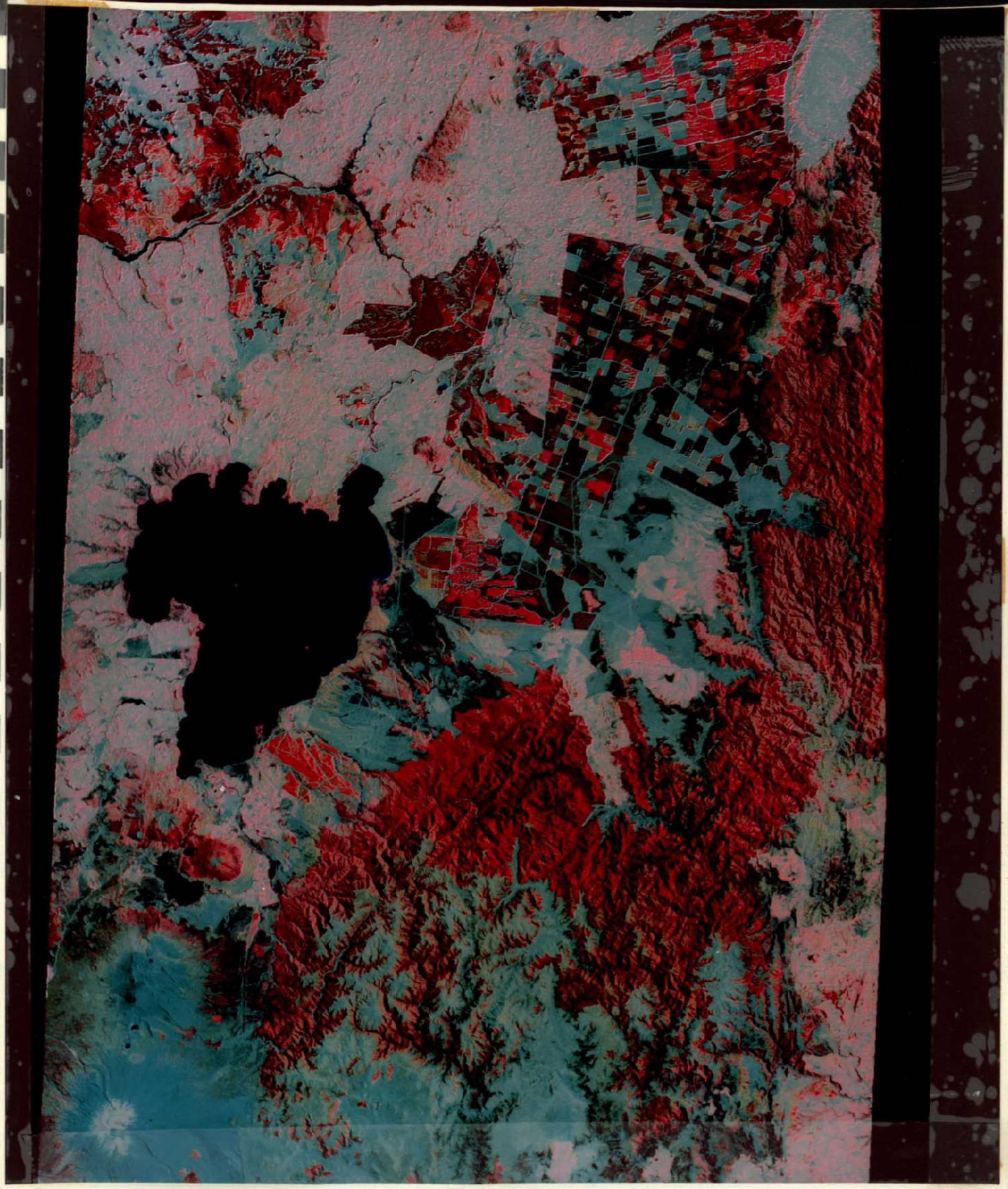

Figure 7.3 A 120 x 80 km part of LANDSAT image 2334-21123 taken on 22 December 1975 and including Lake Taupo and the Kaingaroa State Forest. This image was computer enhanced by histogram equalisation at P.E.L. and written out on an Optronics colorwrite machine. MSS bands 4,5 and 7 are printed as yellow, magenta and cyan respectively.

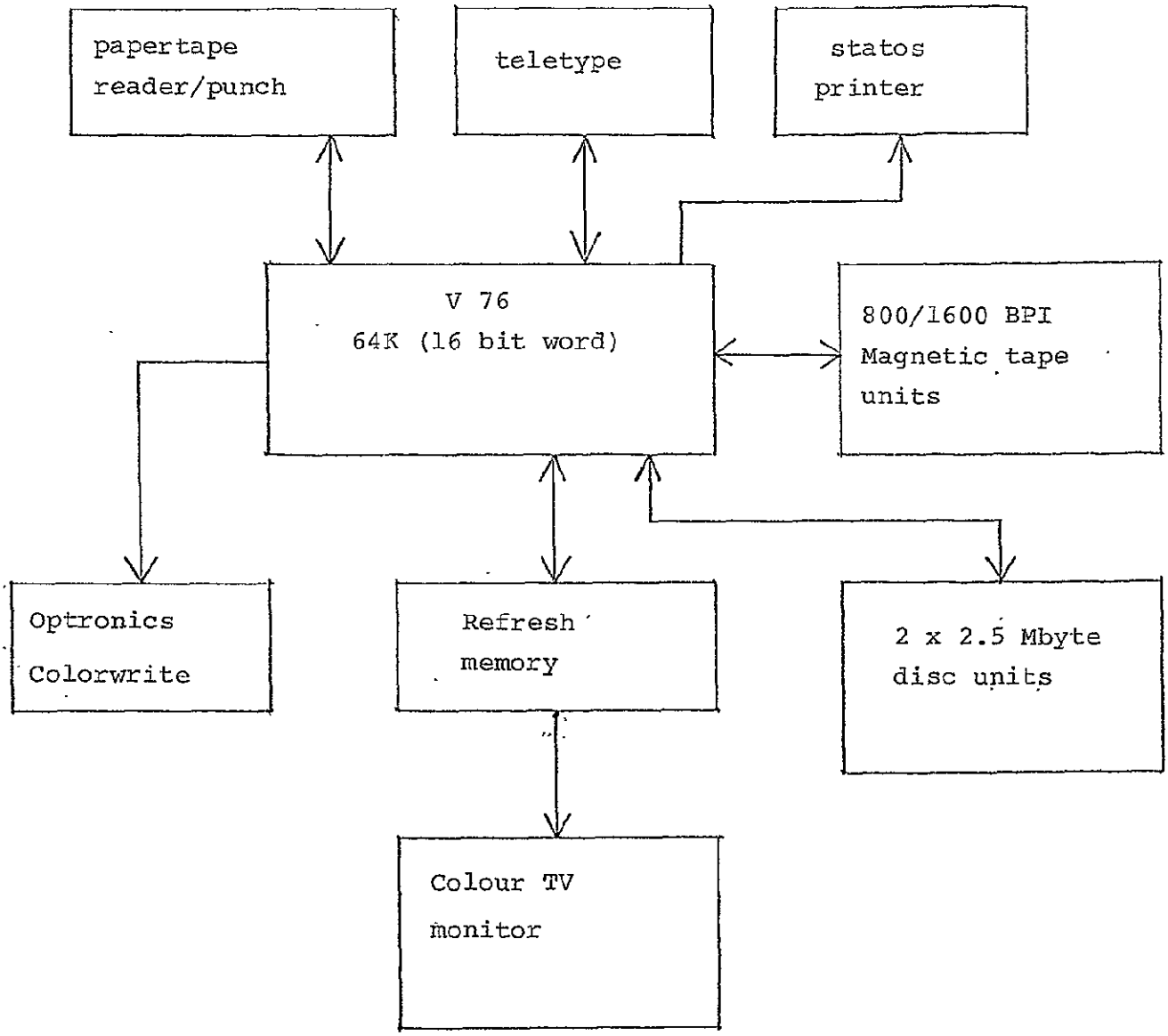

Figure 7.4 System configuration for image processing on the V 76 computer.

CHAPTER 8

DIGITAL IMAGE RECTIFICATION SYSTEM FOR LANDSAT AND AIRCRAFT IMAGERY

M. J. McDonnell

ABSTRACT

A package of HP 2100 computer programs has been developed which uses a minimum of four (but preferably at least ten) ground-control points to derive a simple mapping function which is then used to correct the geometric distortions present in digitised LANDSAT or aircraft imagery. The rectification may be with respect to any desired map projection. The digital image rectification system is explained in this report and some preliminary results are presented.

8.1 INTRODUCTION

Ever since the multispectral scanner of the LANDSAT 1 satellite was first switched on over New Zealand in December 1973, the Remote Sensing Section of the Physics and Engineering Laboratory, DSIR, has been acquiring an extensive multispectral data base of New Zealand. This data is available both as computer compatible tapes (CCT's) containing the original digital data, or as photographic negatives. In addition, negatives from a number of aircraft multispectral photographic surveys are also available at the Physics and Engineering Laboratory. These can be digitised on the Remote Sensing Section's flying spot scanner.

Qualitative research work can often satisfactorily be accomplished using the negatives directly. However, because of the versatility offered by computer processing techniques, serious quantitative work requires the use of digital data. The usefulness of the digital data increases rapidly as the resolution is improved. LANDSAT imagery of the best possible resolution can be obtained if the imagery is corrected for the many geometric distortions present in it and written out on a photographic negative using a photowrite machine. In addition it is usually desirable to have the corrected imagery displayed at a convenient scale in a suitable map projection. This correction process is called image rectification.

We have developed a package of Fortran computer programs for use on the HP2100 mini computer at the Physics and Engineering Laboratory (chapter 7) which will perform a full geometric rectification of a LANDSAT subimage. With this system it is possible to produce a rectified image at any scale in any desired map projection. An uncorrected LANDSAT image typically contains geometric distortions equivalent to about 300 m on the ground, whereas our rectified imagery typically has an r.m.s. error of 50 m which is less than the size of a LANDSAT picture element or pixel. Our system can also be used to rectify aircraft imagery so that it is in register with a map.

The image rectification system developed for use on our HP2100 computer is based on the system developed by Van Wie et al (1975, 1976) at the Goddard Space Flight Center but differs from it in certain key respects. These differences will be made clear as the rectification system is discussed in detail in the following sections.

The reason for developing our own rectification system is mainly financial. The Goddard system would involve us in too much expenditure for computer time on a large computer. However, we have available an HP2100 minicomputer for which we are not charged. (see chapter 7) The Goddard system will rectify whole LANDSAT scenes in the UTM projection. Our system will rectify a LANDSAT subimage on the HP2100 in any desired

mapping projection. The size of the input subimage depends on the extent of the rotation required. This is due to the limited core storage available. For example a small input image (e.g. 128 x 128 pixels) can be fully rotated, whereas a large input image can only be rotated by a small amount.

8.2 DISTORTION SOURCES

There are many sources for the geometric distortions present in LANDSAT imagery. These distortions depend on the detailed technical specifications of LANDSAT and have been discussed in detail by Van Wie et al (1975, 1976) and Bernstein et al (1975). They will now be summarised here before our rectification system is described.

An aspect ratio of 1.4:1 in the LANDSAT imagery is due to the sampling distance being 57 m along but 79 m across scan lines. This is not a serious problem. The angular velocity of the MSS scanning mirror is not constant. This leads to an along scan line distortion in the form of a sine error function which is zero at the end of each scan line and goes through one cycle along each line. The amplitude of the sine error function is about 450 m but varies slowly with time and is different for LANDSAT 1 and 2. This has the effect of decreasing the along scan sampling distance in the middle of each scan line.

Individual MSS bands are misregistered by up to six pixels along scan lines. This is corrected by NASA when preparing the CCT by the insertion of appropriate registration fill characters at the start and end of each scan line.

Additional pixel misregistrations within each band are caused by the delays between sampling each of the 24 individual MSS sensors. An additional offset every six lines is caused by the effect of the earth's rotation during each mirror scan. These errors can be simply compensated for by adding a correction term to each column when a LANDSAT image coordinate (row, column) is calculated.

Variations in the mirror period lead to slight variations in the number of samples in a line. This is compensated for by NASA by regularly inserting synthetic pixels as required so that the resultant line length is constant. These synthetic pixels cause an average error of 28.5 m and can be removed when the CCTs are reformatted. We have not considered it necessary to remove this error.

Further distortion is caused by the satellite's attitude, velocity, and changes of roll, pitch and yaw. In addition the altitude and velocity of the satellite can vary during the 28 seconds or so required to record a whole LANDSAT image.

Panoramic distortion occurs because samples are taken at nominally constant angular intervals of the mirror's movement rather than at equal distances on the ground. A similar effect along scan lines is caused by the earth's curvature.

Because of the central perspective of LANDSAT an object on the ground will appear to be displaced by a distance depending on its height and its distance from the centre of the scan line it is on. This displacement can be as much as 300 m for the top of a mountain of height 3000 m at the edge of a LANDSAT image. This produces a discrepancy when the image is compared to a map produced with an orthogonal perspective. When LANDSAT imagery is viewed, it should be taken into account that it has been correctly produced for a central perspective. The discrepancy between a map and a LANDSAT image produced in this way is only serious for mountain's near the edge of a LANDSAT image.

Further geometric distortions can be introduced in the rectification process by the nature of the map projection in which the LANDSAT image is to be produced. These distortions are negligible for orthogonal map projections such as the Universal Transverse Mercator (UTM) Projection. However, they can be more serious if for example the axes of the map are in latitude and longitude. This can lead to nonlinear effects that are difficult to compensate for using our rectification procedure.

8.3 RECTIFICATION PROCESS

The Goddard approach to the rectification problem is firstly to explicitly correct the input LANDSAT image for the effects of sensor delay, the earth's rotation and the mirror velocity profile to give a corrected input image. The next step is to deduce a suitable mapping function from the UTM map projection to the corrected input image. Let the co-ordinates for the input image, the corrected input image and the map be (R,C), (U,V) and (X,Y) respectively. The Goddard system has available an affine transformation or a polynomial mapping function. For the polynomial mapping fucntion, which is the more accurate, coefficients C_i and D_i are required for the general mapping described by

$$U = C_o + C_1 X + C_2 Y + C_3 X^2 + C_4 XY + C_5 Y^2 + C_6 X^3 + C_7 X^2Y + C_8 XY^2 + C_9 Y^3 + \ldots\ldots\ldots$$

$$V = D_o + D_1 X + D_2 Y + D_3 X^2 + D_4 XY + D_5 Y^2 + D_6 X^3 + D_7 X^2Y + D_8 XY^2 + D_9 Y^3 + \ldots\ldots\ldots$$

The desired order of polynomial is chosen according to the mapping accuracy required. Next the C_i and D_i are computed by means of a least squares fit to a number of known ground control points (GCP's). The coordinates of each GCP are normally measured in both the input LANDSAT image and the map. The input image co-ordinates are then converted to corrected input image co-ordinates and the least squares fit is done between the GCPs in the corrected input image and the map. The above polynomial mapping function is intended to compensate for all errors which have not been explicity corrected in the corrected input image. This technique can compensate for all the errors discussed in the previous section except for those caused by the central perspective of LANDSAT. This error is not correctable by a polynomial mapping function, although it is possible to correct the image for a single chosen height (e.g. sea level). This correction can be achieved by adjusting each GCP by an amount which depends on its altitude and distance from the satellite track through the centre of the image. This correction appears to have been neglected by Van Wie et al. If a GCP is taken on top of a mountain it could cause an error of several pixels.

Our approach is somewhat different. We have noted that the effect of the earth's curvature and the panoramic distortion (for a given height) along rows both have the form of a sine error function to a good approximation. Thus, these errors can be included in the correction for the mirror velocity profile by adjusting the sine amplitude to an optimum value. This optimum value can be simply found by plotting the mean absolute GCP error against sine amplitude, and choosing the amplitude which gives the minimum error. For the example image discussed in section 8.4 this optimum amplitude is 6.55 pixels. The optimum amplitude will vary with the map projection used and it will also vary slowly with time. Correcting for the earth's curvature and perspective distortion at the same time as the mirror velocity profile given a new corrected input image and reduces the need to use a high order polynomial mapping function. We accept the minor constraint that our map image should be a rectangle with sides parallel to the map co-ordinate axes. In this case the function for mapping a rectangle on the map into a quadrilateral in the corrected input image has the form

$$U = C_0 + C_1X + C_2Y + C_3 XY$$

$$V = D_0 + D_1X + D_2Y + D_3 XY$$

A function for mapping from the corrected input image to the map is not required in the rectification process.

This particular mapping function has some special properties. Firstly, straight lines on the map parallel to the co-ordinate axes, map into straight lines on the corrected input image. However, other straight lines on the map, map into curved lines (see for example the diagonals in Fig. 8.1). This is caused by

the XY term in the polynomial. Secondly, and most importantly, the sampling grid in the corrected input image, corresponding to the rectangular desired output image on the map, is formed by the intersection of a grid of straight lines. For each output image row, the endpoint co-ordinates of the corresponding corrected input image sample line are obtained by adding a constant amount to the previously used sample line endpoint co-ordinates. Similarly the sample co-ordinates along each corrected input image line (corresponding to an output image row) are simply obtained by incrementing the previously used sample co-ordinate by a constant amount.

This leads to a considerable saving in computation time. Each sample co-ordinate needed in the corrected input image (corresponding to an output image sample) does not have to be calculated separately by means of the polynomial function above. Van Wie et al overcome the problem of the time required to calculate the polynomial mapping function for each output image sample by superimposing a coarse grid system upon the output image, mapping this grid onto the corrected input image and then performing bilinear interpolation between grid lines. Our system is considerably simpler, but cannot obtain the accuracy possible with the highest order (e.g. 4) polynomial mapping functions used by Van Wie et al. Our model of a sine error function along scan lines, which is implemented efficiently by a table lookup method, compensates satisfactorily for nonlinear distortions along scan lines. However, we have made no attempt to correct for nonlinear distortions which occur across scan lines and are caused mainly by variations in the velocity and pitch of the satellite while scanning an image. We have found these distortions to be minor and a small price to pay for the computational efficiency and simplicity of our rectification procedure.

A further advantage of our quadrilateral mapping function is that, being of low order, it is stable at the edges of the image. Also, although the GCP's should be well spread out, our mapping function is not over sensitive to their location.

For each required geometrically corrected output image sample, its corresponding co-ordinate is calculated first in the corrected input image and then (straightforwardly) in the input image itself. The final radiance value is then obtained by nearest neighbour, bilinear or cubic interpolation as is done by Van Wie et al. Results for an example LANDSAT image are discussed in section 8.4.

Nearest neighbour is the fastest and cubic the slowest, but most accurate interpolation technique. In our experience bilinear interpolation is a satisfactory compromise between the requirements of speed and accuracy.

Our rectification system has been implemented on the HP2100 minicomputer system described in chapter 7. This system has 32 K (16 bit words) of core storage, a single 800 BPI magnetic tape unit and uses a 2.5 M byte disk unit to store the image to be rectified. One output image row is calculated at a time, using data stored in core, after which it is written out to magnetic tape. Data stored in core is updated from disk when required. The size of image which can be rectified is limited either by core storage or disk storage depending on how much the image to be rectified has to be rotated. The amount of this rotation determines how many input image rows are needed in core to calculate each output image row. A 128 x 128 pixel input image can be rotated as much as is desired. A LANDSAT image of an area 13.7 km square can be produced in the Transverse Mercator projection used in the New Zealand inch to the mile map series. This is assuming that the output image has its edges parallel to the map grid lines. In these cases the limit on image size is core storage because of the extent of rotation required. It is possible to define map projections which require very little rotation. From a computational point of view the most suitable projection of this type is the Space Oblique Mercator projection (Colvocoresses 1974). However, for our purposes it is desirable to be able to register rectified imagery with maps in common use in New Zealand. For this reason we are producing rectified images whose edges are parallel to grid lines on a map formed by rotating the standard New Zealand Transverse Mercator grid by -12.5° about its artificial origin. The size of image which can be rectified in this way is limited by our disk storage. A quarter of a full LANDSAT scene can at present be fully rectified. A whole LANDSAT scene can be rectified if only even rows and columns are used in the input image. The resolution obtainable in this way is sufficient for the preparation of a mosaic of New Zealand as discussed in chapter 7.

Later this year it will be possible to use our rectification system on our Varian V76 minicomputer using two 800/1600 BPI magnetic tape units to fully rectify a whole LANDSAT scene. It should be noted that the limitations in image size (in pixels) discussed above apply only to the input image. The size of the output image is generally constrained by the amount of data which can be stored on a magnetic tape. Each rectified image is produced on tape in a form suitable for direct outputting on a photowrite machine.

8.4 IMAGE RECTIFICATION RESULTS

Our rectification system has so far been used on three LANDSAT scenes and one set of multispectral aircraft negatives which had been scanned on an Optronics photoscan device at Massey University. Results obtained for LANDSAT 2 scene 2334-21123 are discussed in this section.

Nineteen points suitable for use as GCPs were chosen by inspection of the LANDSAT scene. Some of these points were the centres of small lakes and forest road intersections, but most were acute water-land interfaces. A number of shaded computer lineprinter outputs and New Zealand standard inch to the mile (1:63360) Transverse Mercator (TM) maps were then obtained which included all the GCPs. The co-ordinates of each GCP in the LANDSAT image and the map were then determined by examining, for each GCP, the appropriate shaded printout and map together. To obtain reasonable accuracy (i.e. ±0.5 pixel in the image row and column co-ordinates and ±20 yards in the map co-ordinates) it is most important that the printout and map should be examined together. Our experience is that the best type of GCP is a land-water interface with the land forming an acute angled peninsula. Such GCPs are readily available throughout New Zealand. An advantage of using land-water interfaces is that only MSS band 7 needs to be printed out to locate the GCP.

In Table 8.1 the input image co-ordinates and the corresponding map co-ordinates are given for the nineteen GCPs. The GCPs were then compensated for the effects of their heights and transformed to the corrected input image. A least squares mapping function was then derived for various amplitudes of the sine error function. The resultant average error in metres is plotted in Fig. 8.2 against the amplitude of the sine error function. From this plot it was deduced that the optimum amplitude was 6.55 pixels in the along scan direction. The resulting mapping error in meters for each GCP using this amplitude in the sine error function is shown in Table 8.1. This error is the distance between the result of mapping the GCP in map co-ordinates to the image, and the GCP measured in image co-ordinates. The distribution of the GCPs and the direction and size of the errors is shown in Fig. 8.1.

It should be noted that the errors for each GCP in Fig. 8.3 and Table 8.1 include contributions from the errors in measuring the GCPs in the map and the image. These contributions may well be the main part of the errors shown in Fig. 8.3. More images need to be processed, and the processed images need to be compared to maps before the mapping accuracy of this method can be fully evaluated. However, initial tests indicate the accuracy is sufficient for our purposes.

Fig. 8.4 is a 2200 x 2200 pixel fully geometrically corrected image produced from LANDSAT scene 2334-21123 taken on 22 December 1975. Lake Tarawera and Mount Tarawera appear in the bottom half of the image. This image is rotated by -12.5° with respect to the standard New Zealand Transverse Mercator projection used in inch to the mile maps. Each pixel covers a 10 yard square area and the bottom right hand corner of the image is at 488000 N, 402000 E. Each band of the image has been enhanced by histogram equalisation as discussed in chapter 7 and MSS bands 4, 5 and 7 are printed as yellow, magenta and cyan respectively. The size of the area covered

by the image is exactly 12.5 miles square. The image was kindly written out for us on the photowrite machine at the Minerals Research Laboratories, C.S.I.R.O., Australia.

8.5 CONCLUSIONS

We have shown that it is practicable to rectify large LANDSAT subimages on a minicomputer system. The geometric accuracy of our rectified imagery is sufficient for a wide range of applications. It is anticipated that our rectification system will be in constant use once the colorwrite device (discussed in chapter 7) is available for outputting images from the computer.

REFERENCES

Van Wie, P, Stein, M (1976) "A LANDSAT digital image rectification system." Report X-931-76-101, Goddard Space Flight Centre, Greenbelt, Maryland.

Van Wie, P, Stein, M, Puccinelli, E, Fields, B (1975) "LANDSAT digital image rectification system - preliminary documentation", Information Extraction Division, Goddard Space Flight Centre.

Bernstein, R, Ferneyhough, D G, (1975) "Digital image processing", Photogrammetric Engineering and Remote Sensing 41, 12, 1465-1476.

Colvocoresses, A P, (1974) "Space Oblique Mercator", Photogrammetric Engineering and Remote Sensing 40, 8, 921-926.

GCP Number	Image (pixels)		Map (yards)		Error (meters)
	Row	Column	Northing	Easting	
1	2001.2	180.2	377180	311220	29
2	1917.0	2155.5	357610	435460	67
3	1412.5	208.0	426220	326610	87
4	1003.0	2188.5	433830	458860	77
5	1166.3	1266.2	432600	397700	86
6	385.0	546.0	508040	371460	95
7	313.8	1402.5	502370	426290	72
8	240.5	2945.5	487700	523490	34
9	1359.3	3205.5	390300	513020	13
10	2024.2	169.6	375350	310050	22
11	1441.2	286.3	422800	330810	24
12	1009.7	2169.1	433550	457590	4
13	413.0	584.0	505050	373250	82
14	253.4	693.4	517110	383770	63
15	255.5	741.5	516220	386610	37
16	300.0	799.2	511750	389170	16
17	347.7	812.0	507580	388840	24
18	385.0	781.8	504890	386060	50
19	393.0	790.8	504100	386450	55
Mean absolute error					49

Table 8.1 Image and map co-ordinates, and mapping errors for 19 GCP's for LANDSAT scene 2334-21123.

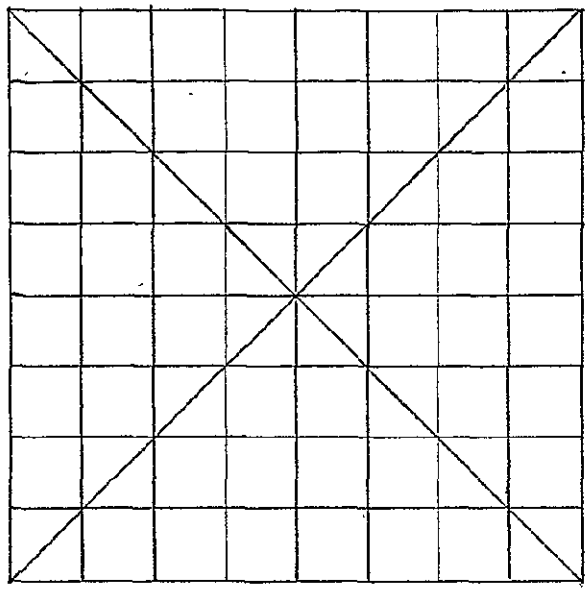

(a)

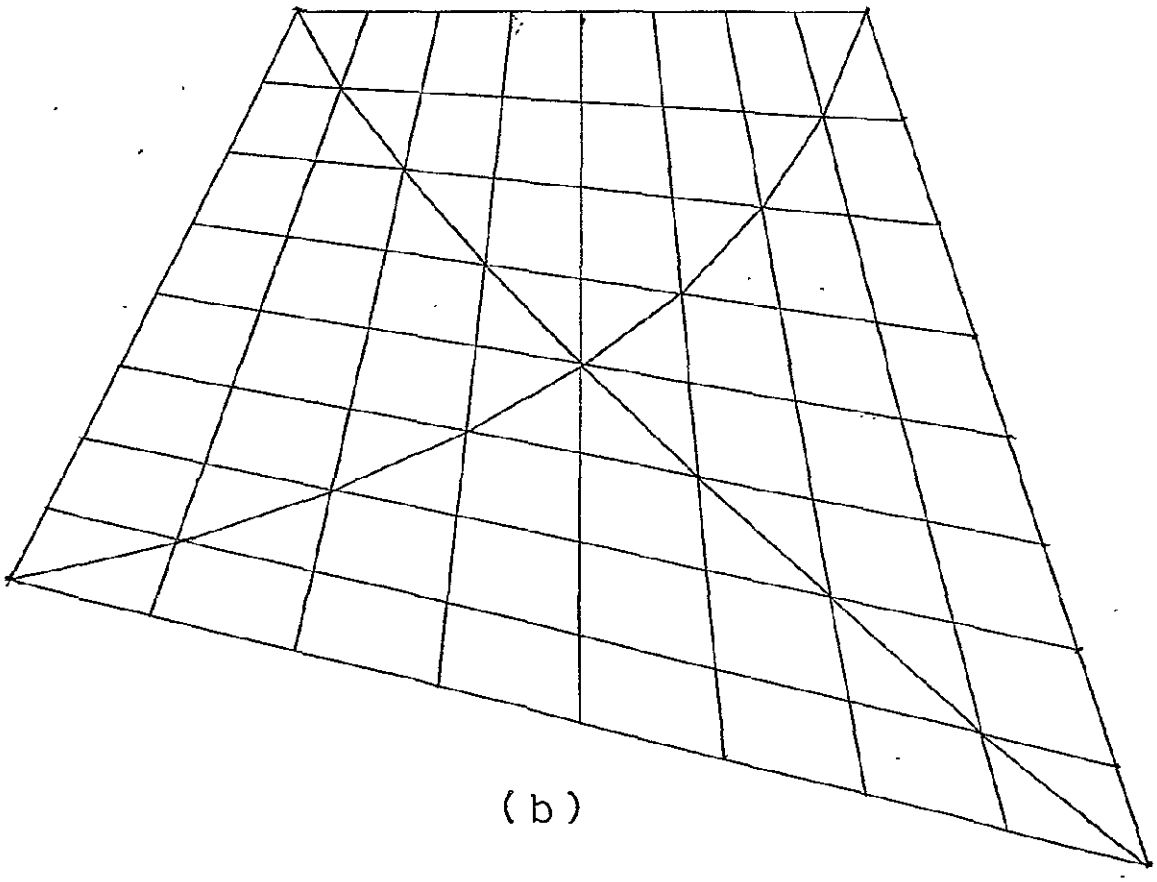

(b)

Figure 8.1 Example mapping of a rectangle on a map (a) into a quadrilateral in the corrected input image (b).

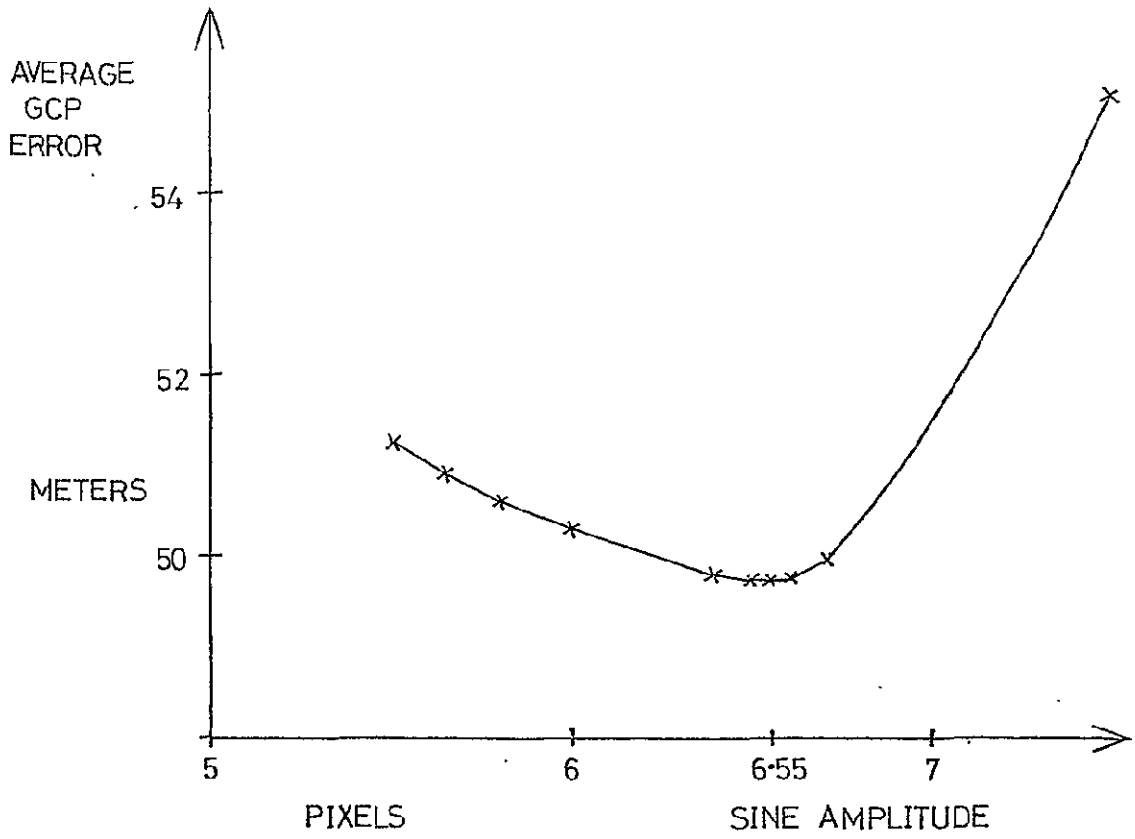

Figure 8.2 Average GCP error in meters versus amplitude of the sine error function in pixels in the along scan direction.

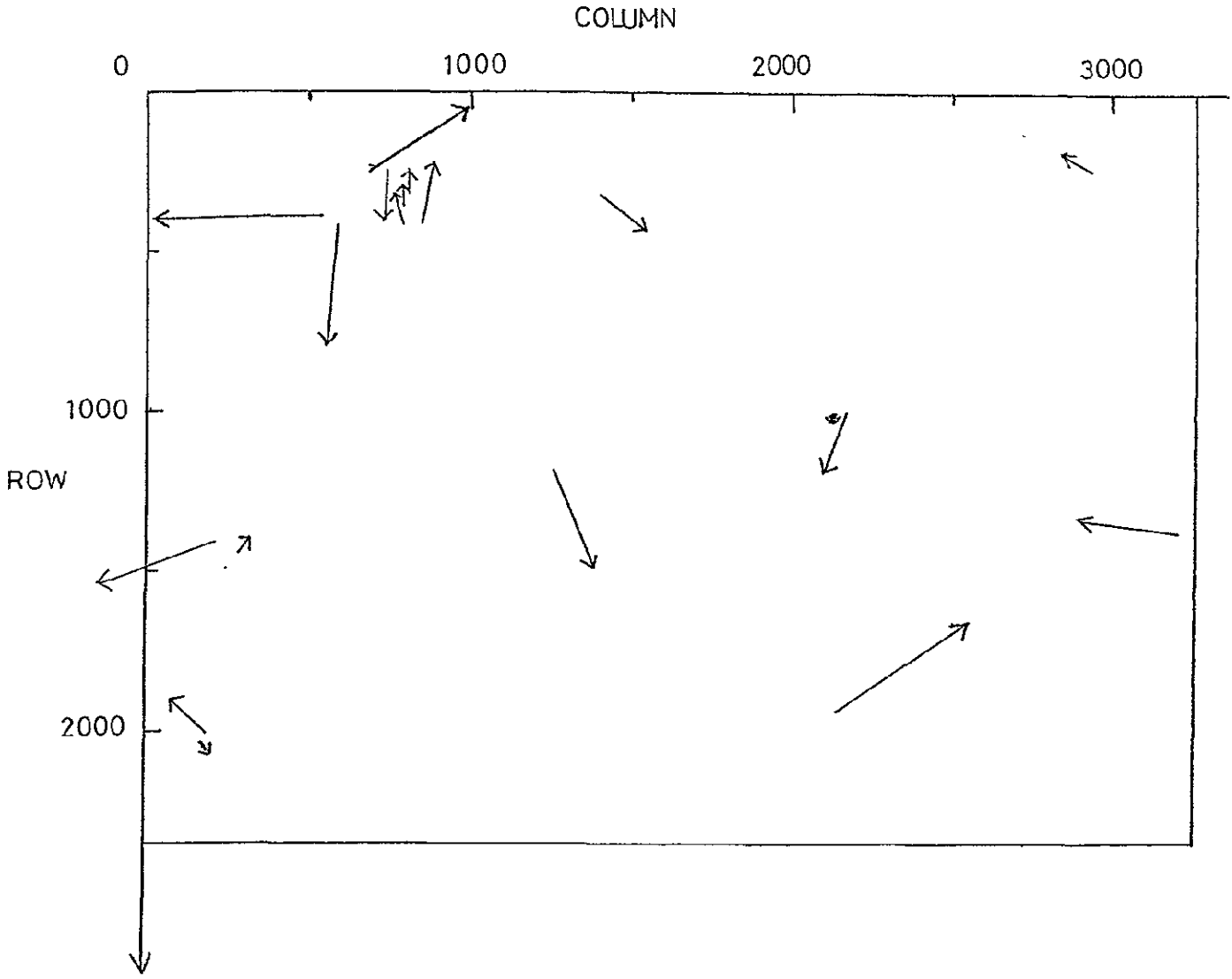

Figure 8.3 The positions of the 19 GCP's used in the geometric correction of LANDSAT scene 2334-21123 are shown by the start of the arrows. The length and direction of the arrows depict the mapping errors for each GCP.

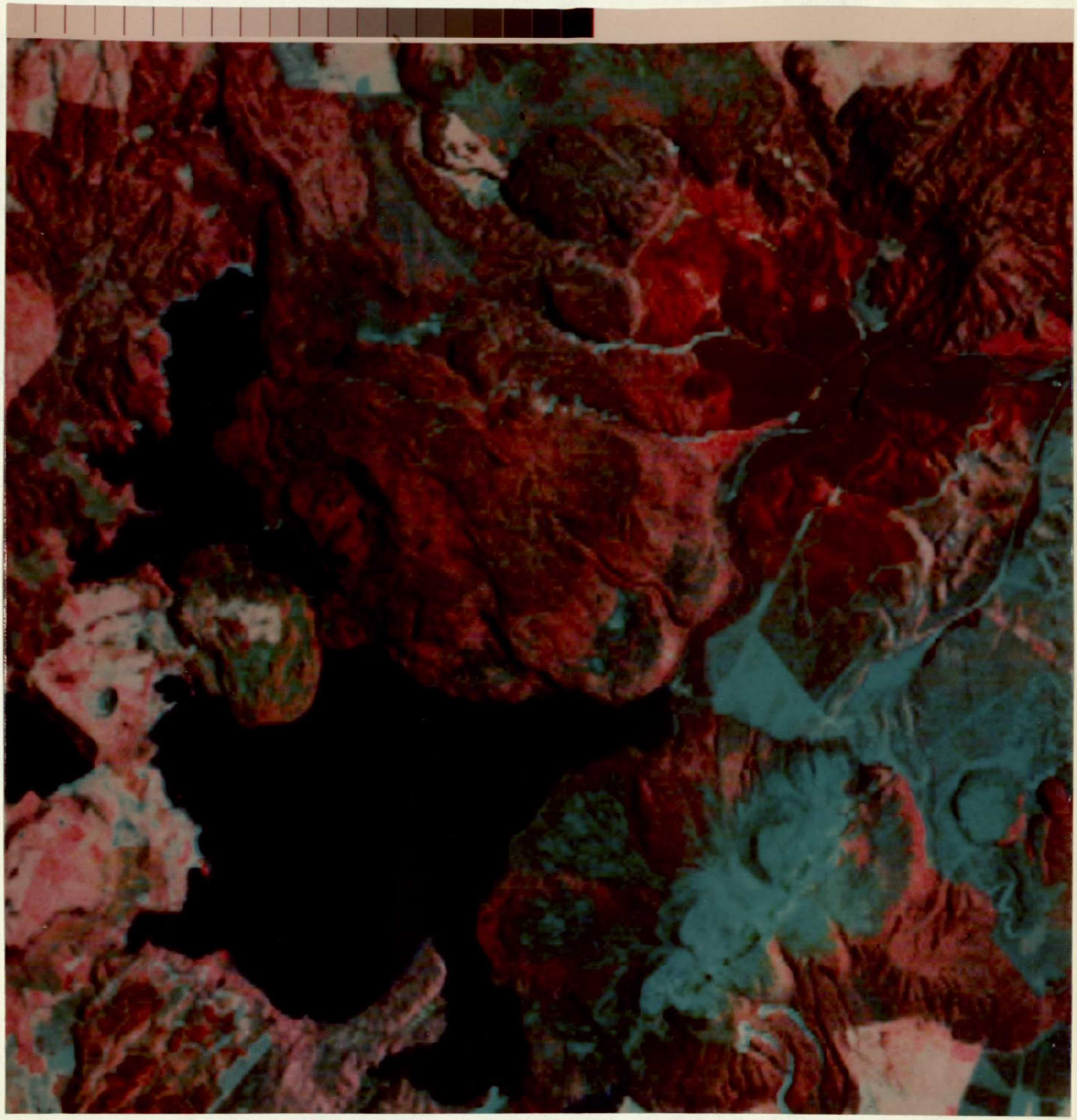

Figure 8.4 A 12.5 mile square image of the Mount Tarawera area which has been enhanced and geometrically corrected on the HP2100 computer at PEL.

CHAPTER 9

SHIP DETECTION FROM LANDSAT

M. J. McDonnell and A. J. Lewis

ABSTRACT

Recent inspection of LANDSAT CCT printouts revealed that the detection of ships is possible. Experience has shown that MSS band 7, because of low radiance values from water and the resultant high S/N ratio, is the best MSS band for a "quick-look" inspection of CCT printouts for possible ships. After verification of the target on CCT printouts of other MSS bands, the ship's size, orientation, state of motion, and direction of movement can be determined from the total number of pixels occupied by the target for each MSS band, the orientation of these pixels, and the target's maximum and total pixel radiance values. This paper presents the procedures used for detecting ships, and discusses the problems and limitations of the overall technique as related to ship parameters, sea state and turbidity, pixel overlap, and relative geometric fidelity between pixels.

9.1 INTRODUCTION

Although the usefulness of LANDSAT data for mapping and monitoring earth resources has been demonstrated repeatedly, one potential application of the data which seems to have been overlooked in ship detection. Recent inspection and analysis of pixels (picture elements) obtained from LANDSAT computer-compatible tapes (CCTs) of New Zealand revealed that not only can ships and their wakes be detected, but that information on the size, state of motion (stationary or moving), and direction of movement can be inferred by calculating the total number of pixels occupied by the vessel and wake, the orientation of these pixels, and the sum of their radiance values above the background level for each MSS band. In this paper the procedures used for detecting ships are presented, and the problems and limitations of the technique as related to ship parameters, sea state and turbidity, pixel overlap, and the relative geometric fidelity between pixels are discussed.

New Zealand is an isolated South Pacific country consisting of two main islands and a number of smaller ones. Inter-island and international shipping activities are very important to the country's economy. It is possible that future satellites such as SEASAT-A will provide a means of monitoring ship movement on a real-time basis. In view of this it was of interest to test the feasibility of using LANDSAT II visible and near-infrared recorded radiometric data for ship detection. SEASAT, with its active imaging microwave sensor, should prove more applicable to ship detection because of its improved resolution and its near allweather and day/night imaging capabilities. However, no satellite data of this type is yet available for evaluation.

Regular scheduling of inter-island ferries between the North and South Islands of New Zealand made it likely that the location of ships would be known at the time of a LANDSAT II overpass. Also, the generally low turbidity of the water in Wellington Harbour and Cook Strait (41.3°S, 174.8°E) simplifies ship detection. For these reasons the Cook Strait area of New Zealand was a logical test site for this investigation.

9.2 SHIP DETECTION PROCEDURE

A set of procedures was established in the early stages of the study to remove much of the subjectivity involved and to help make automatic ship detection through computer processing of LANDSAT data possible in the future. Ship detection was accomplished using coded computer lineprinter outputs which displayed the radiance levels for each LANDSAT MSS band in a 128-pixel-wide strip. Experience has shown that band 7, because of the very low radiance values from water (usually zero), is the best band for a "quick-look" detection of possible ships. The low background radiance values from water in bands 6 and 7 result in a high signal-to-noise ratio (S/N), even though the absolute value of the signal above the background (S-N) is considerably higher in bands 4 and 5. Throughout this paper radiance is expressed in terms of linear LANDSAT quantised units. The maximum radiances for MSS bands 4, 5, 6, and 7 are 2.48, 2.00, 1.76, and 4.00 mW/cm^2 - sr corresponding to CCT radiance levels of 127, 127, 127, and 63 respectively.

The procedure used for establishing the pixels occupied by the target is as follows:

I Locate possible ship on MSS band 7 printout of radiance values. Three levels above the modal background (i.e., the most commonly occurring radiance level for the sea in the printout) is used as the threshold for establishing a possible target. This threshold level was chosen to be above the background noise level, but below the maximum level for a medium sized vessel.

II Analyse the other three MSS bands to confirm that the target is present on all bands. An anomalously high value at the same pixel location as in I is sufficient test (e.g., 50% up on average background).

III Using the pixel with the highest value in band 7 as the ship's center, and the center of a sampling array, five rows and nine columns are sampled in each band. For LANDSAT II, each pixel covers a 79 m square area. The sampling distance between rows is 79 m, but between columns it is only 57 m.

IV A maximum background threshold is established for each band and row sampled in III by finding the maximum of 10 pixel values within the row but outside the sampled area. Where possible five pixel values are taken on each side of the sampled area. This sampling is done separately for each row to eliminate the six-line-striping characteristic of LANDSAT data. The sampling is done away from the suspected ship to prevent target contamination of the background noise level.

V In each band and for each row the maximum background threshold value is then used to eliminate the pixels from III whose radiance values were not affected by the target. Pixel values less than or equal to the threshold are set to zero, as are pixels above the threshold but not in a row or column adjacent to a target pixel. The center pixel in III is taken as the first target pixel.

VI For each band, the average background value for each row is calculated from the ten sampled pixels in IV, and this is subtracted from the radiance value of each pixel not set to zero in V.

VII The result is a 9 x 5 matrix of pixel radiance for each MSS band that defines the number, location, and radiance values of pixels occupied by the ship and its wake.

9.3 ANALYSIS

Two LANDSAT II scenes of Wellington Harbour (2334-21132 taken on GMT 22 December 1975 and 2335-21190 taken on GMT 23 December 1975) were used in this study. Details of five ships known to be in one or both of these images are given in Table 9.1. All of the vessels except HMNZS Rotoiti were successfully located. Table 9.2 gives the CCT radiance levels, before and after the authors' processing, from the four LANDSAT MSS bands for the Aratika, an inter-island ferry, and a given surrounding area.

Our experience is that the location and size of a vessel are better indicated by the radiance values above the average background for the near-infrared bands than the visible bands. This appears to be due to the greater reflectivity of the ship's wake[1]. The direction of ship movement can then be inferred from the position of the wake with respect to the ship (see Table 9.2). At the time of satellite overpass, the Arahanga (GMT 22 December 1975) and the Aramoana (GMT 23 December 1975) are known to have been slow moving or stationary. This explains the low radiance levels for these two ships in Fig. 9.1 and indicates that most of the reflected radiance recorded in MSS bands 4, 5, and 6 is due to the ship's wake. Because band 7 is least influenced by the wake, as indicated by Fig. 9.1 and Table 9.2, it is the best band to use as an indication of the ship's size and position. The low reflectance of the Osco Sailor in band 4 is due to its orange-red colour.

Measurements of the total reflected radiance above background (Fig. 9.1) and the maximum value above threshold (Fig. 9.2) are both subject to considerable error. Errors in the radiance levels as in Fig. 9.1 are introduced by NASA quantisation techniques, the 22 m pixel overlap per 57 m sample spacing, and the authors' processing. Although pixel overlap does not contribute to the maximum radiance errors in Fig. 9.2, it does introduce a larger variation resulting from the positioning of the pixels with respect to the vessel. For example, a ship the length of a pixel may be sampled completely within one pixel or straddle up to six pixels.

The average background radiance along a row is not a source of error, but the range of variation of the background radiance level is. For our images, the background for band 7 was usually level 0, but occasionally level 1 (i.e., a range of 1). The corresponding ranges for bands 4, 5, 6 are 5, 3, and 3 respectively.

The best indication of ship size is given by the total radiance values in MSS band 7 (Fig. 9.1). This is because the total radiance values for a given size are more consistent than maximum radiance levels (Fig. 9.2) and also because of the low near-infrared reflectance of the ship's wake in MSS band 7. The smallest ship positively identified was 112 m long (see Table 9.1). In theory it should be possible to detect vessels 30 m long (such as the Rotoiti) under favourable imaging conditions. For example, based on the average signal per unit ship area produced by the moving ships, the Rotoiti would be expected to produce a total radiance value (after processing) of 3.1, 3.3, 3.4, and 1.0 in bands 4, 5, 6, and 7 respectively. This implies that a small boat may best be found by lowering the threshold level in band 7 to one level above the modal background and then confirm or reject the suspected target by examining the other bands as in step II of the procedure described previously. However, this would lengthen computation time, as many more possible ships would have to be tested.

---

1. The ship's wake is defined by the pixels which, after processing, are zero in band 7 but non-zero in band 4

Fig. 9.3, a plot of signal-to-noise (S/N) ratio against band number for the five positively identified ships[2], indicates that MSS band 7 is the best band for initially locating ships because of the high S/N ratio. In each case the S/N ratio is calculated using the maximum radiance value.

A number of problems were noted which are likely to affect ship detection. For example, the contribution of turbidity to radiance variations in the sea needs to be of low spatial frequency. Also the 22 m pixel overlap along rows needs to be taken into account for determining the most likely position for the vessel, as do the extra pixels NASA have inserted to compensate for variations in scan line length, which could change the apparent orientation of the ship. These particular problems did not affect our results.

Anomalies were found in the data which we were unable to explain adequately. For example, one pixel in the Tasman Sea in band 7 had a radiance value of 63. This is the maximum possible value in band 7 and is at least fifteen times greater than the maximum band 7 radiance for any ship studied. The pixel was surrounded by pixels of value 0. No anomalous radiance value was found nearby in either band 4 or 5, but a high value was found in band 6 which was, however, offset by two pixels along a row. The only plausible, but unlikely, explanation suggested was that the high values were caused by reflections from another satellite passing beneath LANDSAT II, the offset between bands being caused by the slightly different sampling times for bands 6 and 7.

9.4 CONCLUSIONS

The detection of ships via LANDSAT MSS data has been demonstrated. In addition information on ship size, orientation, and movement is obtainable. Band 7 was used for the initial detection followed by confirmation on other MSS bands. Indication of ship size and orientation was also given by band 7. Identification of the ship's wake from MSS bands 4 and 7 indicates motion and direction.

Under low turbidity, as experienced in open seas, the detection of ships 100 m long was verified and detection of ships down to 30 m length theorised. High turbidity and sea state inhibit ship detection by decreasing S/N ratios.

2. A number of other possible ships were also found, but verification of them was not possible.

Table 9.1 -

Description of Ships Present in LANDSAT II Scenes Studied

Ship's Name	Type	Length (m)	Breadth (m)	Tonnage	GMT date	Symbol in Figures
Osco Sailor	Oil Tanker	171.8	26.6	21,275	23 Dec 75	O
Aratika	Inter-island ferry	127.7	18.8	3,879	23 Dec 75	.
Arahanga	Inter-island ferry	127.5	18.8	3,894	23 Dec 75	+
Arahanga	Inter-island ferry	127.5	18.8	3,894	22 Dec 75	-
Aramoana	Inter-island ferry	112.2	18.6	4,160	22 Dec 75	□
HMNZS Rotoiti	Fisheries protection vessel	32.1	6.1	134	23 Dec 75	

Table 9.2 -

LANDSAT Radiance Data for the Aratika

(Source: LANDSAT II scene 2335-21190)

	Before Processing						After Processing					
	Column						Column					
	1462	1463	1464	1465	1466	1467	1462	1463	1464	1465	1466	1467
MSS Band 4												
Row 739	16	16	15	14	14	14	2.2	2.2	1.2			
740	12	16	22	24	19	13		3.0	9.0	11.0	6.0	
741	12	12	13	17	24	19				3.7	10.7	5.7
742	14	14	14	14	14	14						
MSS Band 5												
Row 739	10	11	9	8	8	9	2.0	3.0				
740	8	10	15	19	13	8		2.2	7.2	11.2	5.2	
741	8	8	8	13	20	14				5.0	12.0	6.0
742	8	9	8	9	9	8				1.4	1.4	
MSS Band 6												
Row 739	4	4	4	4	2	2	2.6	2.6	2.6	2.6		
740	2	6	10	12	8	2		3.4	7.4	9.4	5.4	
741	5	4	5	10	16	10				5.3	11.3	5.3
742	5	5	4	5	4	5						
MSS Band 7												
Row 739												
740			2	2					2	2		
741				2	4	2				2	4	2
742												

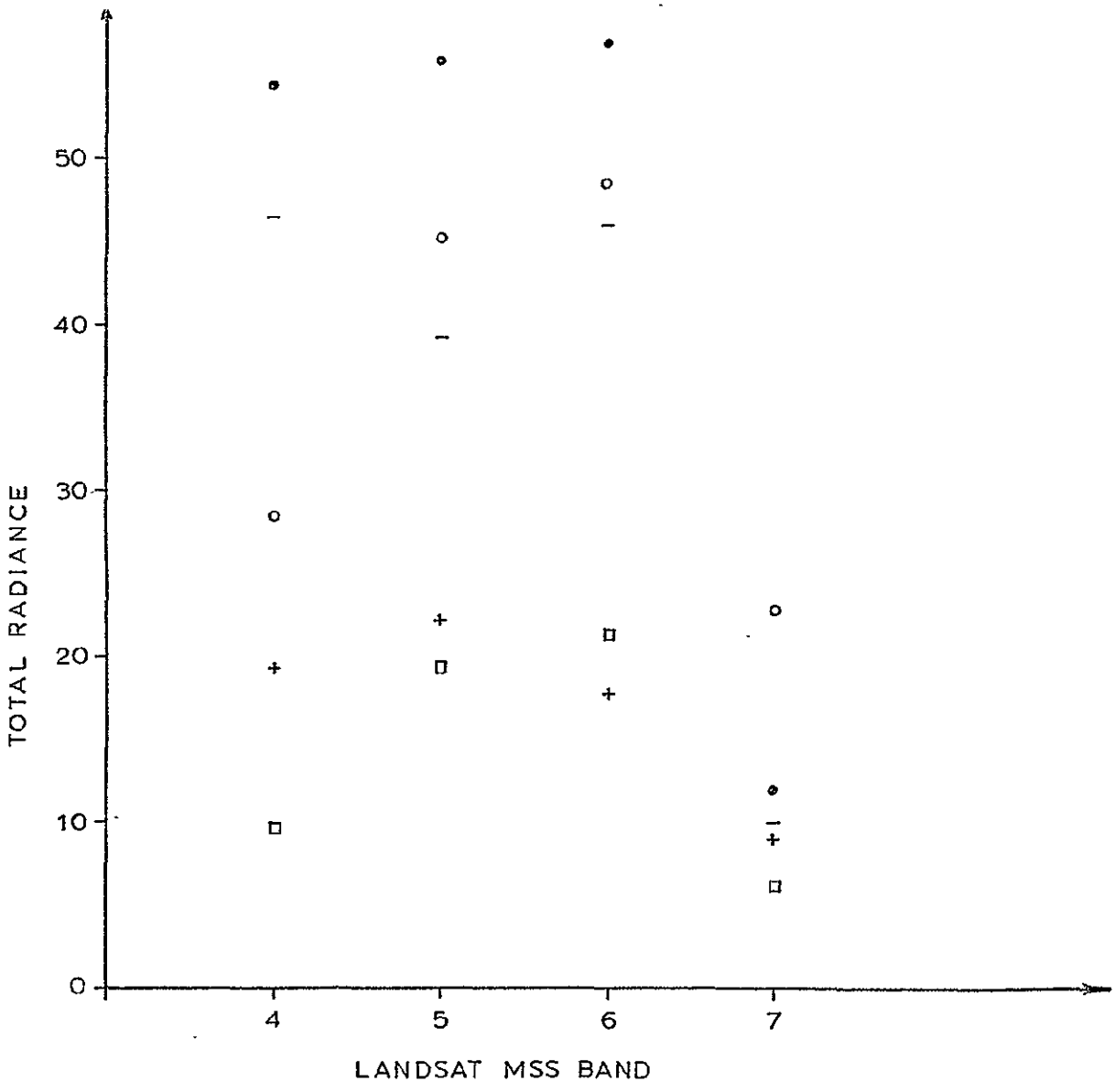

Fig. 9.1 - Total reflected radiance (in LANDSAT quantised units) versus MSS band number for each of the five positively identified ships given in Table 9.1.

O	Osco Sailor	+	Arahanga (GMT 23 Dec 75)
.	Aratika	-	Arahanga (GMT 22 Dec 75)
□	Aramoana		

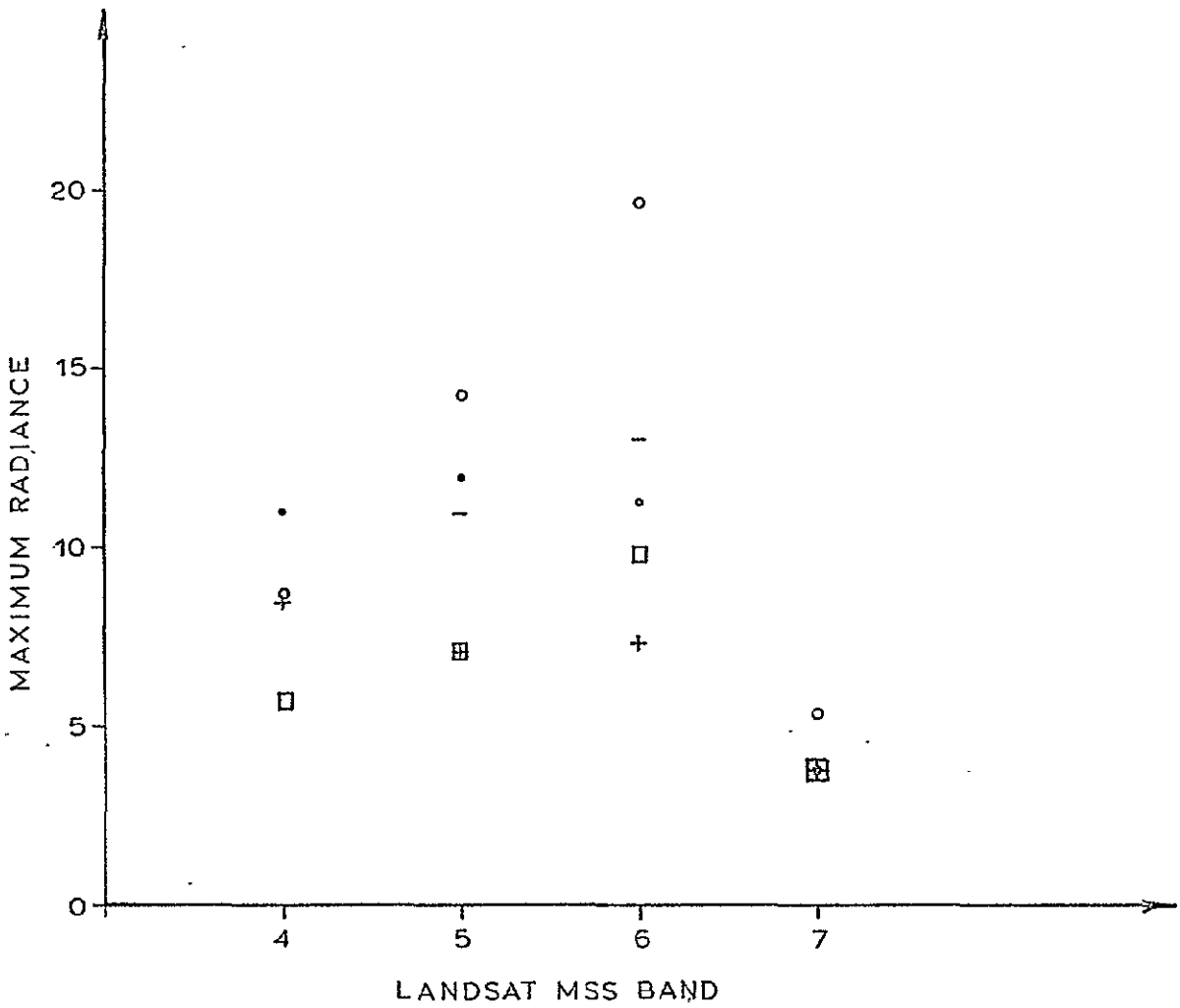

Fig. 9.2 - Maximum pixel value above threshold versus MSS band number for each of the five positively identified ships given in Table 9.1.

O Osco Sailor
. Aratika
□ Aramoana
\+ Arahanga (GMT 23 Dec 75)
\- Arahanga (GMT 22 Dec 75).

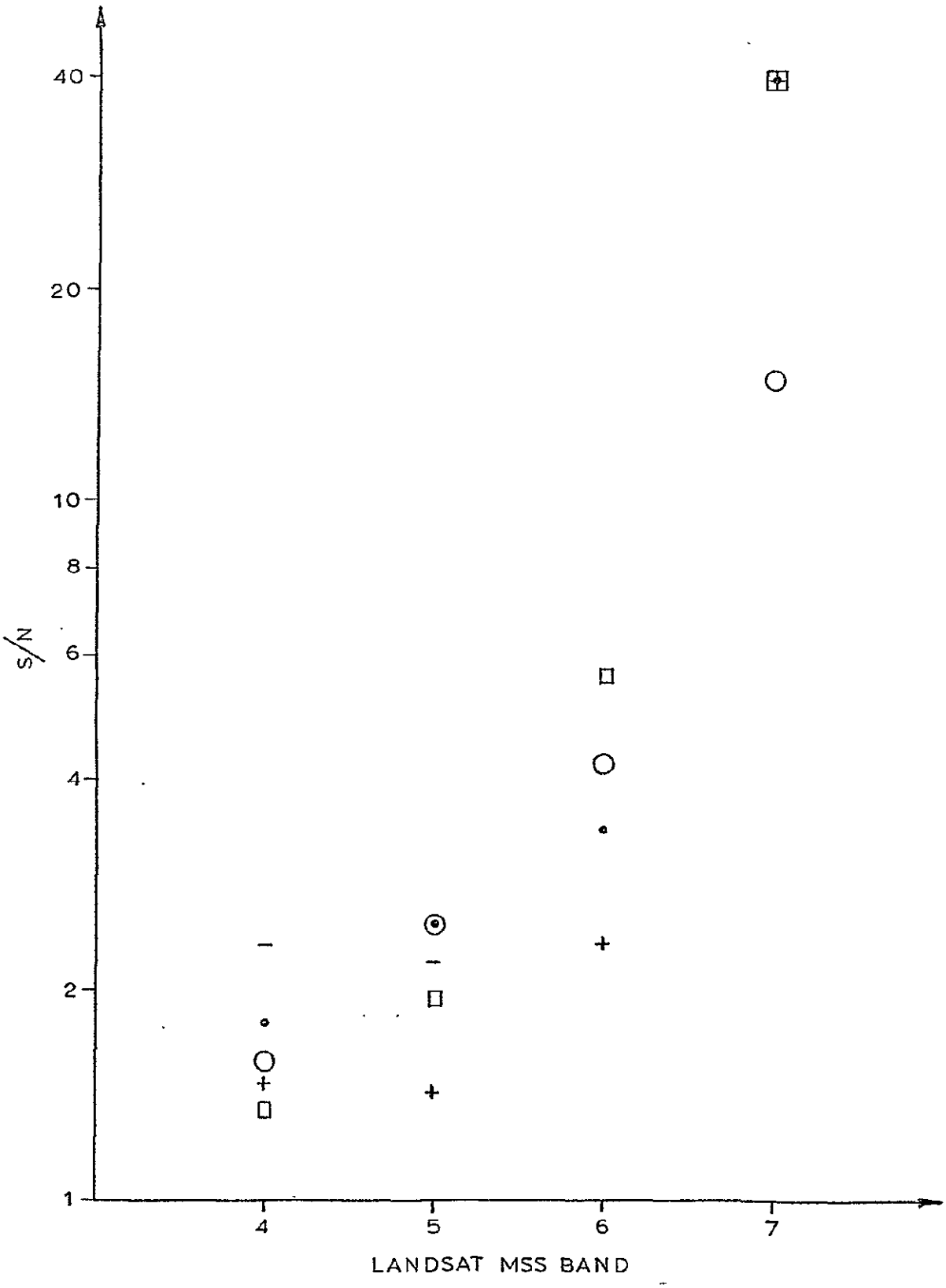

Fig. 9.3 - Signal to noise ratio (S/N) versus MSS band number for each of the five positively identified ships given in Table 9.1.

O Osco Sailor
. Aratika
□ Aramoana
\+ Arahanga (GMT 23 Dec 75)
\- Arahanga (GMT 22 Dec 75)

CHAPTER 10

MONITORING SOME ASPECTS OF NEW ZEALAND'S AGRICULTURAL PROGRAMME WITH LANDSAT : A PRELIMINARY REPORT

I L Thomas, M J McDonnell, P J Ellis,
A D Fowler, R C Child, C T Nankivell, and R S Mason

ABSTRACT

This preliminary report considers the initial results from the Physics and Engineering Laboratory satellite/aircraft/ground truth sub-stage sampling programme as applied to an agricultural investigation. The use of photographic colour composite and computerized parallelepiped supervised clustering techniques in the analysis of such multispectral data is outlined.

It is concluded that simultaneous satellite and/or aircraft coverage must be combined with ground truth data taken by a member of the analysis team over the ground control area for effective extension of such multispectral techniques. The selection of the correct time in the cropping season is mandatory to reduce some of the variations produced in the recorded spectral signatures by differing farming practices, soil types and structures, etc. For cereal crop differentation, this would appear to be between the time at which the crop reaches full (green) ear development and harvest.

From this preliminary analysis, it has proved possible to conclude that:-

(i) LANDSAT is able to map near sub-surface water patterns in well drained soils during the summer season.

(ii) Bare ground is readily identified on both LANDSAT photographic and digital imagery, as well as on aircraft photographic coverage. Areas too may be measured over extended regions using LANDSAT imagery.

(iii) The categories of Water, Urban areas, Forested regions, and crops possessing a high chlorophyll content (e.g. lucerne or alfalfa), together with Bare ground may all be readily identified through all seasons.

(iv) Cereal crops are difficult to detect in winter and spring imagery. More attention to summer delineation is necessary.

The most effective interpretative precedure is believed to consist of a human interpreter using a combination of:-

(a) colour prints composited from three MSS bands,
(b) the interpreter's background knowledge of applicable pattern and texture combined with relevant socio-economic factors, and
(c) multi-band computerized classification mapping.

Ideally, the interpreter should participate in gathering the ground truth in the analysis control area.

CONTENTS

10.1 INTRODUCTION

One of the basic cereal constituents of the New Zealand diet is wheat. The annual consumption is around 313,000 tonnes whilst production fluctuates in relation to price incentives, with importation sometimes becoming necessary: e.g. the 1972-3 yield was 376,111 tonnes whilst that for 1973-4 was 214,590 tonnes (source - New Zealand Official Yearbook, 1976). Consequently, monitoring and possible forecasting of national wheat yield is of importance both to the local diet and to the national balance of overseas funds. The overall aim of this study is to assess the applicability of LANDSAT data to such a monitoring programme and, at this stage, to pose questions that need to be answered as such an assessment programme proceeds.

The province of Canterbury accounts for much of the national cereal production. In 1972-3 it produced 69.7% of the total wheat, 58.9% of the total barley, and 50.5% of the total oats for New Zealand. Since early 1974 the Physics and Engineering Laboratory in conjunction with the Ministry of Agriculture and Fisheries, has been conducting a multistage sampling programme, to reinforce the LANDSAT results, around the township of Darfield (43.48°S, 172.11°E) in the central region of the province.

Over the province a variety of soil types are encountered. They are generally shallow, friable, free draining, and comparatively low in moisture content in summer. To sample a range of soils and climatic conditions a second sampling region closer to the coast has been studied since late 1976. This is sited between the township of Leeston (43.77°S, 172.30°E) and the Rakaia River (43.81°S, 172.19°E).

As will be discussed later, soil moisture not only influences the crops' spectral signature but also, with such soils as prevail in Canterbury, the life of that soil under wind erosion conditions.

Painter (1976) notes that, for the soils of Canterbury, if 1 mm of soil is removed from one hectare of a field the airborne soil load is between 10 and 15 tonnes. He cites a lifting of around 5 tonnes of topsoil per hectare off a monitored field in the course of the day of 26 November 1975. The application of LANDSAT to monitoring areas of bare gound is thus of relevance not only to the viability of cereal cropping but also to the whole agricultural sector in this shallow (15-25 cm) topsoil region.

If one assumes the climatic conditions for Christchurch (provincial capital of Canterbury) to be "typical" for the cropping province, then inspection of table 10.1 leads to the conclusion that this cropping area, during 1975, had a low to medium rainfall, an average amount of sunshine and a slightly higher than usual number of "windy" days. (On 1 August 1975, the Canterbury Plains were subjected to violent windstorm gusts which ranged between 100 and 170 km/hour.)

With such dry shallow soils the availability of sub-surface water becomes important when considering spectral signatures and erosion potential. LANDSAT, with its 185 * 185 km synoptic overview in one image, permits the mapping of subterranean water courses; via the spectral signatures of the less moisture-stressed vegetation atop the water; over areas far too large to consider when using aircraft imagery. This point is made further when discussing the summer image of the Darfield area.

Computerized examination of LANDSAT data is the most desirable manner in which such large areas ($3.4 * 10^4$ km^2) and volumes of data ($3.1 * 10^7$ video data radiance values per image for LANDSAT 1, 2) can be scanned to monitor given targets. This is accomplished through the target's spectral signature - the four radiance values reflected from the crop to the spacecraft after irradiance by the sun and sky. As mentioned previously, such a spectral signature is influenced by crop stresses. These, in part, can be traced back to the underlying soil. (Other factors, such as spraying/fertilizer programmes, sheep or cattle grazing history and, in the Canterbury plains, the deposition of shingle braiding during the formation of the fields, etc, can all influence the resultant spectral signature.)

The features in the plant leading to the formation of a spectral signature are summarized later in this report as are the various soil types prevailing in the test areas.

The more specific aims then, of this project are as follows:

(i) an investigation of the feasibility of using LANDSAT data for the mapping of subsurface moisture over the Canterbury Plains,

(ii) the location and assessment of the area covered by bare ground in the Darfield and Leeston test areas,

(iii) the use of LANDSAT to locate, recognize and assess the area of wheat crops in the two test areas,

(iv) an investigation of the factors that produce variations in spectral signatures for the targets under study in the two test areas, and

(v) the formulation of questions that need to be considered as the study programme proceeds.

10.2 THE CROP SPECTRAL REFLECTANCE AND THE RECORDED MSS RADIANCES A SUMMARY

The LANDSAT 1, 2 Multi-Spectral Scanner (MSS) detects reflected solar irradiance in four bands MSS 4 (500-600 nm) MSS 5 (600-700 nm) MSS 6 (700-800 nm) and MSS 7 (800-1100 nm). Such irradiance is reflected by a ground target possessing a characteristic wavelength dependent reflectance R (λ). The

Table 10.1 Comparison of 1975 Christchurch (Canterbury province) climatic conditions with others around New Zealand (Source - New Zealand Official Yearbook, 1976) (maxima and minima indicated in brackets)

Site	Rainfall (mm)	Bright Sunshine (hours)	Mean Temperature (°C)	Average number of days with winds of 65 km/hour or more (No. of years that were used in average in brackets)
Alexandra	337 (min)	2025	11.0	-
Blenheim	758	2528 (max)	13.4	38 (30)
Christchurch	881	2038	12.2	54 (29)
Hamilton	1306	1981	13.9	22 (min) (8)
Hokitika	2999	1737	11.9	34 (8)
Invercargill	1108	1462 (min)	10.1	98 (27)
Milford	7792 (max)	-	10.6	-
Wellington	1372	2009	13.0	188 (max) (8)

product of the solar irradiance and the crop's reflectance is the radiance detected by the MSS over that target. In general the reflectance for a cereal crop type target is as portrayed in figure 10.1.

Various authors have discussed the spectral reflectance characteristics of plants under differing conditions. A summary of general findings is appended to this chapter (Appendix 10.3) and further discussion is provided by Scott et al (1968), Gates (1970), Myers et al (1970), Myers et al (1975) and the references quoted therein.

Summarising these results for use in this analysis we have that:

MSS 4 monitors the integrated chlorophyll, xanthophyll, carotene, and anthocyanin pigment levels

MSS 5 monitors the chlorophyll status in the plant

MSS 6 monitors the "yellowing" of leaf maturation/deterioration status

MSS 7 gauges the Leaf Area Index and hence allows the crop leaf status to be assessed.

Band ratioing has been advocated for the removal of atmospheric effects and the reduction of sun angle influences in the data. In this project the concept of band ratioing is felt

to be more useful in being able to include a spectral reflectance curve "shape" factor within the standard four band parallelepiped clustering procedures. This will be discussed later when considering the computer analysis but suffice to mention here that one extra gate has been added to the above four that is based on a spectral shape factor defined by the product of the ratios thus:

$$\frac{\text{MSS 5}}{\text{MSS 4}} * \frac{\text{MSS 6}}{\text{MSS 4}} * \frac{\text{MSS 7}}{\text{MSS 4}} .$$

(The ratioed values are the mean spectral signature values for each band for the target. As MSS 4 is more "stable" over the variety of leaf "yellowing" and Leaf Area Index type situations than the other bands it is a useful reference for band ratio comparisons.)

In addition to the above vegetation derived influences, factors such as the sun elevation angle, spectrally dependent atmospheric extinction conditions, terrain slope and aspect etc can all further influence the general spectral signature. Admittedly, for classification over a "flat" agricultural area using one scene, and over an area having sensibly the same atmospheric conditions, these considerations are reduced.

As will be noted when discussing the data base for this preliminary study there are five main types of wheat grown in the two areas under test. These main varieties: Arawa, Kopara, Karamu, Aotea, and Hilgendorf; extend over the whole Canterbury province. Of these varieties, only the Karamu is sown as a spring wheat with the others being sown in late autumn/early winter depending on ground moisture. Initial growth of the Karamu is rapid and some two-months after planting it seems general that the spring wheat ground cover is equivalent to that of the autumn sown wheat. (In appendix 10.3 a brief summary is presented of the development of the more common wheat types and their possible expected similarity/diversity in spectral signature.)

10.3 DATA - ACQUISITION AND BASE

The first LANDSAT scene of New Zealand forwarded to DSIR was 1502-21362 of the Canterbury region recorded by LANDSAT 1 on 7 December 1973 (GMT). Since that time, two further cloud free images of the Canterbury test site have been recorded by LANDSAT 2 (2192-21265 on 2 August 1975 (GMT) and 2282-21254 on 31 October 1975 (GMT)).

Following the construction of the Physics and Engineering Laboratory multi-spectral camera described elsewhere in this report, co-ordinated satellite/aircraft coverage has been striven for since early 1975 to the present. Such multistage sampling has been reinforced by ground measurements of solar and global irradiance in the MSS wavelength bands used by the sensors in the aircraft and satellite.

It was rapidly recognised that timely ground truth data was important to this programme. Staff that were to subsequently analyse the satellite and aircraft imagery visited the contributing farmers and completed the ground truth returns, immediately following the ground irradiance measurements.

Joint satellite/aircraft coverage was obtained for the 2 August and 31 October 1975 scenes. Due to processing difficulties the 31 October coverage was reflown on 14 November 1975 (NZST).

In early 1977 it was realized that combined satellite/aircraft coverage was unlikely during the 1976/7 cropping season. Accordingly a retrospective survey for the October/November 1975 crop was commenced. The original ground truth base was expanded to include more farms in Darfield and to include those that recently had begun contributing in the Leeston area. A total of some 400 fields in the Darfield region and approximately 250 fields in the Leeston area were included in the retrospective survey. In table 10.2 a summary of the ground truth statistics for the wheat crop for this retrospective survey is presented. No allowance has been made for the variation in field size between various farms. Most fields were between 2 and 10 hectares - somewhat different to field sizes in Australia and U.S.A.! Another difference is the variety in cropping carried out in close proximity on the Canterbury Plains. Barley, Oats, Wheat, Lucerne, Peas, Grass for seed, and Grass for sheep/cattle grazing will often all be included in one farmer's holding which in total may extend over only 50 hectares. Thus, a wide variety of spectral signatures may be encountered over a small area - due to cropping and farm management practices alone.

One reason for confining this preliminary study to wheat is that of the available imagery, the best satellite/aircraft and ground data is of the 1975 spring period. At this time the autumn wheat is approximately 30 cm high, as is the spring wheat, whilst the spring sown barley and oats is up to 10 cm high. More distinct signatures are thus expected for the wheat targets than for the other cereal crops. The present study excludes the 2 August 1975 scene.

When discussing moisture stress influences upon the crop, and the erosion potential of the soil, some knowledge of the soils underlying the test area crops is useful. In Table 10.2 the frequency of crop sampling in the two test areas has been broken down according to the underlying soil type. In Appendix 10.1, the basic characteristics of these soils are presented. The data has been extracted from the Soil Bureau Bulletin No 27 (1968) "General Survey of the Soils of South Island, New Zealand". The characteristics of shallow well-drained dry soils on top of alpine derived alluvial deposits are evident throughout the soil categories sampled in the two test areas. The "gley soils" (type nos. 89, 89a) tend to hold more water and organic material than the "yellow grey earths" (type nos. 13, 14, 14a) or "recent soils" (type nos. 95, 95a, 96a, 96c).

Table 10.2 Retrospective wheat crop ground truth inventory for October/November 1975 for the Darfield and Leeston test sites. The soil types are those from DSIR Soil Bureau Bulletin No 27, 1968. Numbers of fields are indicated in each crop class. No allowance is made for variations in field size.

Darfield October/November 1975

wheat / Soil type	Hilgendorf	Arawa	Aotea	Kopara	Karamu	Lucerne (Alfalfa)	Bare Ground	No. of farmers
13				11	7	2	4	4
14	3	4		13	9	11	26	12
14a	5			3	2	5	9	5
95a	2					1	1	1
96a + 96c				5	3		1	2
Totals	10	4	0	32	21	19	41	24

Leeston October/November 1975

wheat / Soil type	Hilgendorf	Arawa	Aotea	Kopara	Karamu	Lucerne (Alfalfa)	Bare Ground	No. of farmers
89				10		4	7	4
89a				3				1
95				9		1		1
96a			4	10		3	1	5
96c			3	4		7	4	2
Totals	0	0	7	36	0	15	12	13

The nutrient status is noted to be greater around the Leeston area, as is the general moisture retention. Leeston also supports a more intensive/extensive cropping programme than the Darfield area. Through both districts the cultivated areas are susceptible to wind erosion.

10.4 DATA PROCESSING

A variety of processing techniques were used on the LANDSAT data. This section details these techniques together with those used in preparing the final aircraft imagery and collectively presenting the ground truth data.

10.4.1 Figure 10.2, Part of LANDSAT scene no. 1502-21362 (P J Ellis)

This segment of the complete scene was processed on the HP 21MX computer at the Commonwealth Scientific and Industrial Research Organization Division of Mineral Physics in Sydney, Australia. The video levels for each band, for this segment, were linearly stretched such that the complete 0-127 level range was utilized over the segment. The data was then written by a "Photowrite" machine to four black and white negatives and recombined using the Physics and Engineering Laboratory colour additive viewer. The "standard" colour balance of:

MSS band 4 negative being printed through a blue filter,
MSS band 5 negative being printed through a green filter,
and MSS band 7 negative being printed through a red filter

was used. This applied to all the colour composite products referenced in this chapter.

10.4.2 Figure 10.4, Part of the aircraft multispectral coverage of the Darfield test site recorded on 14 November 1975. (A D Fowler, R S Mason, C T Nankivell)

Colour composite prints were prepared of the individual 70 mm black and white negative transparencies of each of the MSS band scenes using the standard colour balances for negatives (see above) on the Physics and Engineering Laboratory International Imaging Systems Colour Additive Viewer. A section of this coverage was then mosaiced together and rephotographed for inclusion as a sample of the results from the aerial substage sampling programme. The area covered is just to the north of the Darfield township and includes the Selwyn Forest (to the western edge) and the Waimakariri River in the north eastern corner.

10.4.3 Figure 10.5, Ground truth map for the Darfield region for the 1975 October/November retrospective survey (R C Child)

In April 1977 a field party visited selected farms in the Darfield test area to obtain details for the preparation of a ground truth data base. This extended the data base acquired in November 1975. As the requirement was for the state of the farms in October/November 1975, the information was based on individual farmers' recollection or records of what crop types were in the fields during the 1975 cropping season. The farm plans for grass and clover seed certification had unfortunately not been accurately produced to scale and this subsequently led to difficulties. These plans were already referenced to identify fields and the reference system was adopted for the crop survey. Information on the type of crop growing in the field, the stage of development and any other relevant data was recorded. This information was collated and used to produce a map of the area.

The map was compiled on existing printed topographic maps at 1:25,000 scale. Discrepancies between the field delineation on the farm maps and the topographic maps were corrected with reference to multi spectral airborne photographs taken of the test area. Colour coding of the map crop data was by 'stick-on' foils. The map was then photographed for reproduction in this report.

Comparison of this map with LANDSAT data and the airborne multi spectral photomosaic indicated some discrepancies.

The specifications used to produce the map were that the type of crop would be indicated on the map irrespective of the state of growth. This would ensure that subsequent surveys produce a 'follow on' of the crop development.

Therefore some fields that to the remote sensors looked like bare ground were shown on the map as a crop type if the crop had been planted. The colours adopted for crop coding on the map would be associated with the physical condition of the field, e.g. blue for bare ground and root crops.

The colour coding used on the map is:-

1. Blue for bare ground and associated crop types
   - (a) dark blue for recently worked ground
   - (b) medium blue for potatoes and other root crops
   - (c) light blue for peas and other legumes

2. Green for grass and pasture from heavily grazed to 20-25 cm high seed crop, and associated types
   - (a) light green for grazed pasture
   - (b) medium green for seed grass
   - (c) medium dark green for clover
   - (d) dark green for lucerne

3. Plantations of established exotic trees are blue-green with a black tree symbol on the base map

4. Yellow-orange for cereal crops
   - (a) light orange for spring wheat
   - (b) darker orange for autumn wheat
   - (c) yellow-orange for barley
   - (d) yellow for oats

5 Other crops have a variety of colours
   - (a) purple for fodder beet
   - (b) dark brown for lupins
   - (c) light brown for kale
   - (d) olive green for linseed

Some small discrepancies between the crop type information on the map and the satellite/aircraft data can be attributed to a few doubtful recollections by farmers during this retrospective ground truth survey. The main cause for dissimilarity within either the satellite or aircraft imagery for ostensibly the same crop in the field is the wide variation in state of that crop. The difficulty in obtaining accurate state of crop data for the given LANDSAT overpass increases with time lag from the overpass.

10.4.4 Figure 10.6,Part of LANDSAT scene no.2282-21254 (P J Ellis)

During the visit by one of the authors to the EROS Data Center at Sioux Falls the above scene was raised on the General Electric Image 100 machine. A standard colour composite was produced on the output colour monitor and photographed onto 35 mm slide film. This positive transparency was then enlarged and printed, using the Ciba process at Physics and Engineering Laboratory. No video data manipulations took place in the production of this image.

10.4.5 Figure 10.7,Thematic map for part of the LANDSAT scene no. 2282-21254 (I L Thomas)

A human interpreter is limited by the three types of colour sensitive cones in the human retina to the simultaneous analysis of only three channels of MSS data. Each of the available colours may be made up of the three basic retinal colours; blue, green or red. (Photographic colour material utilizes this very aspect in its three dye layer response to incoming coloured irradiance.)

In the previous photographic processing we have rejected one of the data channels available to us, MSS 6, for this reason, and the fact that for an agricultural target, the MSS 6 content can largely be included in MSS channels 5 and 7 (see Fig. 10.1).

A photographic colour print can contain a range of hues and colours that approaches the human physiological data handling capacity. (For photographic positive print material a practical resolution of 40 line pairs per millimetre is common. Thus one 10 * 8 inch print can contain approximately $8 * 10^7$ elements of information (c.f. the number of picture elements in one LANDSAT 2 scene - approximately $8 * 10^6$).)

For both these reasons computerized classification procedures can aid the human interpreter. The human can call upon information currently not available to the machine for use in the combined decision making process. These data items include: field shape, edge continuity and regularity, field texture, geomorphological texture in the region, rain shadow proximity, social or economic influences in the region; and even allowance for scanner striping influences can be made. This suitably weighted data is currently not available in the computer file accessed by this study.

The final analysis must therefore be compiled by the human interpreter aided, but not superseded, by the classification computer. (For a further discussion, see Hempenius, 1974).

In Figure 10.7, the results of using five dimensional "parallelepiped" histogram supervised clustering on a section of the scene 2282-21254 data for the Darfield region are presented. The colour coding indicates those areas confirmed by the ground truth. (This will be discussed further in the Analysis section.)

This thematic map was produced in the following way. (See also chapter 6.)

Using 57 level single MSS band coded printouts for part of a scene covering a known ground target, bounds were selected for the variation in CCT levels for that target over the four MSS bands. These were then fed as data into the thematic mapping package and used as the upper and lower bounds for a four dimensional parallelepiped (supervised) clustering process applied to a small test area covering only the environs of the known ground target. The programme then determined the mean and standard deviation for those picture elements falling within this four dimensional parallelepiped and output them as shown in Table 10.4, for Kopara wheat.

A revised signature was then calculated by the IBM 370/168 computer to be, for each band, the mean plus/minus one standard deviation (rounded up/down to the next CCT level). This was chosen on the basis that some 65% of the target pixels would be included within these limits. These revised limits were now used as the new parallelepiped bounds and the programme run again for the full test region (e.g. Darfield). During this final run the spectral shape factor option was included. The CCT radiance level scaling tolerance of ±1 level was applied to the mean and this led to the upper and lower limits for the fifth shape factor gate. It was found for each target from the product ratio relation

$$\frac{\text{MSS 5}}{\text{MSS 4}} * \frac{\text{MSS 6}}{\text{MSS 4}} * \frac{\text{MSS 7}}{\text{MSS 4}} .$$

(This product approach was found to be superior to the inclusion of three extra gates based on the individual ratios

$$\frac{\text{MSS 5}}{\text{MSS 4}} , \quad \frac{\text{MSS 6}}{\text{MSS 4}} , \quad \frac{\text{MSS 7}}{\text{MSS 4}} .$$

As outlined in chapter 6 further investigations into more effective classification techniques are continuing.)

If a picture element passed through all the selection gates it was classified. Such pixels formed the data base for the occurrence statistics leading to the mean and standard deviation calculations. For the targets considered here: Bare Ground, Kopara Wheat, Karamu Wheat, Hilgendorf Wheat, Lucerne, Water, Urban and Forest, the spectral signature occurrence statistics are presented in Appendix 10.2.

SPECTRAL FREQUENCY DISTRIBUTION FOR KOPARA WHT
SCENE ID: 2282-2125400 STRIP NO.: 2 OF 4
SCAN LINES: 1840 - 1851
PIXELS: 575 - 615 (WEST TO EAST)

BAND 4		BAND 5		BAND 6		BAND 7	
14.00:	3	13.00:	6	45.00:	0	24.00:	1
15.00:	10	14.00:	6	46.00:	1	25.00:	1
16.00:	5	15.00:	5	47.00:	2	26.00:	4
17.00:	2	16.00:	0	48.00:	1	27.00:	4
18.00:	2	17.00:	0	49.00:	9	28.00:	8
0.00:	0	18.00:	3	50.00:	3	29.00:	4
0.00:	0	19.00:	1	51.00:	2	0.00:	0
0.00:	0	20.00:	1	52.00:	3	0.00:	0
0.00:	0	0.00:	0	53.00:	2	0.00:	0

SPECTRAL SIGNATURE STATISTICS

MEAN FOR BAND 4 IS 15.545 WITH A STANDARD DEVIATION OF 1.143
MEAN FOR BAND 5 IS 15.000 WITH A STANDARD DEVIATION OF 2.160
MEAN FOR BAND 6 IS 49.681 WITH A STANDARD DEVIATION OF 1.912
MEAN FOR BAND 7 IS 27.318 WITH A STANDARD DEVIATION OF 1.358

BASED ON THE ABOVE MEAN AND STANDARD DEVIATION, REVISED SPECTRAL SIGNATURES FOLLOW
(THESE ARE ROUNDED (MEAN +/- ONE STANDARD DEVIATION) CCT LEVELS)
FOR BAND 4 REVISED CCT LEVEL GATE IS FROM 14 TO 17
FOR BAND 5 REVISED CCT LEVEL GATE IS FROM 12 TO 19
FOR BAND 6 REVISED CCT LEVEL GATE IS FROM 47 TO 52
FOR BAND 7 REVISED CCT LEVEL GATE IS FROM 25 TO 29

Table 10.4 Spectral frequency distribution for Kopara Wheat control fields in part of the Darfield test area together with the calculated revised spectral signatures. (Derived from four dimensional parallelepiped histogram supervised clustering.)

The areas calculated as part of this thematic mapping package on the IBM 370/168 were deduced from the number of picture elements that passed all the selection criteria on the assumption that each represented a ground area of 56 m * 79 m (picture element area at a nominal satellite altitude of 920 km.)

In this way, a completely non-qualitative and repeatable selection of spectral signatures is possible.

10.4.6 Bare Ground area measurement with rectified imagery (M J McDonnell)

This section describes an attempt to measure the percentage of bare ground in part of our Darfield test site.

Computing reported in this section was carried out on the HP 2100 computer system (Chapter 7), whereas the other computing reported in this chapter was carried out on the IBM 370/168 (Chapter 6).

The first step was to use LANDSAT scene 2282-21254 taken on 31 October 1975 (GMT) to prepare a rectified image (see Chapter 8) covering a 16,000 x 14,000 yd (about 9 x 8 mile) area around Darfield. (This rectified image was in the Transverse Mercator projection used in New Zealand "inch to the mile" maps, and consequently imperial units are used in this section.) The top left hand corner of the image was at 573,000 yds N, 548,000 yds E, and the sampling distance between rows and columns was chosen to be 50 yds. This image included the farms of our Darfield test site for which we had retrospective ground truth. In addition, aircraft imagery of much of the area had been taken on 14 November 1975.

It should be noted that the above rectification was accomplished using bilinear interpolation (see Chapter 8) which had the effect of smoothing the data and improving classification accuracy. Cubic interpolation on the other hand is more affected by noisy data and would have led to misclassifications.

The main advantage of using the rectified image was due to the increased sampling rate. This increased the number of pixels in each field, thus making it much easier for our later processing to distinguish between fields and small potentially misclassified areas.

Lineprinter printouts were then produced which included the test sites and for each band displayed the radiance of each pixel as a unique coded character on a 0 to 127 overprinting scale. These printouts were then analysed with reference to the ground truth data and the aircraft imagery. As field boundaries were shown on the map it was easy to find the position of any field on the rectified printouts from the corresponding map co-ordinates of its centre. Using these printouts, a range of radiance values for each band was determined for those pixels near the centre of

each field which was verified as being bare ground from both the ground truth and the aircraft imagery. Only central pixels were used to reduce the effect of neighbouring fields. It soon became clear that the signature range for bare ground derived in this way included a number of fields planted with potatoes, barley, or peas. At the time of the satellite overpass, these fields were bare, or appeared bare, because not enough of the crop was showing to significantly alter the signature. Consequently the signature range shown in Table 10.5 for bare ground is interpreted as including bare ground, and emerging crops for which the bare ground contribution to the signature dominated that of the crop. The signature range in Table 10.5 did not include river bed or heavily grazed grass, both of which were distinguishable from bare ground. The stage of growth at which a crop moves out of the signature range in Table 10.5 has not been precisely defined. This does not lead to serious classification problems, however, as the time taken for a crop to change from being apparently bare ground, and to move out of the signature range in Table 10.5 is short (e.g. two weeks).

The spectral signature range derived as above correctly classified the central portions of all bare fields in our test site. No anomalous fields were found, although several small areas (typically a couple of pixels each) incorrectly appeared to be bare. This was usually caused by the misclassification of pixels at the boundary between two fields. If the signature range in Table 10.5 had been widened slightly, it would still have classified the bare fields correctly but the number of pixels incorrectly classifed as bare would have increased considerably.

The next step was to measure the area of bare ground within a specified rectangular subimage of the rectified image. This was achieved by first assigning a value of 1 or 0 to each pixel depending on whether or not its spectral signature fell within the range in Table 10.5. Next, the area count was carried out by summing the contributions of each individual pixel to the total area of bare ground. The contribution of each pixel depended upon whether or not that pixel had been classified as bare ground, and the number of neighbouring pixels (out of the eight nearest neighbours) that had also been classified as bare ground. This contribution was assigned to each pixel according to Table 10.6. The contribution values given in this table were chosen empirically and have proven to be satisfactory. In general these coefficients depend upon the ratio of the size of a pixel to the average field size and have the effect of significantly reducing localised misclassifications.

The total area of bare ground is then obtained by multiplying the above area count by the area of a pixel and a scaling factor. A scaling factor is necessary because only the central portion of fields has been counted by the above procedure. The size of the scaling factor required depends upon the spectral signature range, the coefficients in Table 10.6, the sampling rate in the rectified image, and the distribution of field sizes in the region under study. The scaling factor is determined by dividing the area of bare ground known to be in a test area by the

area determined as above from the rectified LANDSAT image. This scaling factor can then be used in measuring the bare ground area in much larger regions so long as the same spectral signature applies, and the distribution of field sizes in the test area is similar to that over the entire region.

Using the above area measurement technique and a scaling factor of 1.42, the area of bare ground in two test areas was estimated to be 128 and 215 acres, which compares favourably with the known areas of 131 and 210 acres respectively. These areas were determined from careful measurement of our scaled aircraft imagery. The same scaling factor was then used to estimate the area of bare ground in a 10,000 yd square area with its North-West corner at 570,000 yds N, 550,000 yds S, and including the Selwyn forest and part of the Waimakariri river bed. The estimated area was 2256 acres which is 10.9% of the total area of 20700 acres. We are satisfied, from the aircraft imagery and corresponding LANDSAT printouts, that the signature used was valid over this full area. As ground truth is not available for the full area we are unable to compare our estimate of 2256 acres with the true area. Nevertheless, we are confident that the error in our figure is less than 10%.

The procedure outlined in this section can be used to measure the area of bare ground or any other desired classification (e.g. a crop or forest species) over an entire region, provided that a suitable spectral signature range is available. More work needs to be done to establish over how wide a region a spectral signature range for bare ground is applicable. Insufficient bare ground areas were included within our Leeston ground truth to determine whether the same spectral signature range was applicable in this region.

Table 10.5 LANDSAT Spectral signature range for bare ground

MSS band	4	5	6	7
CCT radiance levels	22-29	28-40	35-55	14-24

10.5 RESULTS AND DISCUSSION OF INDIVIDUAL INVESTIGATIONS

As outlined in the Introduction there are four major investigations being carried out as part of this preliminary study. The results from each are to be discussed in turn.

It rapidly became apparent that the lack of confirmatory multispectral aircraft coverage of the Leeston test area

Table 10.6 Average fraction of a pixel which is bare ground as a function of whether or not the pixel has been classified as bare ground, and the number of its nearest neighbours (from 0 to 8) which have been classified as bare ground.

Number of neighbours classified as bare ground	0	1	2	3	4	5	6	7	8
Pixel bare ground	0.0	0.1	0.6	0.8	0.9	1.0	1.0	1.0	1.0
Pixel not bare ground	0.0	0.0	0.0	0.2	0.5	0.8	1.0	1.0	1.0

reduced the applicability of the retrospective ground truth data. Such supporting photography would have helped to explain some of the wide variations detected in the spectral signatures processed by the computer of this area for identical crop types.

Consequently the following comments are all restricted to the Darfield test area.

10.5.1 Mapping sub-surface moisture

Subterranean moisture will retard the drying out of surface vegetation. For a given vegetation class then, referring to figure 10.2, the chlorophyll absorption band in MSS 5 will be less pronounced for the drier vegetation. The spectral reflectance in MSS channels 6 and 7 will increase for drier vegetation (see Appendix 10.3).

Let us now consider how an increased target reflectance level is portrayed on the final colour composite product. For a given MSS channel an increased reflectance is recorded as an increased radiance level on the computer compatible tape (CCT) product and as an increase in density on the photographic negative product. (That is, low radiance levels are represented by low density regions on the photographic negative.) When this photographic negative is printed, as in the colour additive viewer, increased fluxes of light are passed by the low photographic density (low target reflectance) regions onto the photographic positive print material. Consequently a high photographic density in the representative colour for that MSS channel signifies a low target radiance being recorded by the sensor. This concept is referred to here as "inverse reflectance" and these values are recorded on the final colour composite print.

In Table 10.7 "inverse reflectances" for a variety of ground targets are given on an arbitrary scale of 0 to 5. A low target reflectance is thus portrayed as having a high inverse reflectance signifying a high density, in that band, on the colour composite print. To derive arbitrary reflectance levels the tabulated "inverse reflectance" value should be subtracted from 5. (Another approach to this derivation of inverse reflectances is to consider the photographic colour wheel and how the different impressed light fluxes appear when transposed in the final print.)

On the basis of the foregoing and assuming that the same varied cropping pattern exists throughout the sub-image portrayed as Fig. 10.2, the morphology of subterranean moisture is easily mapped in the summer scene. The "moist" vegetation will display increased chlorophyll absorption in MSS 5 and a higher leaf area index in MSS 7, due to thicker, more turgid leaves, than will the "drier" vegetation. Consequently red/brown vegetated tracks are taken to be indicative of subsurface water with blue/orange/brown tracts being indicative of the drier areas. Applying this criterion to Fig. 10.2 yields the interpretative map of Fig. 10.3.

The assumption that the same varied cropping pattern persists over both "moist" and "dry" areas is not strictly valid as farmers will tend to utilize both areas to the full by selecting crops that profit from the subsurface conditions. This revised cropping pattern will reinforce the patterns based on a more uniform varied cropping practice.

As mentioned earlier, the Canterbury Plains are subjected to substantial wind erosion. Fertile topsoil may be deposited in certain places over the Plains, dictated by wind patterns and topography. Before accepting the sub-surface moisture patterns suggested here, allowance must be made for such wind blown soil accretion as it too will influence the vegetation growth sensed by the spacecraft.

The sub-surface moisture patterns deduced here from LANDSAT imagery have been compared with groundwater profiles taken over the same region of the Canterbury Plains (Donaldson, 1977, personal communication). Good agreement has been found for the plains region shown in Figs. 10.2 and 10.3 and further work using LANDSAT in this field will be pursued.

This application of LANDSAT data is well-suited by the light soils atop drained alluvial gravels that characterise the Canterbury Plains. Summer imagery (e.g. Fig. 10.2) is the most suitable for detecting such variations in moisture stress induced in the covering vegetation.

10.5.2 Location and area assessment of bare ground regions

Bare ground is one of the easier targets to reliably identify. An inspection of Figs. 10.2, 10.4, 10.6, 10.7, and 10.8 confirms this. As discussed previously, bare ground is expected to show as blue, if the standard colour balance is used in composite preparation.

Table 10.7 Expected "inverse reflectance" contributions to the colour composite positive print for various ground targets. (The "inverse reflectance" is defined such that a low target reflectance in a MSS band produces a low density on the photographic negative for that band and hence a high density on the positive product. In short, a low target reflectance is revealed as a high signal on the positive print product; that is, as a high "inverse reflectance".) (Values given on an arbitrary scale of 0 to 5.)

Target	MSS 4 (yellow)	MSS 5 (magenta)	MSS 7 (cyan)	Composite colour (very approx.)
Deep Water	3	4	5	dark blue
Shallow Water	2	3	5	blue
Forest	4	4	2	brown
Bare ground	1	1	3	blue
Low dry stubble (e.g. grazed grass)	2	2	2	blue/orange
"Dry" vegetation (e.g. ripe wheat)	3	3	2	orange/brown
"Moist" vegetation (e.g. lucerne)	4	4	1	red/brown

In the "Data Processing" part of this chapter, a technique has been presented for measuring the area of bare ground in a target region using rectified imagery prepared on our HP 2100 computer.

The thematic mapping techniques discussed above led to the mapping portrayed as Fig. 10.7.

10.5.3 Location and area assessment of wheat crops

A more extensive set of ground truth data limited this preliminary analysis to the spring 1975 imagery. A similar computerized analysis was however conducted for the summer 1973 image and the results are presented without ground truth for superficial comparison only.

An inspection of Fig. 10.4 soon permitted various ground targets to be located and the variety in spectral signatures to be initially appriased.

Applying the data presented in Table 10.7 allows the following targets to be identified:

Shallow water	-	blue
Forest	-	brown
Bare ground	-	blue
Some thin ground cover (e.g. grass just surfacing)	-	green
Grazed grass or cut crop	-	light blue to light orange (closely to lightly grazed)
Long grass/lucerne	-	red
Wheat	-	russet brown/red

These categories are rather subjective and reference to the ground truth map (Fig. 10.5) should be made. With the aid of the ground truth map the categories of : bare ground with peas showing, Hilgendorf wheat, Kopara wheat, Karamu wheat, and Zephyr barley can often be distinguished on this aircraft derived photographic product. However, the variation in spectral signature within the fields is also extremely evident and this makes machine classification difficult. Differences in farming practice, soil moisture, soil type, soil nutrient level, time of sowing, ploughing patterns, fertiliser/spraying history, alluvial braiding in the sub-soil, windblown soil accretion/depletion patterns: all lead to variations in the resultant spectral signature. The trained human interpreter here has the (integrating) advantage over the (differentiating) machine.

Turning now to Fig. 10.6, recorded some two weeks previously, the need for ground truth to be acquired as close as possible to satellite overpass/aircraft overflight time is immediately evident when this figure is compared with Fig.10.4. (Compare the state of ploughing at the north western corner of the Selwyn Forest, other bare ground areas, and grazing patterns, between the two figures.)

On viewing Fig. 10.6 alongside the ground truth map, Fig.10.5, the classes of Kopara, Karamu and Hilgendorf wheats may be distinguished only in places. The Karamu is a spring sown wheat and it may be deduced that some paddocks have been sown much closer to overpass time than others. Again the human interpreter integrates over some variations in spectral signature in performing his crop classification.

Turning now to the machine classified thematic map for the spring scene (Fig. 10.7), it is immediately evident that the variety of spectral signatures for each field of a particular

target does not allow a tight classification to be made for the wheat crop on the basis of this spring imagery. If instead of requesting a classification for each of the three wheat types sought in Fig. 10.7, a blanket "all wheats" category was sought, a range of other targets would also be included. The spectral signatures for the wheat types studied in Fig. 10.7 and shown in Appendix 10.2, would also include some grasses and stages of the lucerne crop as well. This spring imagery can thus not support either tight or general machine classification of the wheat crop. Rather a combined human/machine interpretation approach is needed.

It is noted that often lucerne and lush grass fields are classified together as are urban and bare ground targets. The former may be resolved by a judicious choice in the time of image acquisition. The latter could be resolved by subdividing the bare ground category into soils with different moisture contents. It is expected however that rural townships will approach, in spectral signature, some classes of bare ground due to their low population density as compared to a city target.

It is conceivable that some farmers may graze their autumn sown wheat over the winter period. This, combined with a range of planting times for the spring sown wheats, makes the usefulness of spring imagery somewhat dubious. However, it represents the best data base currently available to us.

In Fig. 10.7 only those fields that are confirmed by the ground truth data - which led to Fig. 10.5 - are colour shaded. Obviously by reference to the aircraft imagery (Fig. 10.4) the classification "success" rate could be improved. This however does rely on a human interpreter, being trained by the ground truth, extending his analysis area without check. Similarly Fig. 10.6 leads to increased confidence in the machine classification results. This type of "begging the question" analysis would be resolved were our ground truth data base increased. The areas where improved ground truth is needed are to the immediate north, north-east, and south-east of Darfield.

To ascribe a figure of merit to such a machine classification process Kalensky and Wightman (1976) define the mapping accuracy M_i of class i to be

$$M_i(\%) = \frac{N_i}{N_i + E_i} * 100$$

where N_i = number of correctly classified pixels in class i

and E_i = number of erroneous pixels in class i (those omitted completely plus those incorrectly classified)

The absence of an adequate ground truth data base did not permit the inclusion of such a mapping accuracy determination.

The data base was deficient for the following reasons:

(i) it was based on memory rather than actuality, due to its retrospective character,

(ii) two weeks separated the LANDSAT overpass and acceptable recording of airborne imagery, and

(iii) gaps existed in the ground truth mapping around Darfield leading to only moderate statistical sampling.

Similarly area measurements, whilst simple to compute, are meaningless except for major categories such as bare ground, forest, etc., using this spring, highly varied, data base.

Arising from this thematic mapping analysis, we may conclude:

(i) summer (close to harvest) imagery is necessary for cereal inventory studies

(ii) the ground spectrometer programme is vital to the reasoned development of spectral signature studies

(iii) the ground truth data base needs to be extended

(iv) simultaneous satellite/aircraft overpasses are needed of the training area

(v) the ground truth must be collected by a member of the analysis team as close to overpass/flight time as possible

(vi) such ground truth must include data on crop type, date of planting, crop status, spraying programme, etc.

The only available summer imagery is the first LANDSAT scene received in New Zealand (scene no. 1502-21362). Part of that scene is protrayed in Fig. 10.2. Ground truth is very limited for this scene. In Fig. 10.8 a thematic mapping of the Darfield area based on this scene is presented. (Note that the symbol "2" in this case represents all wheats, whilst in Fig. 10.7 it represented Kopara wheat.) Fig. 10.8 has also been derived by five dimensional histogram parallelepiped clustering. In the absence of detailed ground truth only a speculation as to the mapping accuracy is possible. However based on general knowledge that the Physics and Engineering Laboratory group have built up of the areas, the results encourage the pursuit of summer imagery for cereal differentiation.

10.5.4 Spectral signature variations in the test area

Aside from all the influences upon a spectral signature discussed previously, it has been noted that the outermost plants in a field protect the inner crop stands. This screening effect which can extend for some metre or two into the field will change the spectral characteristics of the edges. The extent of this change, with respect to the centre of the field, awaits the ground spectrometer programme.

For a variety of reasons, already discussed, we have limited our study to the one time frame (spring 1975) and the one area (Darfield). Nonetheless the diversity in farming practice, crop development, and influences such as alluvial braiding in the subsoil influencing relative crop growth across a field, etc, have made spectral signature determination, let alone comparisons, difficult.

Accordingly we must await summer imagery to complete this part of the study.

In appendix 10.2 the occurrence statistics are presented for the spectral signature groups used for the eight targets protrayed in Fig. 10.7.

10.6 CONCLUSIONS

Over the course of this preliminary study LANDSAT has demonstrated its applicability for providing rapid location data and, in some cases, ready area measurements for a restricted range of ground targets.

Ground targets, such as: water, forest, urban areas, bare ground and high chlorophyll content crops (e.g. lucerne), may be readily identified over a range of seasons. Small farming urban areas have like characteristics to surrounding bare ground targets.

It is believed that a judicious choice of phase in the crop maturation cycles is necessary to enable the location and area measurement of cereal crops to be accomplished. Further work utilizing the airborne multispectral camera and the ground spectrometer is currently planned.

LANDSAT has demonstrated its capability of mapping some areas of subsurface moisture within well drained soils, but again the correct choice of season (summer) is mandatory.

For the most meaningful results simultaneous ground truth data in the control area taken by the analysis staff must be combined with simultaneous satellite and/or aircraft coverage.

The aircraft programme has pointed out many of the reasons for the difficulties encountered in the computer classification of ground targets. Variations in time of planting, ploughing pattern fertilizer/spraying history, alluvial braiding in the sub soil, windblown soil accretion/depletion patterns, all lead to variations in the spectral signature for fields containing the same nominal crop.

The human interpreter using the photographic colour composite usually integrates over these spectral signature variations and currently his crop identification/location record is better than that of the computer. Further work is necessary on the computer recognition of signatures for the whole paddocks, including allowance for the above variations.

Currently, the human interpreter can usually recognize, in the spring scene, the three main wheat classes in the Darfield test area. The computer at the moment cannot equal this. Again analyses at different seasons may improve the automatic recognition and area assessment record.

The most powerful combination would thus seem to be the trained human interpreter using a colour composite prepared from the three MSS bands 4, 5 and 7; aided by his background knowledge of pattern recognition, textural trends etc; and further aided by the computer condensed classification map. This latter map would be based on all MSS channels together with a "shape" relation and other data manipulations that have a solid base in the crop spectral response.

At this time the Physics and Engineering Laboratory group is acquiring the human expertise needed for the above interpretative package and the computer software is being developed.

Many of the previously detailed influences that perturb the spectral signature diminish in importance as crop maturity approaches and maximum ground cover is combined with crop nominal uniformity. Consequently the best time for intra-cereal crop differentation studies would thus appear to be from just before the time the crop reaches its full (green) ear development to the time it is harvested. For inter-crop differentiation the best time is suggested as being when the earlier maturing crop is entering the above "green-ear-development-to-harvest" phase. Further combined satellite/aircraft/ground truth/spectrometer work is advocated during the forthcoming New Zealand summer months.

REFERENCES

Coles, G D, Wrigley, C W, "Laboratory methods for identifying New Zealand wheat cultivars" N.Z. J. of Agric. Res. Vol.19 p 499, 1976.

Donaldson, I.G, Personal Communication, 1977.

Gates, D M, "Physical and Physiological properties of plants" Chapter 5 "Remote Sensing with special reference to agriculture and forestry" published by Nat.Acad.Sciences, Washington, USA 1970.

Hempenius, S A, "The ITC 8-image Caroussel Comparator and its possible use in ERTS and EREP investigations." The ITC Journal No. 2 p 167, 1974.

Kalensky, Z and Wightman, J M, "Automatic Forest Mapping Using remotely sensed data: XVI IUFRO World Congress, Oslo, Norway, June 1976.

Myers, V I, et al "Soil, Water and Plant Relations" Chapter 6 "Remote Sensing with special reference to agriculture and forestry" published by Nat.Acad.Sciences, Washington, USA, 1970.

Myers, V I, et al "Crops and Soils" Chapter 22 "Manual of Remote Sensing" published by American Society of Photogrammetry, Virginia, USA, 1975.

New Zealand "Official Yearbook 1976" published by Department of Statistics, NZ Government, Wellington, 1976.

Painter, D J, "What cost wind blown soil?" New Zealand Farmer Vol. 97, p 47, 1976.

Scott, D, Menalda, P H, Brougham, R W, "Spectral analysis of radiation transmitted and reflected by different vegetations" NZ Journal of Botany, Vol. 6 p 427, 1968.

ACKNOWLEDGEMENTS

This project has proceeded jointly with the assistance of the Ministry of Agriculture and Fisheries staff in Wellington and in the Christchurch and Darfield offices. In particular the support and material help rendered by Mr J Scott of M.A.F. Head Office, and by Messrs L Bennetts, R Riddell and G Fergusson of the Canterbury offices has been greatly appreciated.

The personal and professional hospitality so willingly extended to us on so many occasions by the contributing farmers in the Darfield and Leeston areas has aided the program immensely. We are continually grateful for this support from the following farmers, aided by their ladies:

J Anderson, B Gillanders, T Mulholland, C Stott, G Loe, C Reveley, B Steele, B Youngman, N Claridge, R Steele, T Sadler, A Colee, P Sadler, M Robertson, W Judd, R Innes, F O'Boyle, T Brankin, H Jenkins, O Osborne, H Relling, M McEvedy, W Moorhead, J Moorhead, M Moorhead, W Lowery, A Tong, R Tong, W Heslop, R Wylie, A Moorhead, N Moorhead, G Benny, J Lay, and L Lay.

During the preparation of this preliminary report we have greatly benefited from discussions with our colleages at the Physics and Engineering Laboratory, in particular Mr G M Allcock (reviewing the manuscript) Dr I G Donaldson (comments on the sub-surface moisture patterns) and Dr J H Troughton (guidance in presenting the summary of plant optical properties).

The patient reduction of the manuscript to legible form has been the province of Ms P Humphries and we are grateful for her cheerful forbearance in this task.

FIGURE CAPTIONS

Fig. 10.1 General crop reflectance profile (400-1200 nm).

Fig. 10.2 Colour composite of part of scene 1502-21362 prepared on the CSIRO Photowrite and Physics and Engineering Laboratory colour additive viewer.

Fig. 10.3 Ground key for Fig. 10.2 showing the subterranean moisture patterns deduced from Fig. 10.2

Fig. 10.4 Mosaic of part of aircraft multispectral coverage of Darfield test site 14 November 1975.

Fig. 10.5 Colour coded ground truth map for the contributing farms in the Darfield test area for the October/ November 1975 retrospective survey. (The colour coding is as discussed in section 10.4.3.)

Fig. 10.6 Colour composite of part of scene 2282-21254 prepared from a colour slide taken from the G E Image 100 output tube at E.R.O.S. Data Center Sioux Falls.

Fig. 10.7 Coded line-printer prepared thematic map for part of the Darfield test area for the LANDSAT scene no. 2282-21254. The colour coding indicates those classes confirmed by ground truth data. Symbols represent the following targets: W - Water, U - Urban, F - Forest, 1 - Bare Ground, 2 - Kopara Wheat, 3 - Karamu Wheat, 4 - Hilgendorf Wheat, 7 - Lucerne. (Colour coding is as discussed in section 10.4.3.)

Fig. 10.8 Coded line-printer prepared thematic map for part of the Darfield test area for the LANDSAT scene no. 1502-21362. Symbols represent the following targets: W - Water, U - Urban, F - Forest, 1 - Bare Ground, 2 - All Wheats, 7 - Lucerne.

APPENDIX 10.1 Summary of Soil Conditions in test area. Source: Soil Bureau (DSIR) Bulletin No 27 (1968)

Area: Darfield

Soil Ref No.	Soil Generic Name	Individual Soil Name	Parent Material	Representative Profile	Natural Nutrient Status	Present* Carrying Capacity (ewes/ha)	Liability to Soil Erosion
13	Yellow grey earth	Lismore soil (silt loams and shallow silt loams)	Greywacke gravel with thin cover of loess	15 cm crumb stony silty loam, friable 15 cm blocky stony silty loam, firm on v. stony soil	Low	4 - 8	Wind where cultivated
14	Yellow grey earth	Chertsey soil (silt loams and shallow silt loams)	Greywacke alluvium with thin cover of loess	20 cm granular/nutty silty loam, friable 23 cm blocky silty loam friable 15 cm sandy gravels, compact on gravels	Medium to low	5	Wind
14a	Yellow grey earth	Hatfield soil (silt loams)	Greywacke alluvium and loess	25 cm nutty/granular silty loam, friable 40 cm blocky silty loam, firm on gravels with silt matrix	Medium	5	Wind where cultivated
95a	Recent soil	Waimakariri shallow soils (sandy loams to silt loams, shallow and stony loams)	Greywacke alluvium, some fine sandy loess and some sand	25 cm granular/crumb sandy loam, friable 15 cm massive/granular stony sandy loam, friable on gravels	Medium to low	$2\frac{1}{2}$	Wind

* 1957-63 averages for similar plots in area

APPENDIX 10.1 Summary of Soil Conditions in test area. Source: Soil Bureau (DSIR) Bulletin No 27 (1968)

Area: Darfield

Soil Ref No.	Soil Generic Name	Individual Soil Name	Parent Material	Representative Profile	Natural Nutrient Status	Present* Carrying Capacity (ewes/ha)	Liability to Soil Erosion
96a and 96c	Recent soil	Templeton Soil (silt, stony, sandy loams) Eyre-Paparua soil (shallow silt loams, sandy loams)	Greywacke alluvium - some thin loess	20 cm nutty/granular stony silty loam, friable 25 cm nutty, very stony silty loam, very friable on sandy gravels	Medium	5	slight wind

* 1957-63 averages for similar plots in area

Appendix 10.1 Summary of Soil Conditions in test area. Source: Soil Bureau (DSIR) Bulletin No 27 (1968)

Area: Leeston

Soil Ref No.	Soil Generic Name	Individual Soil Name	Parent Material	Representative Profile	Natural Nutrient Status	Present* Carrying Capacity (ewes/ha)	Liability to Soil Erosion
89	Gley Soils	Temuka Soils (silt to clay loams)	Greywacke alluvium	15 cm granular silty loam, firm 18 cm prismatic/blocky clay loam, v. firm on massive clay loam, firm	Medium to High	8	
89a	Gley Soils	Waterton Soils (silt loams)	Greywacke alluvium	23 cm nutty silt loam, firm 8 cm blocky clay loam, firm 18 cm blocky clay loam, firm on greywacke gravels	Medium	8	
95	Recent Soils	Waimakariri Soils (sandy to silty loams)	Greywacke alluvium	23 cm fine sandy loam, friable weak medium granular structure 18 cm fine sandy loam, friable weak coarse blocky structure on fine sand over loose greywacke gravels	High to Medium	$8\frac{1}{2}$	

1957-63 averages for similar plots in area

Appendix 10.1 Summary of Soil Conditions in test area. Source: Soil Bureau (DSIR) Bulletin No 27 (1968)

Area: Leeston

Soil Ref. No.	Soil Generic Name	Individual Soil Name	Parent Material	Representative Profile	Natural Nutrient Status	Present* Carrying Capacity (ewes/ha)	Liability to Soil Erosion
96a	Recent soils	Templeton Soils (silt and sandy loams)	Greywacke alluvium - some thin loess	20 cm silt loam medium granular structure, friable 15 cm medium nutty structure, silt loam 30 cm very firm coarse prismatic structure silt loam on greywacke gravels and sand	Medium to High	6	
96c	Recent soils	Eyre-Paparua soils (shallow stony sandy silty loams)	Mostly stony Greywacke alluvium	20 cm nutty/granular stony silt loam friable 25 cm nutty very stony silt loams, v. friable on sandy gravels	Medium to Low	4	Slight wind erosion potential

1957-63 averages for similar plots in area

Appendix 10.2 Summary of occurrence statistics for the spectral signatures of the eight classes classified in the thematic mapping package applied to the 31 October 1975 LANDSAT scene (2282-21254). Such thematic mapping is based on five dimensional parallelepiped supervised clustering as discussed in the text. The spectral shape factor, the fifth dimension, has a tolerance of ±1 CCT level

SPECTRAL FREQUENCY DISTRIBUTION FOR BARE GRND.
SCENE ID: 2282-2125400 STRIP NO.: 2 OF 4
SCAN LINES: 1720 - 1876
PIXELS: 535 - 649 (WEST TO EAST)

BAND 4		BAND 5		BAND 6		BAND 7	
22.00:	7	26.00:	18	37.00:	9	16.00:	16
23.00:	80	29.00:	47	38.00:	21	17.00:	43
24.00:	65	30.00:	58	39.00:	40	18.00:	56
25.00:	106	31.00:	36	40.00:	25	19.00:	58
26.00:	7	32.00:	56	41.00:	10	20.00:	42
0.00:	0	0.00:	0	42.00:	59	0.00:	0
0.00:	0	0.00:	0	43.00:	22	0.00:	0
0.00:	0	0.00:	0	44.00:	19	0.00:	0

SPECTRAL SIGNATURE STATISTICS

MEAN FOR BAND	4 IS	24.353	WITH A STANDARD DEVIATION OF	0.878
MEAN FOR BAND	5 IS	30.302	WITH A STANDARD DEVIATION OF	1.795
MEAN FOR BAND	6 IS	40.740	WITH A STANDARD DEVIATION OF	1.972
MEAN FOR BAND	7 IS	18.311	WITH A STANDARD DEVIATION OF	1.237

SPECTRAL FREQUENCY DISTRIBUTION FOR KOPARA WHT
SCENE ID: 2282-2125400 STRIP NO.: 2 OF 4
SCAN LINES: 1720 - 1876
PIXELS: 535 - 649 (WEST TO EAST)

BAND 4		BAND 5		BAND 6		BAND 7	
14.00:	7	12.00:	2	47.00:	16	25.00:	16
15.00:	94	13.00:	21	48.00:	12	26.00:	43
16.00:	108	14.00:	48	49.00:	89	27.00:	79
17.00:	61	15.00:	82	50.00:	34	28.00:	80
0.00:	0	16.00:	63	51.00:	66	29.00:	52
0.00:	0	17.00:	14	52.00:	73	0.00:	0
0.00:	0	18.00:	40	0.00:	0	0.00:	0

SPECTRAL SIGNATURE STATISTICS

MEAN FOR BAND	4 IS	15.825	WITH A STANDARD DEVIATION OF	0.806
MEAN FOR BAND	5 IS	15.425	WITH A STANDARD DEVIATION OF	1.468
MEAN FOR BAND	6 IS	50.188	WITH A STANDARD DEVIATION OF	1.529
MEAN FOR BAND	7 IS	27.403	WITH A STANDARD DEVIATION OF	1.142

SPECTRAL FREQUENCY DISTRIBUTION FOR KARAMU WHT
SCENE ID: 2282-2125400 STRIP NO.: 2 OF 4
SCAN LINES: 1720 - 1876
PIXELS: 535 - 649 (WEST TO EAST)

BAND 4		BAND 5		BAND 6		BAND 7	
14.00:	21	13.00:	91	57.00:	51	33.00:	84
15.00:	197	14.00:	169	58.00:	50	34.00:	99
16.00:	191	15.00:	156	59.00:	72	35.00:	130
17.00:	147	16.00:	140	60.00:	53	36.00:	159
0.00:	0	0.00:	0	61.00:	47	37.00:	98
0.00:	0	0.00:	0	62.00:	56	0.00:	0
0.00:	0	0.00:	0	63.00:	120	0.00:	0
0.00:	0	0.00:	0	64.00:	107	0.00:	0

SPECTRAL SIGNATURE STATISTICS

MEAN FOR BAND	4 IS	15.834	WITH A STANDARD DEVIATION OF		0.862
MEAN FOR BAND	5 IS	14.620	WITH A STANDARD DEVIATION OF		1.033
MEAN FOR BAND	6 IS	61.118	WITH A STANDARD DEVIATION OF		2.362
MEAN FOR BAND	7 IS	35.115	WITH A STANDARD DEVIATION OF		1.308

SPECTRAL FREQUENCY DISTRIBUTION FOR HILGOF WHT
SCENE ID: 2282-2125400 STRIP NO.: 2 OF 4
SCAN LINES: 1720 - 1876
PIXELS: 535 - 649 (WEST TO EAST)

BAND 4		BAND 5		BAND 6		BAND 7	
16.00:	85	16.00:	130	60.00:	59	33.00:	73
17.00:	209	17.00:	54	61.00:	44	34.00:	115
18.00:	505	18.00:	230	62.00:	125	35.00:	207
19.00:	226	19.00:	302	63.00:	126	36.00:	228
0.00:	0	20.00:	301	64.00:	234	37.00:	254
0.00:	0	0.00:	0	65.00:	140	38.00:	148
0.00:	0	0.00:	0	66.00:	73	0.00:	0
0.00:	0	0.00:	0	67.00:	224	0.00:	0

SPECTRAL SIGNATURE STATISTICS

MEAN FOR BAND	4 IS	17.850	WITH A STANDARD DEVIATION OF		0.857
MEAN FOR BAND	5 IS	18.575	WITH A STANDARD DEVIATION OF		1.303
MEAN FOR BAND	6 IS	64.208	WITH A STANDARD DEVIATION OF		2.065
MEAN FOR BAND	7 IS	35.896	WITH A STANDARD DEVIATION OF		1.452

SPECTRAL FREQUENCY DISTRIBUTION FOR LUCERNE
SCENE ID: 2282-2125400 STRIP NO.: 2 OF 4
SCAN LINES: 1720 - 1876
PIXELS: 535 - 649 (WEST TO EAST)

BAND 4		BAND 5		BAND 6		BAND 7	
14.00:	4	12.00:	48	82.00:	42	50.00:	129
15.00:	260	13.00:	283	83.00:	83	51.00:	155
16.00:	171	14.00:	146	84.00:	61	52.00:	109
17.00:	42	0.00:	0	85.00:	96	53.00:	50
0.00:	0	0.00:	0	86.00:	87	54.00:	34
0.00:	0	0.00:	0	87.00:	58	0.00:	0
0.00:	0	0.00:	0	88.00:	1	0.00:	0
0.00:	0	0.00:	0	89.00:	64	0.00:	0

SPECTRAL SIGNATURE STATISTICS

MEAN FOR BAND	4 IS	15.526 WITH A STANDARD DEVIATION OF		0.665
MEAN FOR BAND	5 IS	13.205 WITH A STANDARD DEVIATION OF		0.604
MEAN FOR BAND	6 IS	85.291 WITH A STANDARD DEVIATION OF		2.061
MEAN FOR BAND	7 IS	51.381 WITH A STANDARD DEVIATION OF		1.190

SPECTRAL FREQUENCY DISTRIBUTION FOR WATER
SCENE ID: 2282-2125400 STRIP NO.: 2 OF 4
SCAN LINES: 1720 - 1876
PIXELS: 535 - 649 (WEST TO EAST)

BAND 4		BAND 5		BAND 6		BAND 7	
26.00:	16	27.00:	5	21.00:	9	4.00:	0
27.00:	45	28.00:	26	22.00:	16	5.00:	27
28.00:	27	29.00:	51	23.00:	5	6.00:	54
29.00:	41	30.00:	35	24.00:	43	7.00:	57
30.00:	29	31.00:	25	25.00:	47	8.00:	28
31.00:	22	32.00:	18	26.00:	16	9.00:	14
0.00:	0	33.00:	20	27.00:	26	0.00:	0
0.00:	0	0.00:	0	28.00:	12	0.00:	0
0.00:	0	0.00:	0	29.00:	6	0.00:	0

SPECTRAL SIGNATURE STATISTICS

MEAN FOR BAND	4 IS	28.488 WITH A STANDARD DEVIATION OF		1.533
MEAN FOR BAND	5 IS	30.016 WITH A STANDARD DEVIATION OF		1.632
MEAN FOR BAND	6 IS	24.950 WITH A STANDARD DEVIATION OF		1.941
MEAN FOR BAND	7 IS	6.711 WITH A STANDARD DEVIATION OF		1.135

SPECTRAL FREQUENCY DISTRIBUTION FOR URBAN
SCENE ID: 2282-2125400 STRIP NO.: 2 OF 4
SCAN LINES: 1720 - 1876
PIXELS: 535 - 649 (WEST TO EAST)

BAND 4		BAND 5		BAND 6		BAND 7	
22.00:	4	25.00:	21	47.00:	25	22.00:	15
23.00:	58	26.00:	56	48.00:	44	23.00:	70
24.00:	140	27.00:	27	49.00:	101	24.00:	86
25.00:	74	28.00:	69	50.00:	14	25.00:	70
26.00:	6	29.00:	69	51.00:	54	26.00:	39
0.00:	0	30.00:	40	52.00:	44	0.00:	0

SPECTRAL SIGNATURE STATISTICS

MEAN FOR BAND	4 IS	24.070 WITH A STANDARD DEVIATION OF	0.779
MEAN FOR BAND	5 IS	27.812 WITH A STANDARD DEVIATION OF	1.531
MEAN FOR BAND	6 IS	49.567 WITH A STANDARD DEVIATION OF	1.554
MEAN FOR BAND	7 IS	24.170 WITH A STANDARD DEVIATION OF	1.112

SPECTRAL FREQUENCY DISTRIBUTION FOR FOREST
SCENE ID: 2282-2125400 STRIP NO.: 2 OF 4
SCAN LINES: 1720 - 1676
PIXELS: 535 - 649 (WEST TO EAST)

BAND 4		BAND 5		BAND 6		BAND 7	
10.00:	12	9.00:	28	27.00:	19	14.00:	9
11.00:	76	10.00:	42	28.00:	34	15.00:	21
12.00:	63	11.00:	52	29.00:	33	16.00:	47
13.00:	19	12.00:	19	30.00:	10	17.00:	52
14.00:	12	13.00:	20	31.00:	37	18.00:	36
15.00:	11	14.00:	12	32.00:	24	19.00:	19
0.00:	0	15.00:	9	33.00:	15	20.00:	9
0.00:	0	16.00:	11	34.00:	17	0.00:	0
0.00:	0	0.00:	0	35.00:	4	0.00:	0

SPECTRAL SIGNATURE STATISTICS

MEAN FOR BAND	4 IS	12.875 WITH A STANDARD DEVIATION OF	1.222
MEAN FOR BAND	5 IS	11.455 WITH A STANDARD DEVIATION OF	1.963
MEAN FOR BAND	6 IS	30.310 WITH A STANDARD DEVIATION OF	2.237
MEAN FOR BAND	7 IS	16.922 WITH A STANDARD DEVIATION OF	1.450

11

Appendix 10.3 Biophysical basis of optical properties of vegetation over the 400-1200 nm wavelength range

Of the solar radiation incident on the leaf, that between 400-700 nm is highly absorbed by the pigments in the leaf associated with photosynthesis, while between 750-1200 nm, much more of the radiation is reflected. In the 400-700 nm range there are peaks of chlorophyll absorbtion at 450 and 680 nm. The higher transmission and reflectance in the green portion of the spectrum gives vegetation its characteristic appearance. The human eye also has its highest sensitivity in daylight in this same spectral range. Absorption of solar irradiance due to liquid water occurs with major values at 1400, and 1900 nm and with minor absorptions at 980 nm and 1100 nm.

MSS channel 4 senses an amalgam of pigment responses from the leaves of a crop. These are the pigments based on the chlorophyll, xanthophylls, carotenes and anthocyanins, in healthy foliage.

The major feature in MSS channel 5 is the chlorophyll absorption band at ∿680 nm. As the chlorophyll content of the leaf varies, so too will the level in MSS 5 vary (inversely). The autumnal yellowing of foliage, or crops as they approach harvest, is due to a breaking down of the chlorophyll in the leaf thus allowing the presence of the carotenes and xanthophylls to become apparent.

The ratio of the radiances recorded in MSS channels 5 and 4 can thus give an indication of the maturity of a crop.

MSS 6 acts as a "bridging" band between the chlorophyll absorption in MSS 5 and that irradiance/mesophyll interaction well covered by MSS 7. With plant deterioration the yellow and orange carotene and red anthocyanin colours appear as the green chlorophyll pigment is lost and the chlorophyll absorption band weakens. Such leaf senescence can be brought on by droughts and high temperatures, amongst other causes.

It is expected that careful monitoring of the MSS 5 and 6 channels will yield much information that will assist in the differentiation of similar crop types.

Little of the wavelength region 800 - 1100 nm is absorbed by the leaf. Most is reflected and much of the remainder transmitted - where it may be reflected by underlying layers. As the irradiance ray penetrates the leaf cuticle into the mesophyll it undergoes many critical reflections as it passes between cells. These critical reflections occur at cell walls as the ray transits from high refractive index hydrated cell walls to low refractive index intercellular air spaces. Obviously the extent to which this "random walk" by the irradiance ray continues depends upon the density of cells in the mesophyll,

the thickness of the leaf, and the water content of the mesophyll. Throughout this progression through the mesophyll the ray is subject to the liquid water absorption band at around 980 nm.

As a leaf matures, it usually progresses from having few air spaces in its mesophyll during its juvenile days, to the sponginess of many air spaces in later life. This increase in the number of air spaces leads to increased reflectance in the 800-1100 nm region.

Another important application of MSS 7 is the monitoring of the Leaf Area Index (LAI). The LAI for a crop at a certain stage in its maturity is the ratio of leaf area to ground area. It has usually been found (Myers et al, 1970) that an increase in LAI is accompanied by an increase in reflectance in the 800-1100 nm region whilst reflectance in the 500-600 nm region remains essentially constant. (This result is consistent with the above discussion on the irradiance absorption in MSS 4 and transmittance in MSS 7).

The LAI, derived from LANDSAT data, is likely to be most meaningful for emergent crops (LAI low, say, 1 to 3). As LAI increases a decreasing percentage of the total irradiance will be reflected from the lowermost leaf layers - until the returned signal is lost in the data 'noise'.

MSS 7 can thus provide a measure of the relative leaf growth of a crop, within LAI limits, together with possible moisture stress influences.

For a further discussion on these topics the reader is referred to Gates (1970), Myers et al (1970), Myers et al (1975), and Scott et al (1968).

As the Canterbury Plains are subjected to drying winds, have a low to medium rainfall, and the crops are grown on shallow free draining soils, the influence upon the spectral reflectance of a decreasing crop moisture level is important to overall monitoring in this area. Myers et al (1975) found that as the moisture content decreased, over all the MSS bands, the reflectance increased.

Just as the human eye can distinguish spectral, and hence genetic, differences between various cereal crops so too may the multispectral scanner be expected to sense genetic differences. Obviously improvement in such differentiation will be aided by finer wavelength resolution in the sensing equipment.

There are five main types of wheat commonly grown over the two test areas. These are Arawa, Kopara, Karamu, Aotea and Hilgendorf. Genetically, it is interesting to note (Coles and Wrigley, 1976) that the red grained Hilgendorf combined with the white grained Aotea and Arawa, and other strains, led to the red grained Kopara progeny. (The grain colour is determined by soaking the grain in 5% sodium hydroxide at room temperature). The red grained Karamu

comes from a completely independent immediate parentage background. On this basis, spectral signature differences could be expected between Karamu and the other varieties. A similarity between the other two commonest varieties, Hilgendorf and Kopara, could be expected although some parent/daughter differences would be anticipated.

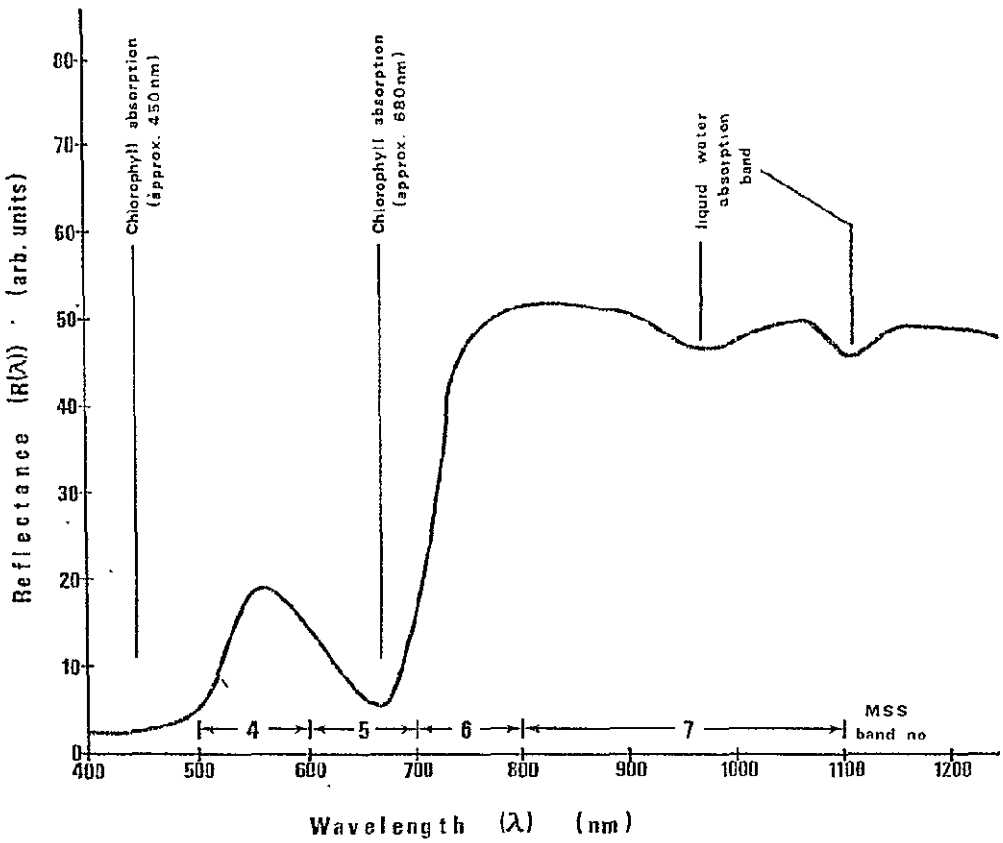

Fig. 10.1 General crop reflectance profile (400 - 1200 nm)

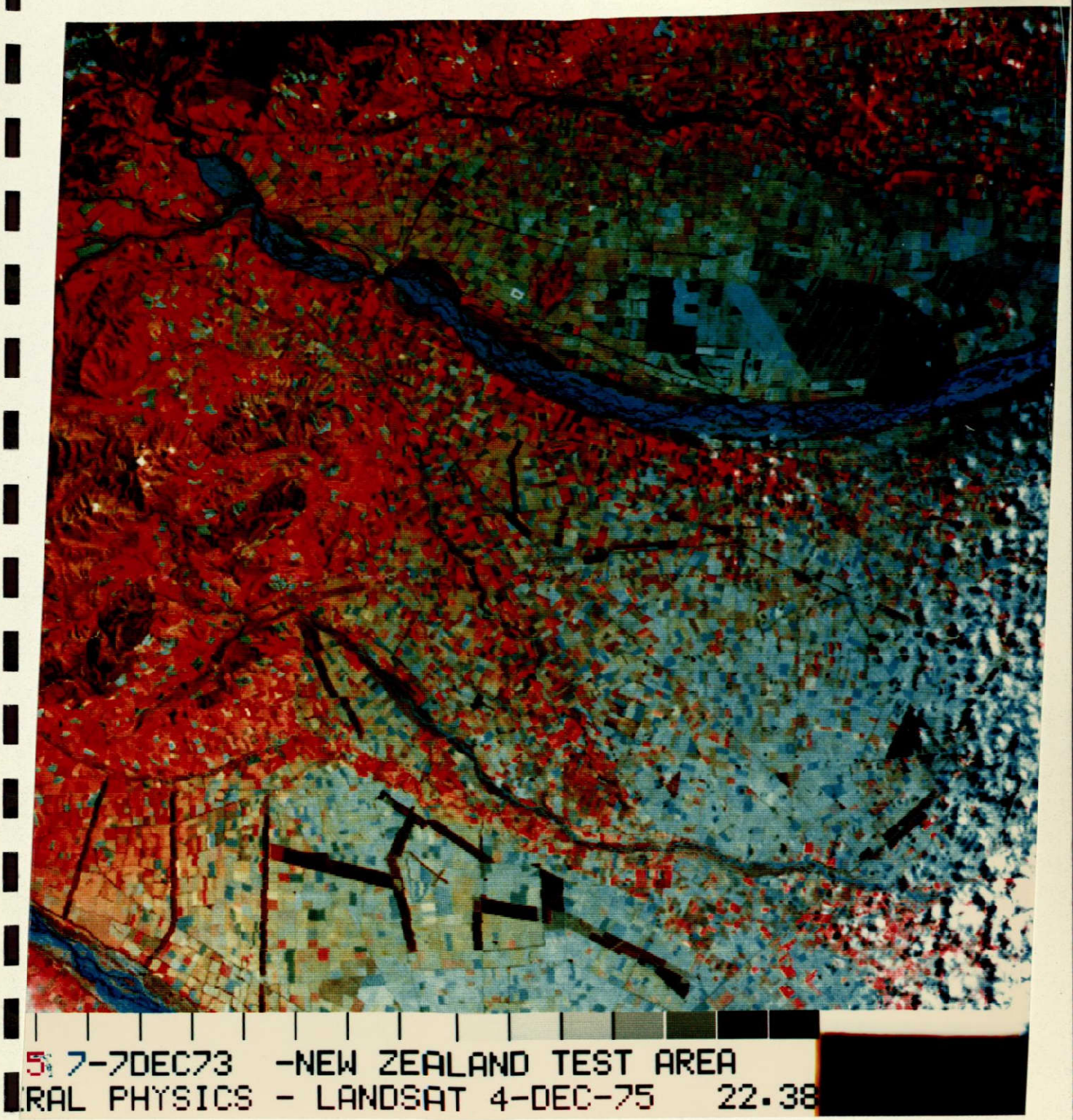

Fig. 10.2 Colour composite of part of scene 1502 - 21362 prepared on the C.S.I.R.O. Photowrite and P.E.L. colour additive viewer.

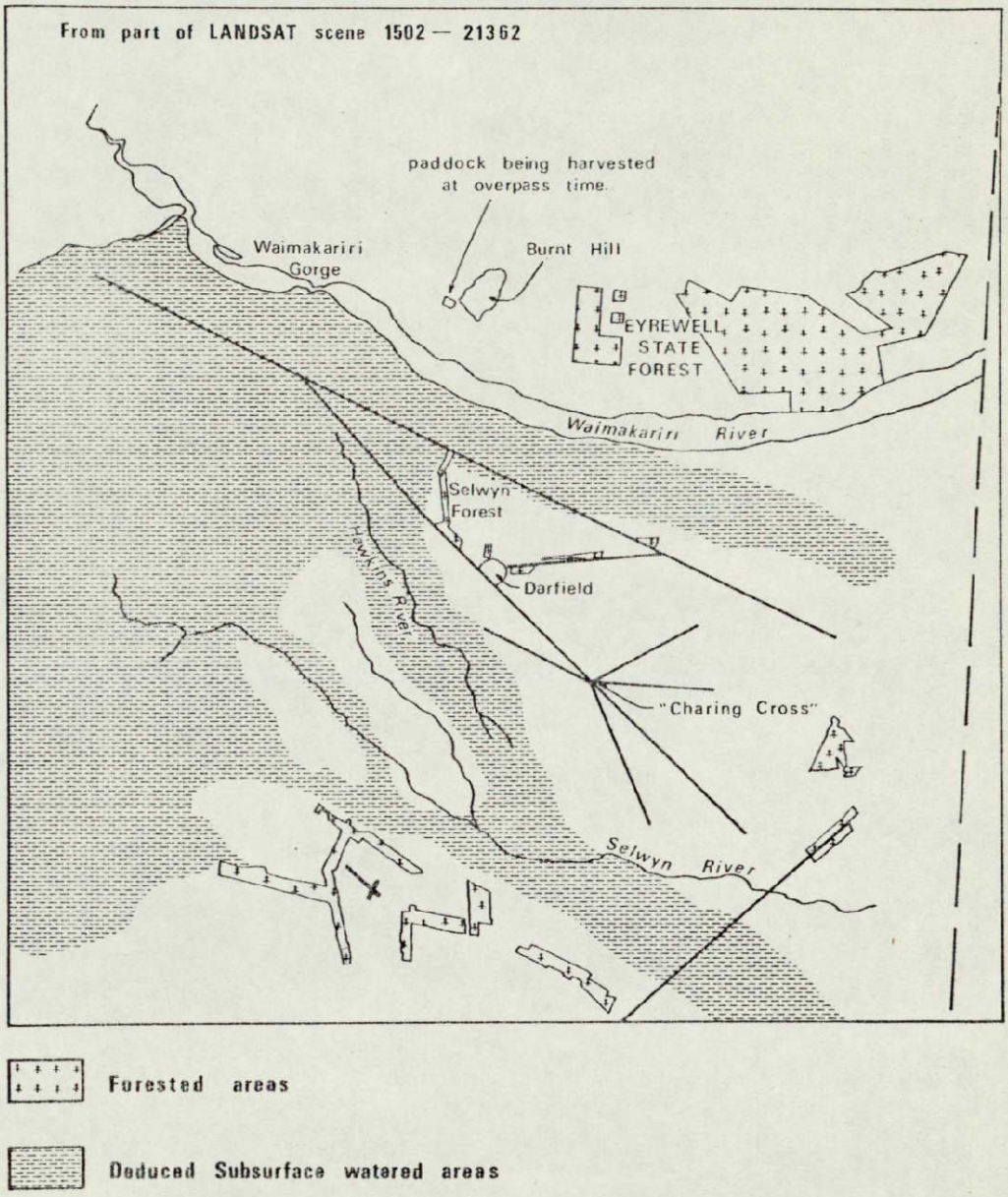

Fig. 10.3 Ground key for fig. 10.2 showing the subterranean moisture patterns deduced from fig. 10.2

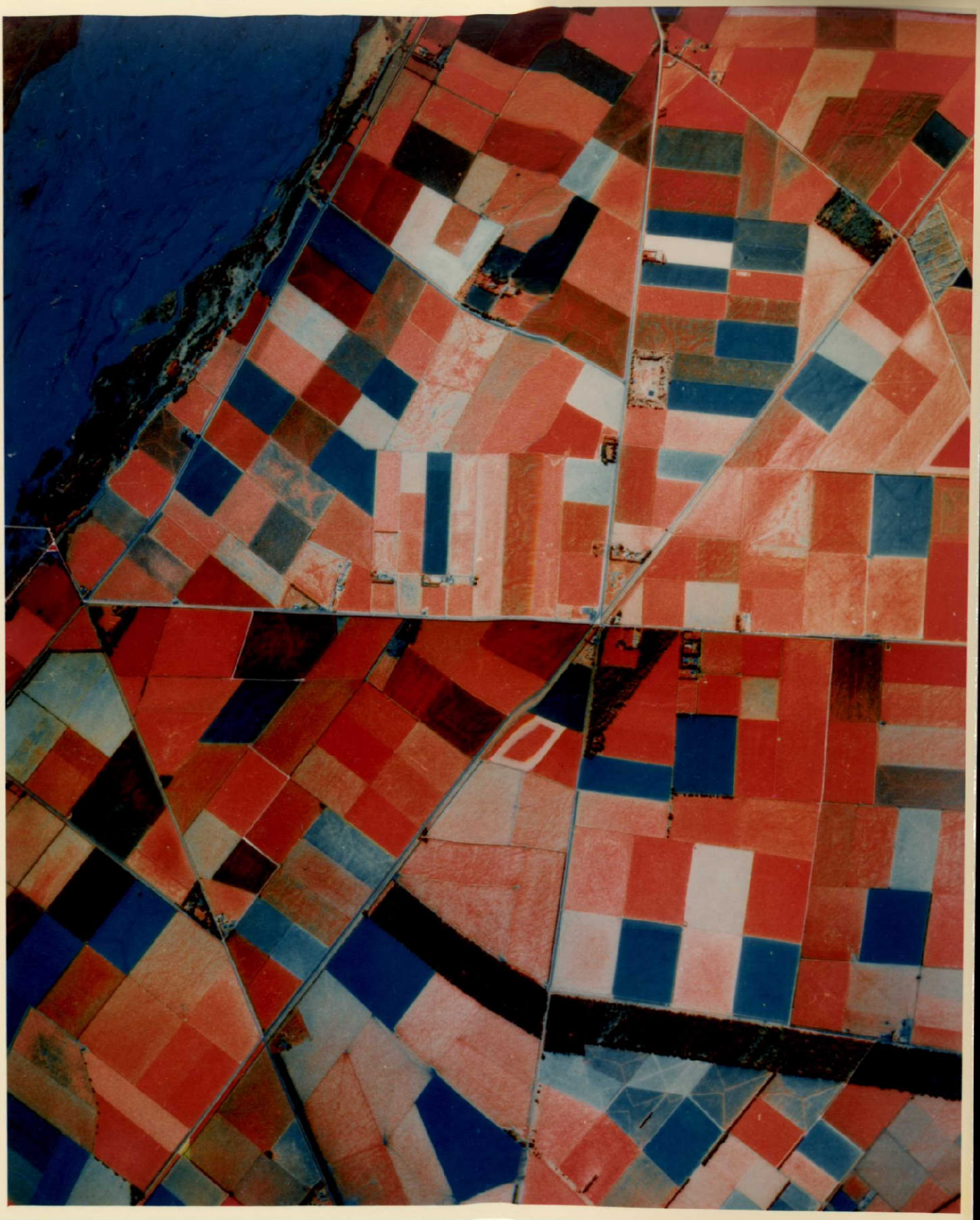

Fig. 10.4 Mosaic of part of aircraft multispectral coverage of Darfield test site 14 November 1975.

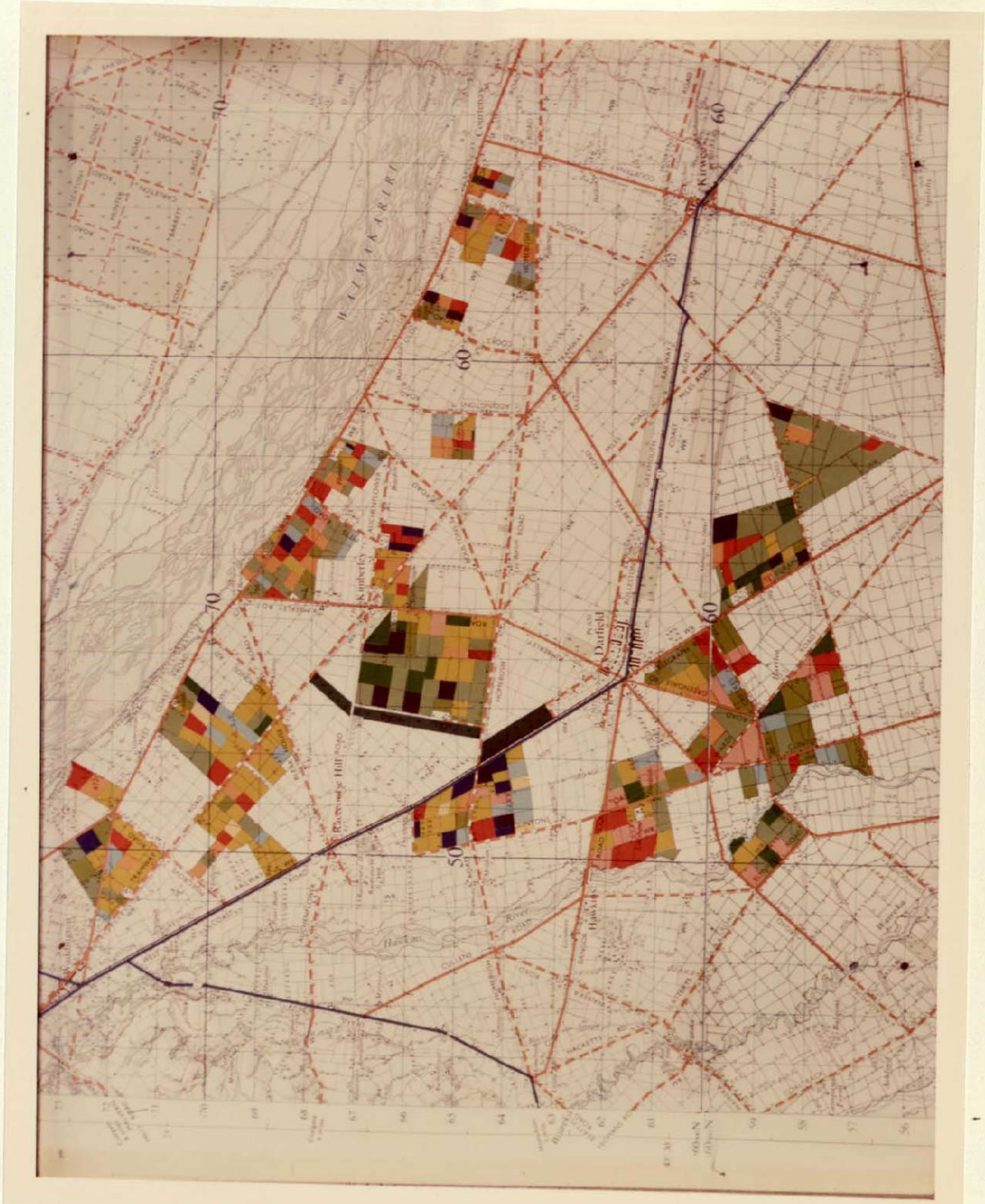

Fig. 10.5 Colour coded ground truth map for the contributing farms in the Darfield test area for the Oct/Nov 1975 retrospective survey. (The colour coding is as discussed in section 10.4.3)

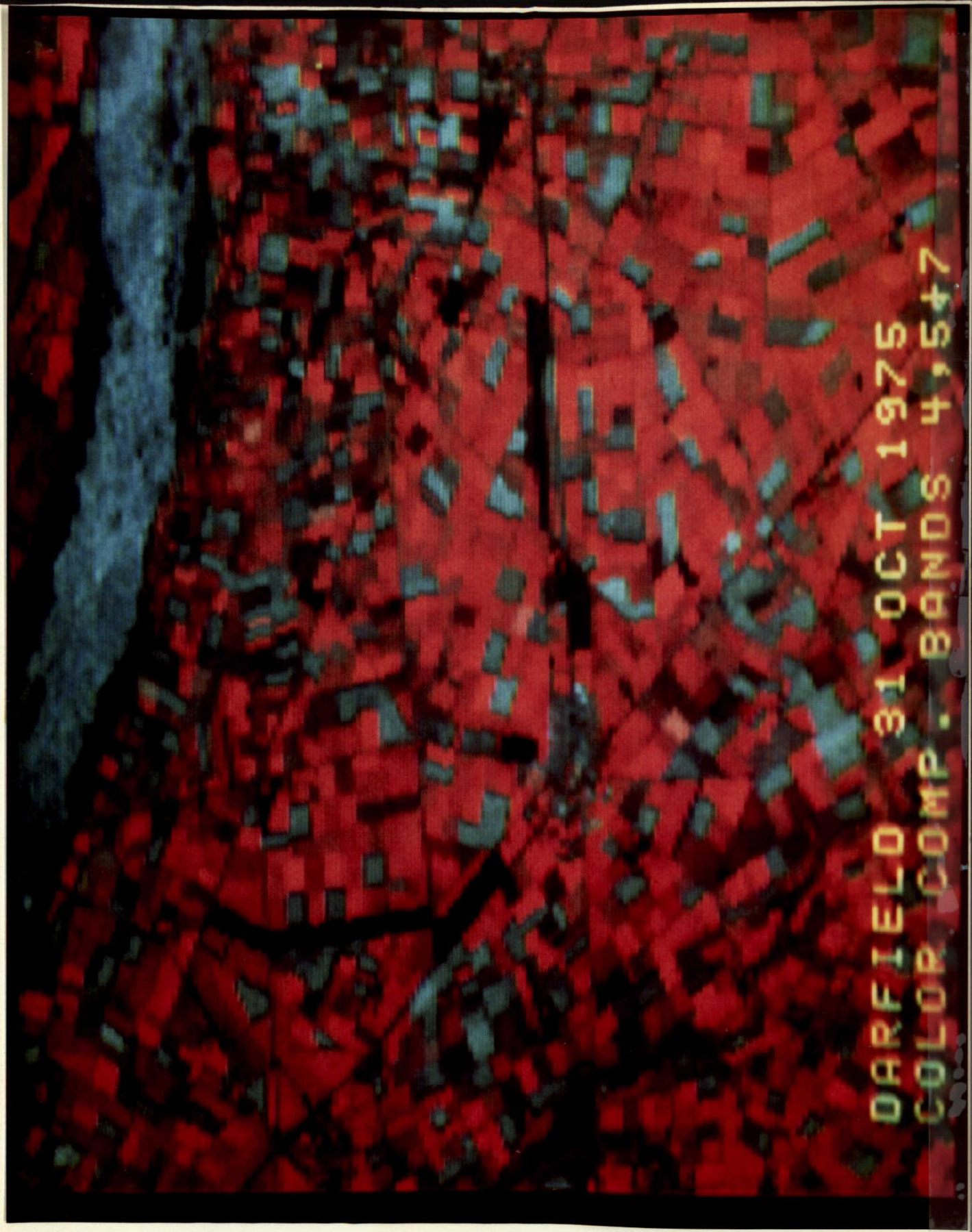

Fig. 10.6 Colour composite of part of scene 2282 - 21254 prepared from a colour slide taken from the G.E. Image 100 output tube at E.R.O.S. Data Center Sioux Falls.

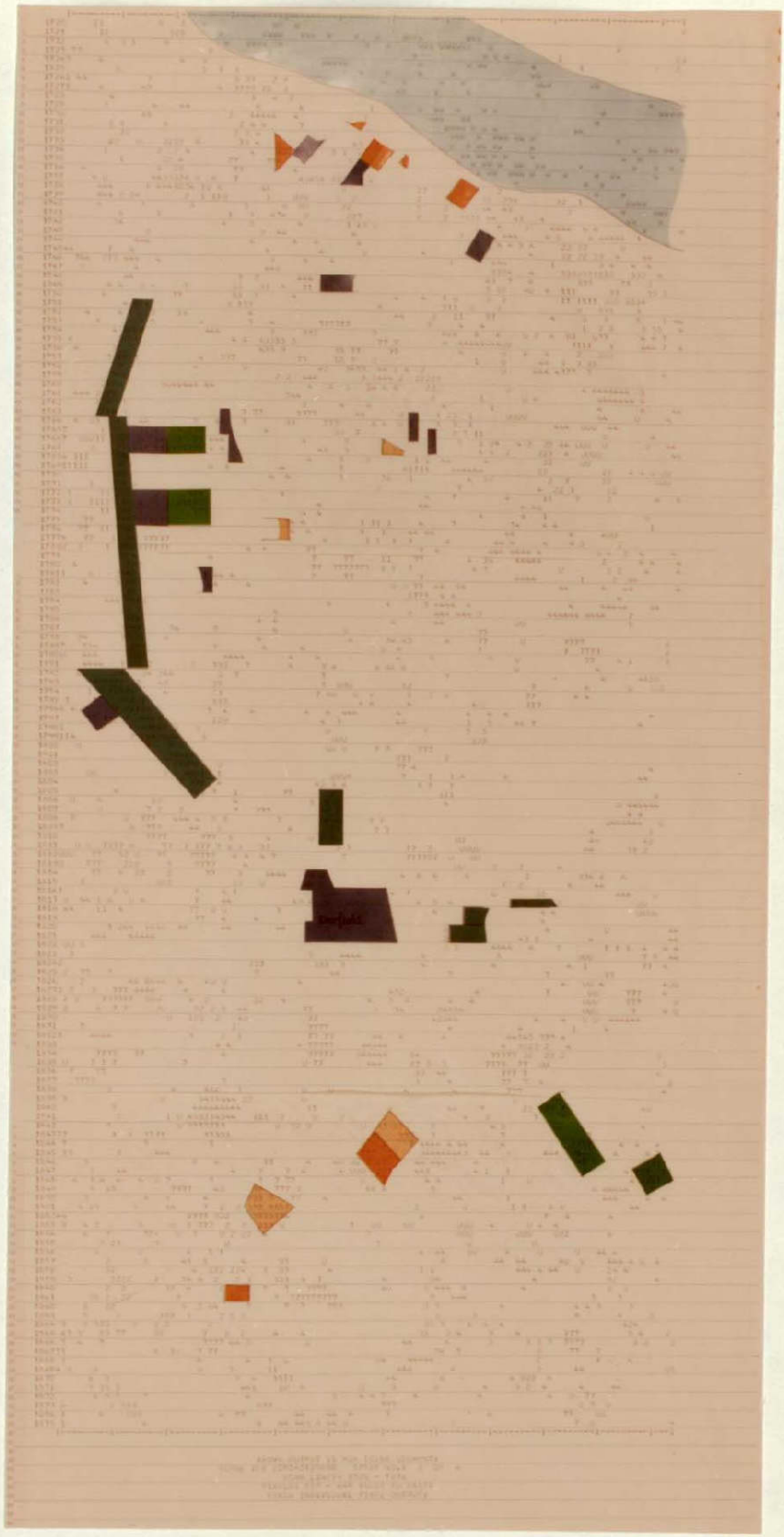

ORIGINAL PAGE IS
OF POOR QUALITY

Fig. 10.7 Coded line-printer prepared thematic map for part of the Darfield test area for the LANDSAT scene no.2282-21254. The colour coding indicates those classes confirmed by ground truth data. Symbols represent the following targets: W - Water, U - Urban, F - Forest, 1 - Bare Ground, 2 - Kopara Wheat, 3 - Karamu Wheat, 4 - Hilgendorf Wheat, 7 - Lucerne. (The colour coding is as discussed in section 10.4.3)

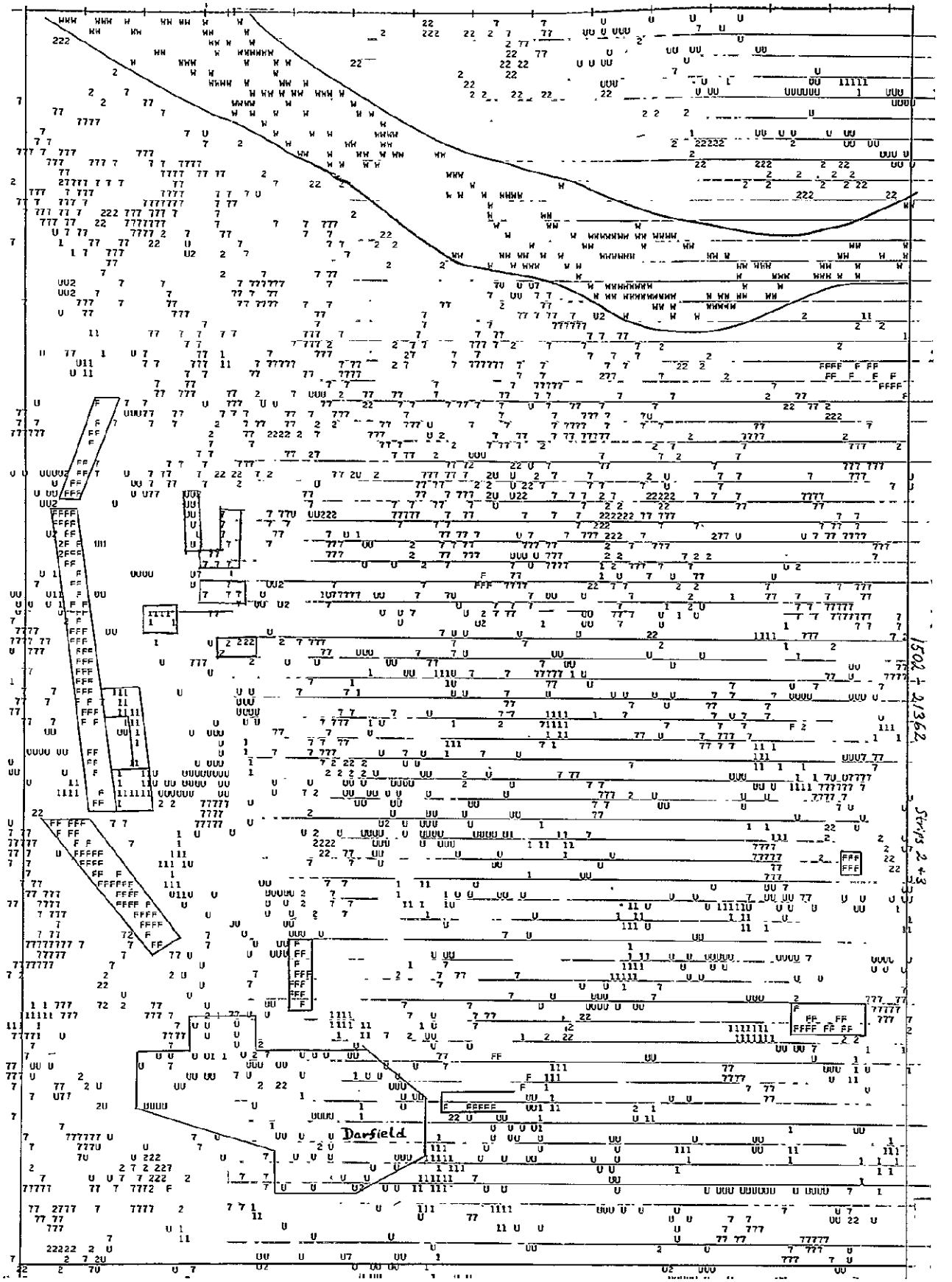

Fig. 10.8 Coded line-printer prepared thematic map for part of the Darfield test area for the LANDSAT scene No. 1502 - 21362. Symbols represent the following targets: W - Water; U - Urban; F - Forest; 1 - Bare ground; 2 - All wheats; 7 - Lucerne.

CHAPTER 11

SNOWFIELD ASSESSMENT FROM LANDSAT

I. L. Thomas, A. J. Lewis* and N. P. Ching

ABSTRACT

The potential use of LANDSAT MSS data for routine monitoring of the area and condition (type/depth) of a snowfield is explored. Area measurements are readily possible from the photographic product and the CCT data. The CCT data may also reveal variations in snow density and/or moisture content. This study demonstrates that LANDSAT MSS data have the potential for contributing to rapid assessment and management of snowfield resources, especially if repetitive satellite coverage is obtained.

Although further work relating actual snow conditions to the recorded radiances is necessary, the importance of using absolute radiance values from CCT data and of considering the effect of topography on recorded snow reflectance is demonstrated.

*On sabbatical leave from Department of Geography and Anthropology, Louisiana State University, Baton Rouge, Louisiana, U.S.A.

11.1 INTRODUCTION

The acquisition of meaningful information on snow cover and snow conditions from LANDSAT data has been the object of many projects. One NASA publication deals entirely with snow cover observations from satellite data (Rango 1975). It is repeatedly reported that the accurate determination of snowline and snow cover area is easily accomplished. However, Bartolucci et al. (1975) have suggested that snow typing, depth, and other snowpack parameters are not readily obtainable from LANDSAT data.

In response to a request from the New Zealand National Parks Authority, the New Zealand Forest Service and the Remote Sensing Section of the Physics and Engineering Laboratory (PEL), Department of Scientific and Industrial Research, initiated a joint study to assess the relative merits of extending an existing skifield (Mt Robert (41.85°S; 172.80°E), or opening a new area (Six Mile Creek Basin (41.88°S; 172.85°E)), for such development.

LANDSAT MSS data with their 56 by 79 m resolution (at nominal spacecraft altitude), multispectral sensitivity, and potential for sequential coverage provide a likely source of valuable information for snowfield assessment. The particular questions of access, wind exposure, and general terrain conditions applicable to any skifield assessment are left to the skiing fraternity.

11.2 METHODS

The study has been divided into three stages: transect selection, areal planimetry, and analysis and interpretation of CCT data for snow depth/typing. This last stage compares radiance data along three transects within the Six Mile Creek Basin with that along one transect line in the existent ski basin - the Mt Robert skifield. All stages use the one cloud-free LANDSAT scene available of the study area (Scene ID no. 2282-21252 recorded on 31 October 1975 (GMT)).

11.2.1 Transect Selection

The first stage was the selection of a suitable transect line within the Six Mile Creek Basin for a continuing programme of ground measurements on snow depth/type. This transect line was located on the basis of an analysis of the MSS 4 positive transparency using a Datacolor 703 isodensitometer.

New Zealand Forest Service field inspection of snow conditions began in early November 1976, at the end of the Southern Hemisphere ski season. A transect 3940 ft long was established from 5200 ft to 5900 ft elevation above sea level. Six permanent stations were positioned so that snow depth and surface conditions could be recorded. These stations consist of a centre pole with measurements taken at 10 locations each 33 ft apart to the right and left of the six centre poles. Similar data will be collected at regular intervals corresponding to future satellite overpasses during future snow seasons. Occasional aerial surveys will accompany the ground surveys, and ground photographs are to be taken during the field surveys.

11.2.2 Planimetry and Snow Area Measurements

The second stage of the study, again executed by the New Zealand Forest Service, used the colour-coded isodensitometer product, obtained from the MSS 4 positive transparency, to derive the area covered by each of the four highest intensity levels recorded on the photographic product. This was done by projecting the 35 mm colour slide, photographically taken from the Datacolor 703 screen, on to a base map. This map/projector system was suitably oriented to counteract distortions and scale differences. After transferral of the four highest regions, standard planimetric techniques led to the deduced percentage areas presented in Table 11.1. The regions chosen in each basin for this area assessment were bounded on three sides by ridge lines. The fourth side, closing the area, was a line drawn between the lateral spurs to the basin (see Figs 11.1 and 11.2).

Table 11.1—Percent of Area by Intensity Categories: Six Mile Creek and Mt Robert

Intensity Category	Percent of total area studied	
	Mt Robert	Six Mile Creek
I. Highest level (purple)[1]	26%	43%
II. Second (white)[1]	36%	30%
III. Third (yellow)[1]	35%	19%
IV. Lowest level[2] (red)[1]	2%	7%
Total Area (ha)	193.9	498.4

Source: MSS band 4 positive, Scene # 2282-21252

1. The colours are those in Fig. 11.1 (see also Probine et al. 1976).
2. Interpreted as open ground - no snow cover.

11.2.3 Analysis of CCT Data

The third stage, conducted by PEL, was directed at relating the radiance profiles along the transects derived from the Computer Compatible Tape (CCT) product to the likely snow conditions at the time of the overpass. Snow of all types has MSS radiances that usually place it in a region of compressed dynamic range on the photographic scene radiance/film density curve. For this reason snow typing is best performed using the CCT data.

In further assessing the two snowfield areas, Mt Robert and Six Mile Creek, 47 level coded character printouts of each MSS band of the CCT data for the 31 October 1975 scene (no. 2282-21252) were prepared on an IBM 370/168 computer.

11.2.3.1 CCT Transect Lines

Four transect lines were selected for study: one approximately along the existent Mt Robert skifield towline and three in the Six Mile Creek Basin (Fig. 11.2). Transect (D-A) was placed along the New Zealand Forest Service snow sampling line. Transect (D-C) was established to approximate the sun illumination angle on the Mt Robert transect (E-F), and transect (D-B) was set up on the predominantly sunward slope approximately opposite the (D-A) transect.

Aided by black and white enlargements of the area for each MSS band and topographic maps, ground control points were transferred to the coded computer printouts.

The computer user has no control over the column or row spacing, or over the character size used in the line printer output. Consequently mapping distortions are present in the line printer products, particularly when sampling is oblique to the LANDSAT scan lines. To partially overcome this distortion the control points were always established by measuring direction and distance either parallel or perpendicular to scan lines, from a known location. This procedure was used in the analysis of each MSS band's printouts and thus avoided possible pixel misregistration due to the inclusion of the registration fill characters in the production of the CCTs. As a consequence a positional accuracy of ± 2 pixels may be ascribed to the relationship between the ground feature and the CCT-derived radiance. (Each LANDSAT pixel, for the nominal altitude of 920 km, samples an area of 56 m cross track by 79 m along track.)

11.2.3.2 Determination of the Radiance Levels from the CCT Data

The CCT level data were converted to radiance data (in milliwatt per steradian per square centimetre per unit bandwidth) for the following reasons:

1. Small variations in spectral radiance could signify different melt/freeze histories or density regimes in the snow (O'Brien and Munis 1975). For these variations to be assessed and interrelated, it is desirable for the recorded radiances to be expressed in common absolute terms.

2. The low-gain mode in three of the four MSS channels has approximately the same full-scale radiance response, but such is not the case for MSS 7.

3. The CCT data for MSS 4, 5, and 6 are decompressed (range 0-127), whereas the MSS 7 data are in the linear mode (range 0-63).

The unit bandwidths of MSS 4, 5, and 6 are all nominally the same at 100 nm, but that for MSS 7 is nominally 300 nm. This last MSS band spans a number of water vapour absorption bands in the atmosphere, whose contribution is largely uncertain. Consequently the radiance of each band is expressed in "bandwidth" terms rather than in "nanometer" terms.

The pixel radiance values were plotted together with the topographic elevation profile and presented in Figs 11.3, 11.4, 11.5, and 11.6. (The uncertainties in the four MSS band radiances are ±0.03 (mw $ster^{-1}$ cm^{-2} $bandwidth^{-1}$) for MSS 4, ±0.02 for MSS 5, ±0.02 for MSS 6, and ±0.09 for MSS 7.)

11.2.3.3 Criteria for Boundary Selection

The next step was the determination of the snow region boundaries along each transect. Obviously in regions where the snow cover is sparse the uncovered terrain will contribute to the final recorded radiance levels for each pixel.

The realisation that snow will always increase the recorded radiance over that of the basic ground terrain leads to two major criteria for selecting a boundary between terrain and snow and then between types of snow.

(a) "Radiance Block Criterion"

The first criterion involves (i) plotting the frequency of occurrence of radiance values within selected intervals for each MSS band (Fig. 11.7), (ii) noting the groupings of increased frequency of radiance occurrence ("radiance blocks"), and (iii) determining the boundaries to these blocks.

Data from all four transects were used in these plots so that the "radiance block" criterion would apply to both the Mt Robert Basin and the adjacent Six Mile Creek Basin. A three-point running mean of the frequency data is then plotted. Boundaries to each "radiance block" were then chosen after inspection of the three-point running mean plot for each band. They were selected as the minimum value on the lower radiance side of the maxima. A range of at least one radiance sampling interval was assigned to each boundary about the minimum, greater ranges being given to minima having greater radii of curvature. (The maxima or modal values are regarded as being the most frequently occurring within each "radiance block", i.e., postulated snow type.) These "radiance block" boundaries were now further scrutinised in the light of published results on the variation of snow radiances with wavelength.

On the basis of SKYLAB S192 scanner data (spanning the wavelength range 410 nm to 2350 nm) Barnes and Smallwood (1975) concluded that the reflectance of snow decreased with increasing wavelength. Consequently MSS 4 is expected to reveal more variations in the snowpack than MSS 7 (from snow signal to background noise considerations). Thus the "radiance block" boundaries already derived from the MSS 4 data are regarded as the major "radiance block" boundaries for use in snow region boundary determination. In the absence of simultaneous ground measurements we are forced to consider only the gross changes in the three-point running mean plot as being of significance. Accordingly the boundaries advanced in Table 11.2, in particular those from MSS 4, were combined with the second criterion for ultimate boundary selection.

Table 11.2—Snowfield "Radiance Block" Boundaries - from Fig. 7

MSS 4	MSS 5	MSS 6	MSS 7
0.1 - 0.3	0.1 - 0.3	0.2 - 0.4	0.4 - 1.2
0.6 - 0.8	0.8 - 1.1	0.6 - 0.8	
1.0 - 1.2			

units are all (mw $ster^{-1}cm^{-2}$ $bandwidth^{-1}$)

Though three major "radiance blocks" and hence possibly three different snow types are apparent in the MSS 4 frequency data in Fig. 11.7, the number of evident radiance blocks decreases with increasing wavelength. Two, or possibly three, blocks are apparent in the MSS 5 data, two in MSS 6, and one in MSS 7. Barnes and Smallwood's (1975) conclusion on the decreasing reflectance of snow with increasing wavelength, together with the finding of O'Brien and Munis (1975) that denser or wetter snow also exhibits a decreased reflectance, suggests that this observed decrease in the number of apparent "radiance blocks" may be due to different snow conditions. However, in the absence of simultaneous ground truth this contention is regarded as conjectural in this study, but it underlines the need for simultaneous observations.

(b) Radiance Gradient Criterion

The second criterion relies on all bands responding to changing terrain/snow or snow/snow boundaries by all recording increased or decreased radiances together when compared to the previous MSS radiance values, as inspection progresses along the transect. If this trend is maintained in all MSS channels for at least two pixels, in this analysis a "radiance gradient" boundary was allocated to that position along the transect.

Thus, in advancing the location of any snow type boundary along a transect the "radiance gradient" criterion is used first to indicate the likely positions. If the MSS 4 radiance values at the chosen locations along the transect fall within the previously determined "radiance block" boundary ranges and in general satisfy the MSS 5, 6, and 7 "radiance block" ranges, the location is suggested as being a boundary between different snowpack regions.

The Six Mile Creek Basin is regarded as the "control" basin, as the three transect lines spanned a range of sun illumination angles under essentially the same climatic regime. As a final check, the selected boundaries were marked on Fig. 11.3, 11.4, 11.5, and 11.6, and the topographic elevations noted. Within the "control" basin a similar altitude would be expected for the boundary to each class of snow.

11.2.3.4 Boundary Selection

Using the criteria advanced above the boundaries were selected and marked by vertical bars on each of the four transects (Figs 11.3, 11.4, 11.5, and 11.6). The topographic elevations, and the applicable variations, were now read from the plots (Figs 11.3, 11.4, 11.5, and 11.6) and the results are presented in Table 11.3. For transect D-A above 5500 ft inter-band correlation decreased. If the snow had been uniformly denser/wetter, the radiance in all bands would have been expected to show sympathetic variations along the transect. Similarly, if topography had been the sole influence, sympathetic variation in all band radiances would be expected. Such is not the case, and thus, in the absence of simultaneous ground truth, a combination of varying topographic reflectances and wavelength-dependent shadowing effects is postulated as the source of these variations.

Table 11.3—Topographic Elevation (in feet), and Variation of Various Ground Cover/Snow and Snow/Snow Boundaries[1] extracted from the Radiance Transect Plots of Fig. 11.3, 11.4, 11.5, and 11.6

Transect	D-A	D-B	D-C	E-F
Ground/snow	4850 ± 50	4700 $^{+100}_{-200}$	4600 ± 50	4650 ± 50
	A	A	A	A
Snow/snow	5300 ± 50	5200 $^{+100}_{-200}$	4900 ± 150	
	A	A	A	
Snow/snow	5500 ± 50	5650 $^{+100}_{-50}$	5300 ± 50	
	B	A	A	
		Overload obscures extra regions	Overload obscures extra region	

1. These snow/snow boundaries labelled A would seem to indicate less dense/drier history snow at higher elevations. That labelled B could mark denser/wetter history snow at higher elevations.

11.3 FIELD DATA COLLECTION

Several light aircraft overpasses were made to take hand-held oblique colour photographs during September and October 1976. The photographs taken on 29 October 1976 have been used to aid the analysis of LANDSAT CCT (31 October 1975) data. The time lag of approximately one year is partly reconciled by inspection of New Zealand Meteorological Service climatic data for September and October of 1975 and 1976. Monthly summaries of temperature and precipitation for the Lake Rotoiti station (located between the two basins) indicate that there was little difference between the two

years. Monthly mean temperature differences were less than 1°c and monthly precipitation differences were less than 4 mm. Snowfall for Lake Rotoiti station indicates that at the times of both the overpass and the overflight, conditions were similar. One week before each overpass fresh snow fell to the same elevation (2,500 ft). Sun elevation and azimuth angles differ between the overpass and the 29 October 1976 aircraft flight due to the different times. The sun elevation and azimuth were 44° and 65° respectively for the LANDSAT overpass and 60° and 21° for the aircraft flight.

Field data and hand-held photographs were also acquired by one of the authors (AJL) during November 1976.

11.4 INTERPRETATIONS AND CONCLUSIONS

The primary objective of this study, to compare snow conditions in the two basins, has been accomplished using LANDSAT data. Comparison of transects of MSS radiance values from the Six Mile Creek (Fig. 11.5) and Mt Robert (Fig. 11.6) leaves little question that there were great differences between the two basins in the percentage of snow-covered area (see Table 11.1) and the lower elevation of 100% snow cover. The Six Mile Creek Basin transect (D-C) has similar radiance values below 4,600 ft; slightly higher values between 4,600 and 5,000 ft; and much higher radiance values above 5,000 ft than the Mt Robert Basin transect (E-F). It is therefore concluded that the differences in radiance levels indicate a greater areal snow cover in Six Mile Creek Basin, and that the effect of lower radiance values from vegetation/snow regions contributes to the sample within the pixels in the Mt Robert area. Comparison of the two visible bands (MSS 4 and 5) for the two basins demonstrates this difference. Over 50% of the transect in Six Mile Creek Basin has radiance values higher than the maximum radiance values in the Mt Robert Basin.. This conclusion is substantiated by the colour oblique photography of the two basins at different times but, as mentioned previously, with similar snow conditions.

The LANDSAT data can be divided into different radiance/topographic categories that show similarity between transects (Table 11.3). Although a correlation of these numerical categories with natural conditions of snow is deemed possible, confirmation requires simultaneous field and satellite cover.

Several general observations have been made from the data that should help future interpretation of MSS radiance values from snow-covered areas. The most important of these is the effect on the radiance from the snow of local slope angles and orientation along an altitude contour line. The effect of orientation with respect to the sun is evident in a comparison of transects D-A (Fig. 11.3), a south-facing slope directed away from the sun, and D-B (Fig. 11.4), a north-facing slope directed towards the sun. Higher radiance values and even overloading in three bands were recorded for the sun-facing slope. In aircraft photographs taken in September 1976 of the Six Mile Creek Basin, local hot spots from solar reflection appear at several locations along transect D-C. Overloading of the MSS 5 sensor well below the crest suggests that a similar phenomenon has occurred on the satellite overpass, i.e.,

strong solar reflection from a local slope facet resulting in a hot spot.

The area of a snowfield is easily assessed from the LANDSAT data and requires little data manipulation. The snow/vegetation boundary is also easily determined. However, further information may be deduced from the natural breaks that occur in the MSS CCT data. Although not corroborated, in this case, by ground data, the breaks suggest there were variations in snow type, depth, history, or some combination of the three at the time of satellite overpass.

The general increase in radiance values in the three Six Mile Creek Basin transects strongly suggests that the snow is fresher and drier as the elevation increases. This relationship of snow radiance and the condition and/or moisture content of snow was reported by O'Brien and Munis (1975). Along with the natural breaks in the data, this has been used with apparent success to categorise and classify these snow transects into four regions (Table 11.1). The two higher levels are interpreted to be potentially skiable snow; the two lower levels are probably non-skiable, the lowest radiance region being below the snowline.

It has become evident that co-ordinated ground-satellite data collection is necessary for further progress to be made in relating snow type to recorded LANDSAT radiances. Such ground data should be on an areal scale compatible with the LANDSAT pixel resolution and should include data on snow age, density, temperature, and moisture content.

11.5 ACKNOWLEDGEMENTS

The assistance of New Zealand Forest Service staff in all aspects of the field programme and areal planimetry is gratefully acknowledged. In particular the support of Mr R. Hodder, Dr J. Hayward, Mr S. Corboy, and Miss D. Laurenson has aided this study. The study was spurred by the inquiry and interest of Mr A. P. Thomson of the National Parks Authority. The assistance rendered in this pilot study by Dr P. J. Ellis, Mr G. M. Allcock, and Mr A. D. Fowler of Physics and Engineering Laboratory has been greatly appreciated.

11.6 REFERENCES

Barnes, J. C. and Smallwood, M. D. 1975: Synopsis of current satellite snow mapping techniques with emphasis on the application of near infrared data. In: Operational Applications of Satellite Snowcover Observations (NASA SP-391), A. Rango (ed.). Scientific and Technical Information Office, NASA, Washington DC, pp 200-14.

Bartolucci, L. A., Hoffer, R. M., and Luther, S. G. 1975: Snowcover mapping by machine-processing of SKYLAB and LANDSAT MSS Data, In: Operational Applications of Satellite Snowcover Observations (NASA SP-391), A. Rango (ed.). Scientific and Technical Information Office, NASA, Washington DC, pp 295-312.

O'Brien, H. W. and Munis, R. H. 1975: Red and near-infrared spectral reflectance of snow, In: Operational Applications of Satellite Snowcover Observations (NASA SP-391), A. Rango (ed.). Scientific and Technical Information Office, NASA, Washington DC, pp 345-60.

Probine, M. C. Suggate, R.P., McGreevy, M. G., and Stirling, I. F. 1976: Third Quarterly Report LANDSAT II Investigation Programme No. 28230. Physics and Engineering Laboratory Report No. 553. Department of Scientific and Industrial Research, Lower Hutt, New Zealand.

Rango, A. (ed.) 1975: Operational Applications of Satellite Snowcover Observations (NASA SP-391). Scientific and Technical Information Office, NASA, Washington DC, 426 pp.

FIGURE CAPTIONS

Fig. 11.1 Colour-coded isodensitometer image of the MSS 4 positive transparency of part of scene 2282-21252 that was used in assessing the area of snow in the two basins and selecting the location of the transect. Inset: location map for the study.

Fig. 11.2 The location of transect lines for CCT radiance comparisons in the Mt Robert and Six Mile Creek Basins. The shaded area signifies bush. (Note that the location of the CCT radiance transect lines have a positional tolerance of ±2 pixels - see text.)

Fig. 11.3 The variation in MSS radiance along the D-A transect, and the ground topography profile. Suggested snow region boundaries marked by vertical bars.

Fig. 11.4 As for Fig. 11.3 for transect D-B. Overload regions shown as oooooooooo.

Fig. 11.5 As for Fig. 11.4 for transect D-C.

Fig. 11.6 As for Fig. 11.3 for transect E-F.

Fig. 11.7 The differential and three-point running mean of radiance occurrence for each of the MSS bands. (This plot includes the data from all four transects D-A, D-B, D-C, E-F.) (Those radiance values leading to sensor "overload" are plotted immediately above the maximum sensor response level - indicated on the plots.)

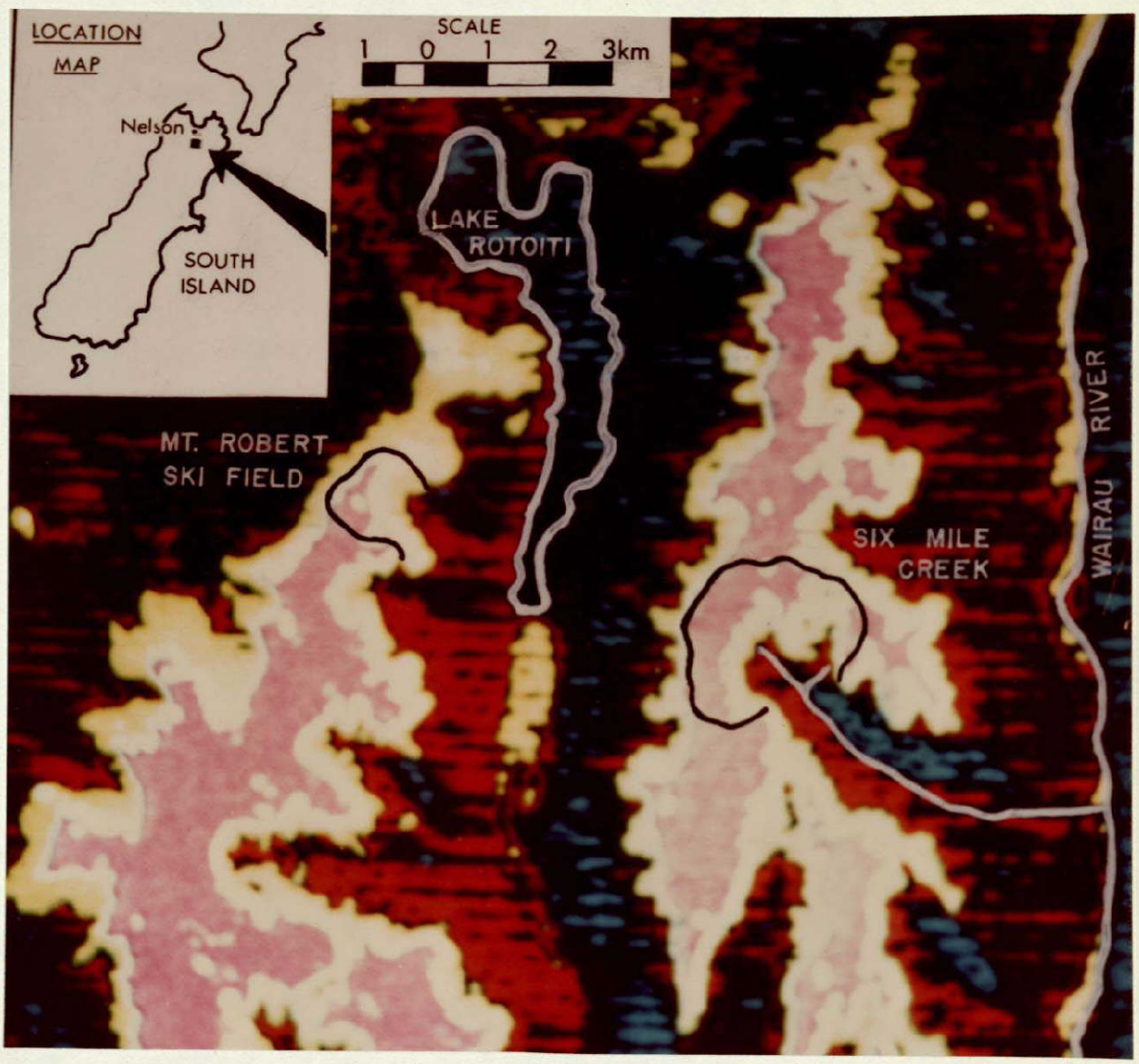

Fig. 11.1 Colour-coded isodemsitometer image of the MSS 4 positive transparency of part of scene 2282-21252 that was used in assessing the area of snow in the two basins and selecting the location of the transect. Inset: location map for the study.

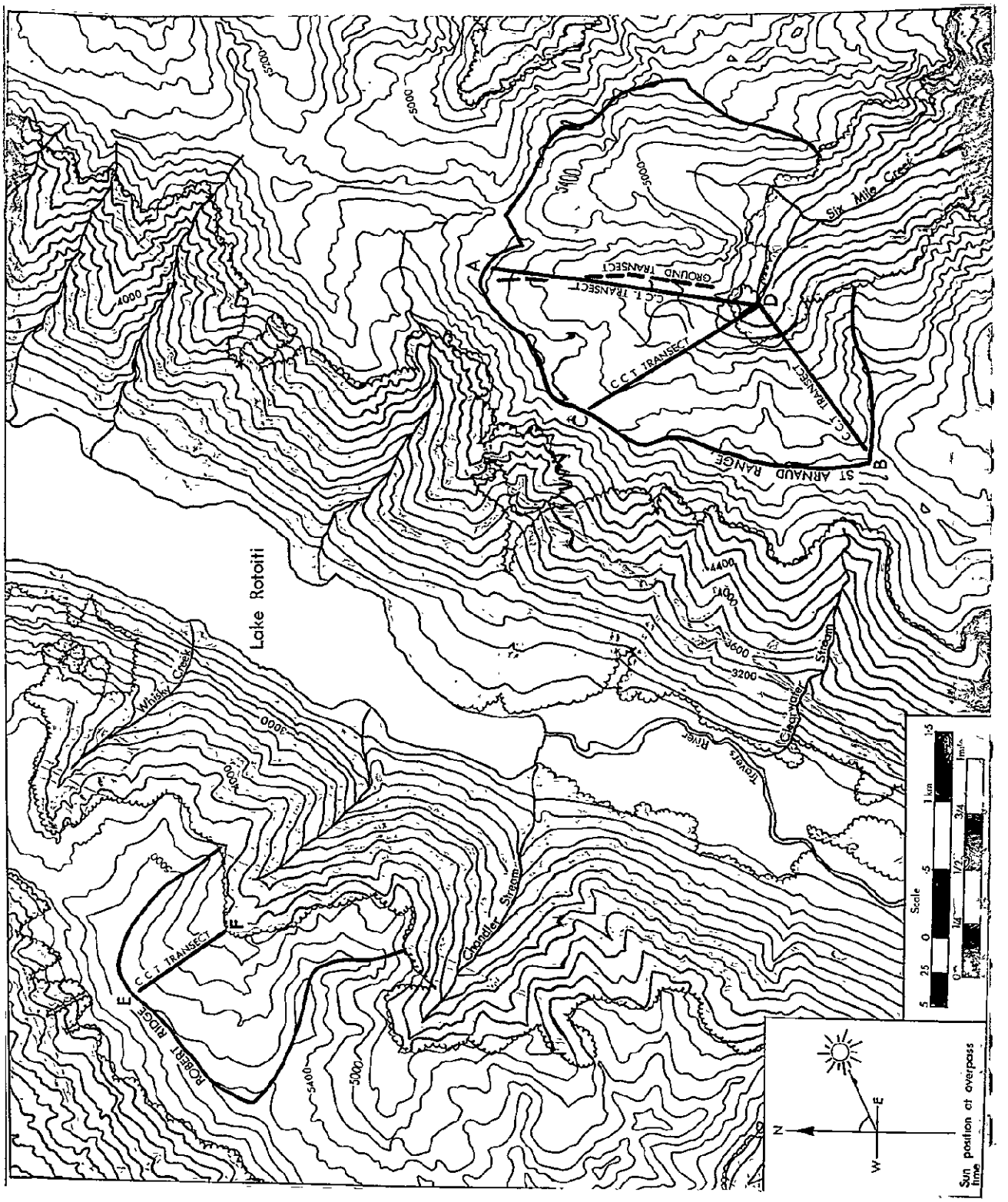

Fig. 11.2 The location of transect lines for CCT radiance comparisons in the Mt Robert and Six Mile Creek Basins. The shaded area signifies bush. (Note that the location of the CCT radiance transect lines have a positional tolerance of ±2 pixels - see text.)

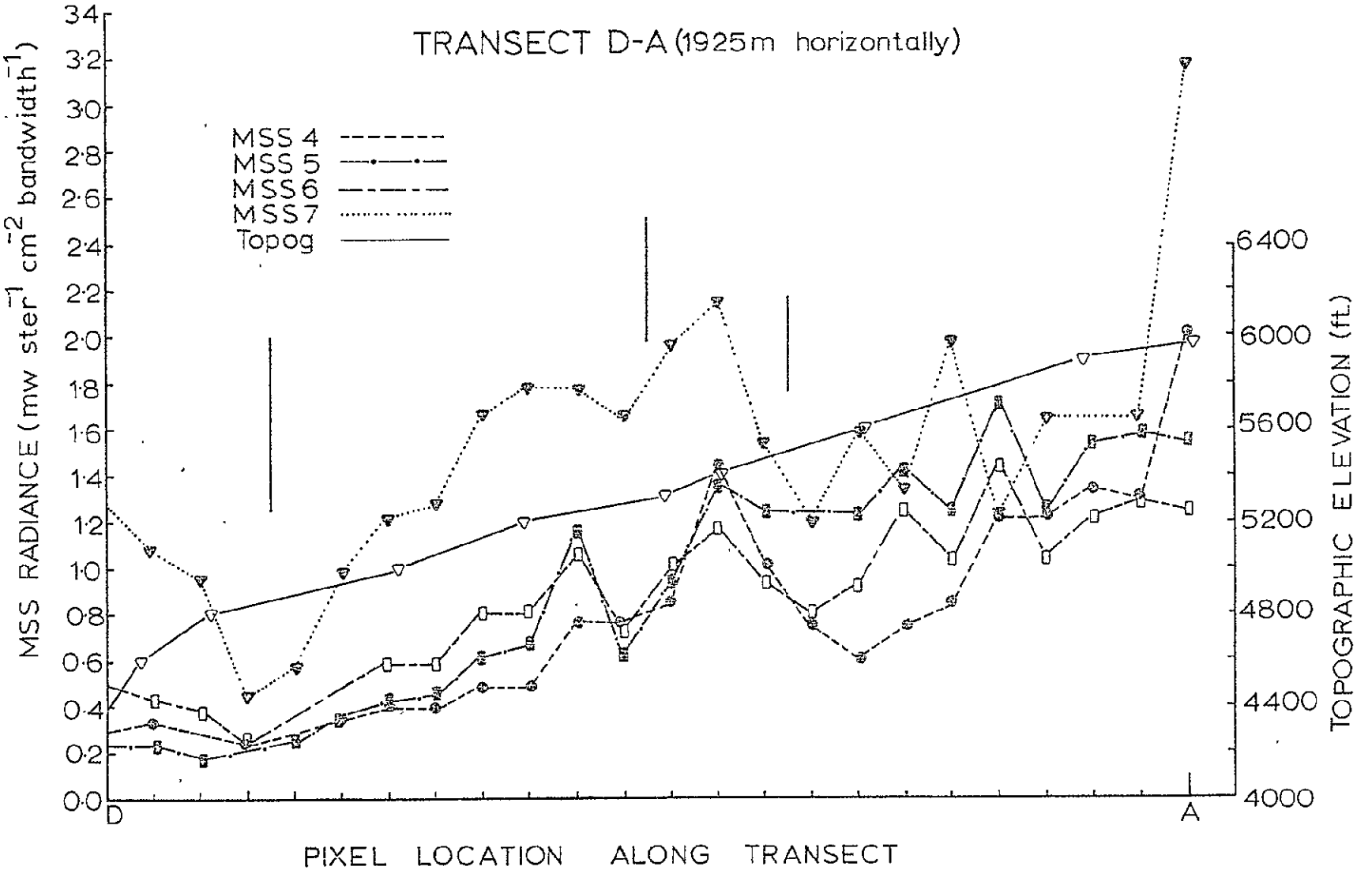

Fig. 11.3 The variation in MSS radiance along the D-A transect, and the ground topography profile. Suggested snow region boundaries marked by vertical bars.

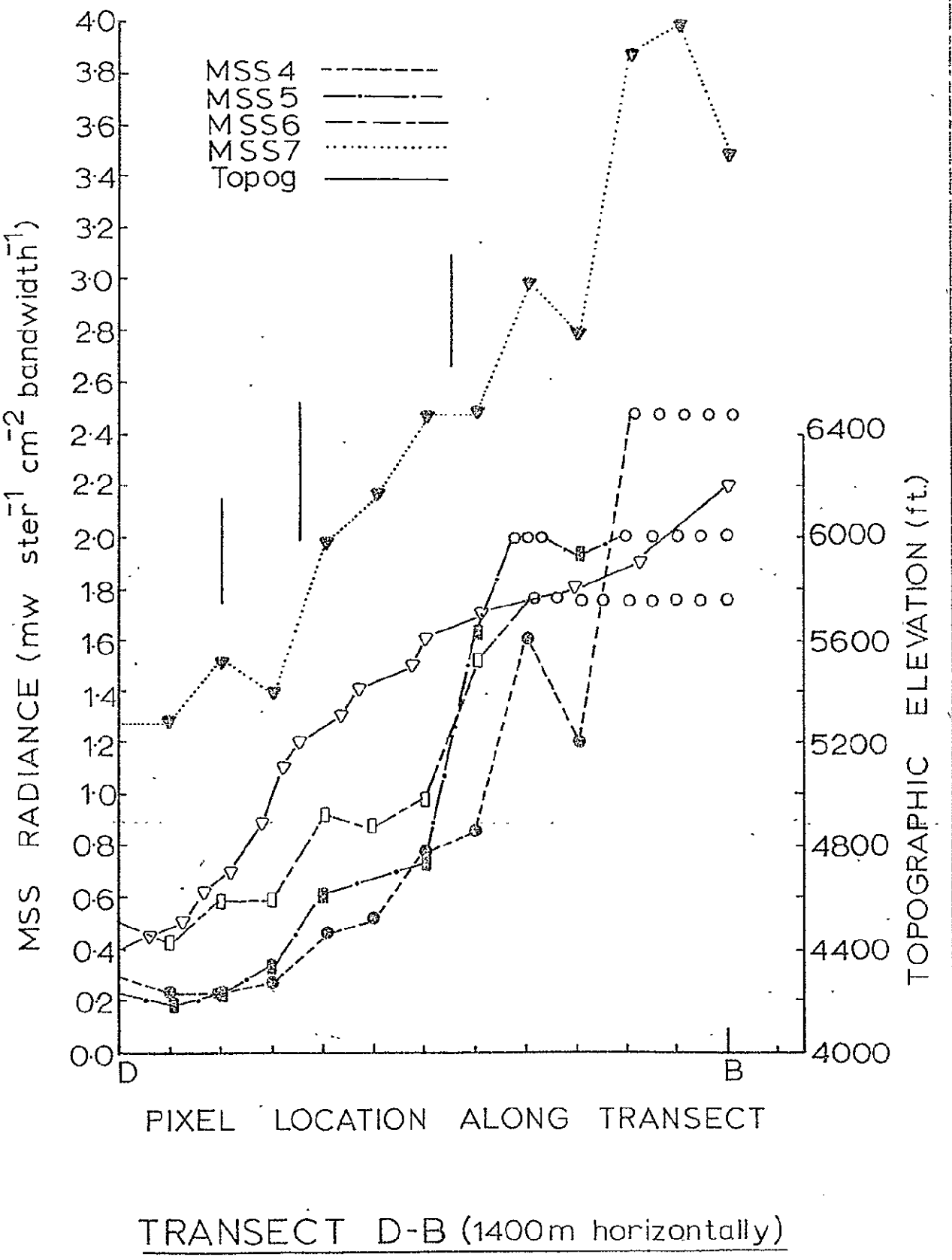

TRANSECT D-B (1400m horizontally)

Fig. 11.4 As for Fig. 11.3 for transect D-B. Overload regions shown as oooooooooo.

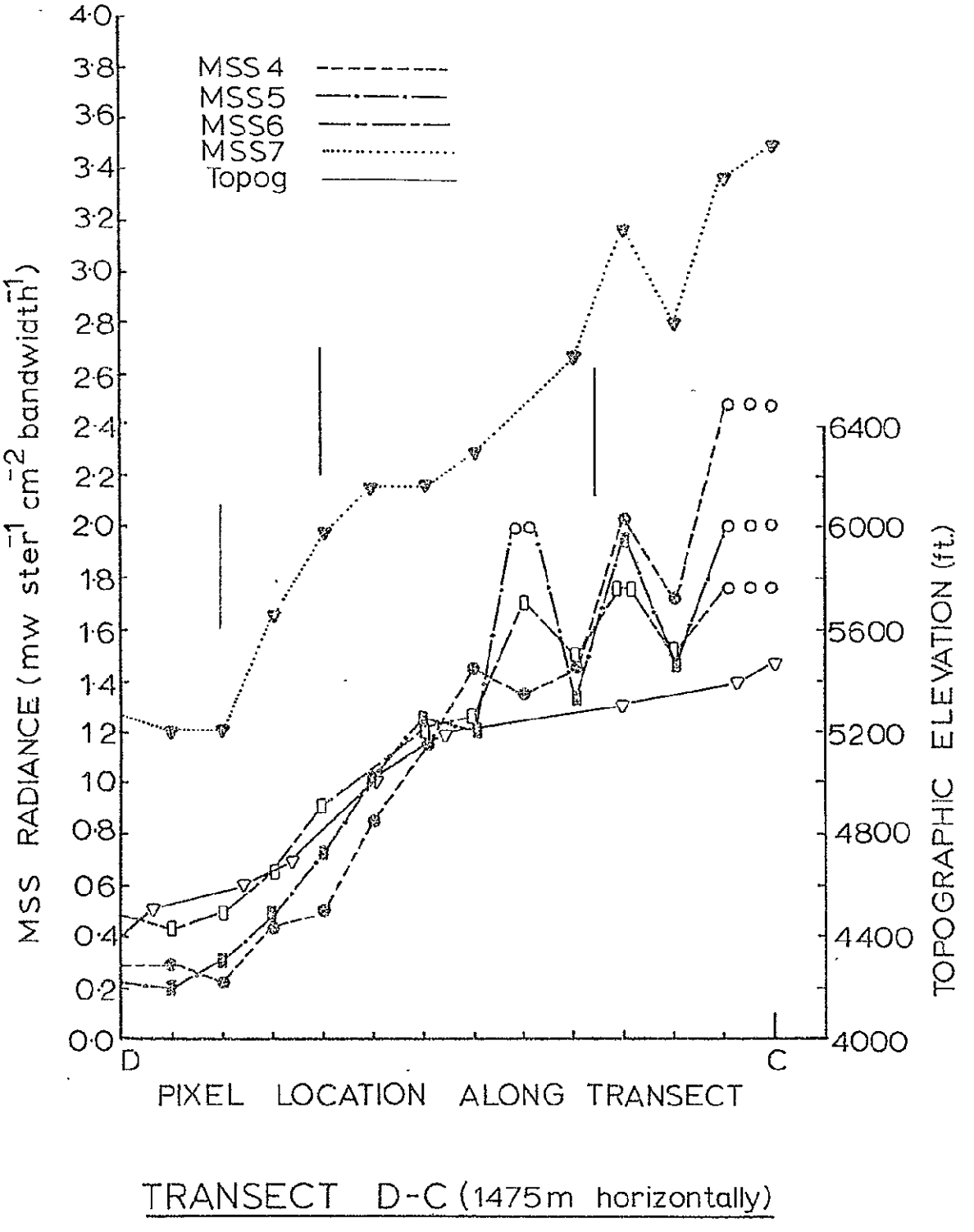

Fig. 11.5 As for Fig. 11.4 for transect D-C.

C 2
91

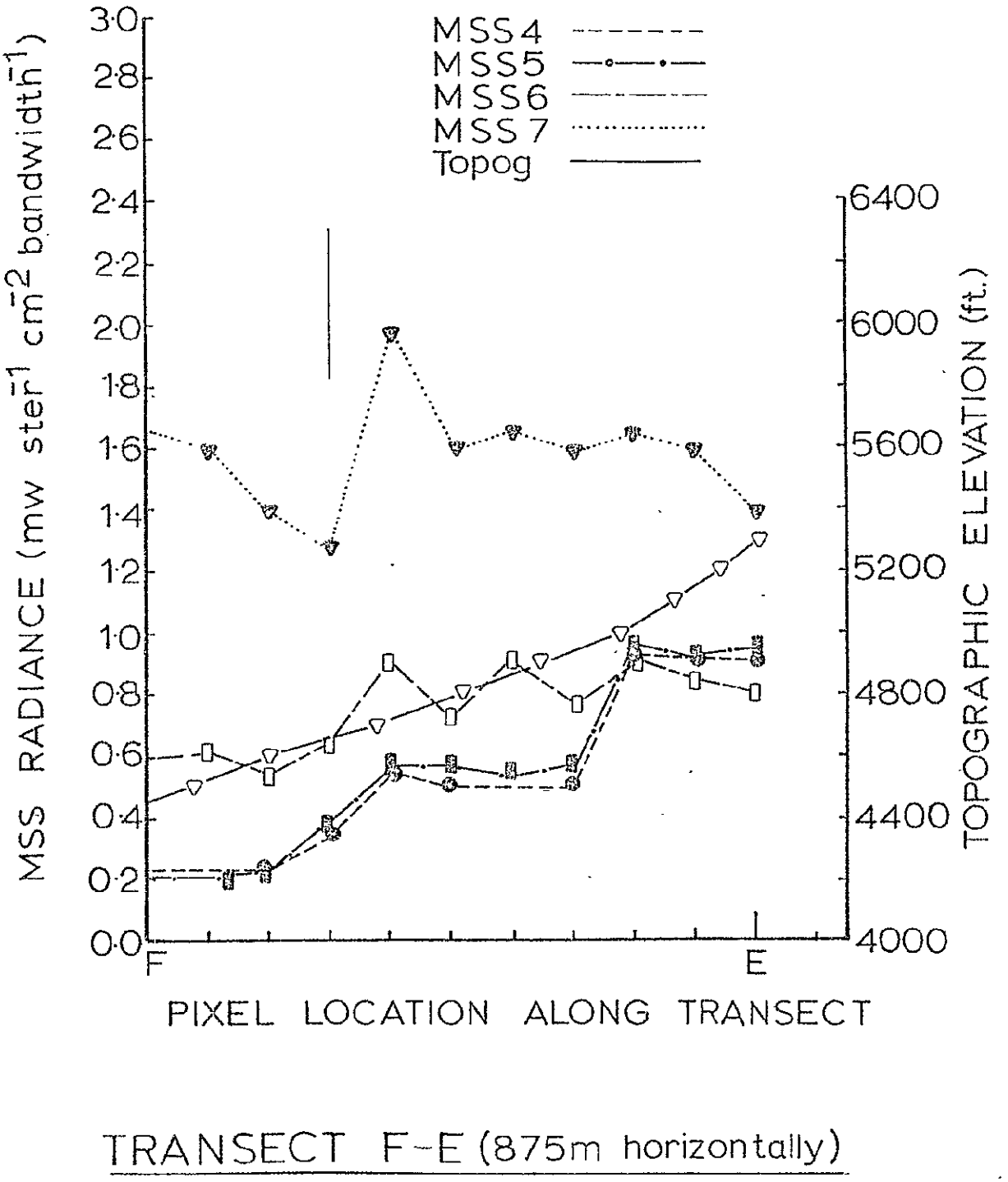

Fig. 11.6 As for Fig. 11.3 for transect E-F.

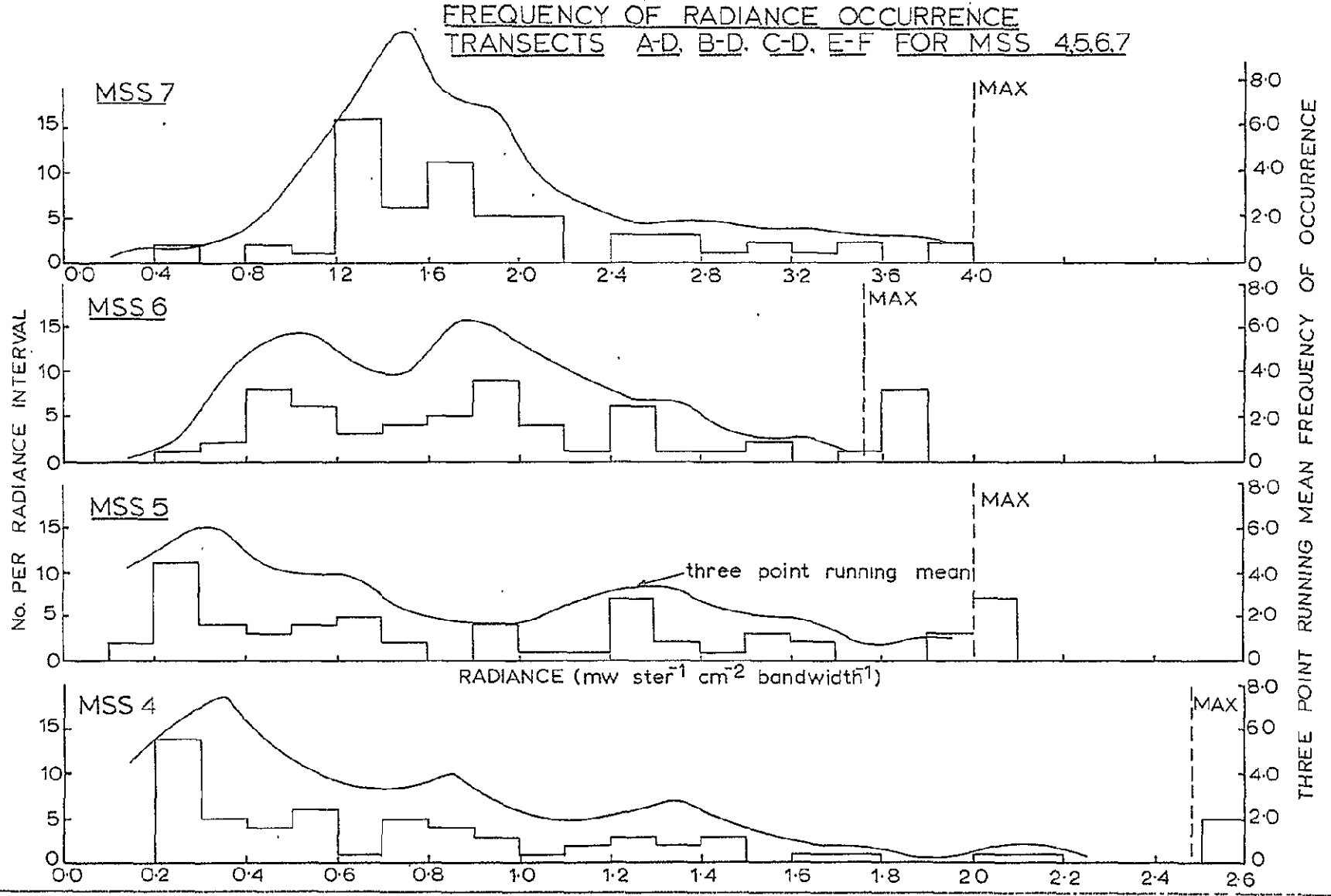

Fig. 11.7 The differential and three-point running mean of radiance occurrence for each of the MSS bands. (This plot includes the data from all four transects D-A, D-B, D-C, E-F.) (Those radiance values leading to sensor "overload" are plotted immediately above the maximum sensor response level - indicated on the plots.)

CHAPTER 12

Sediment/Siltation Monitoring within a Tidal Basin Using Repetitive LANDSAT MSS Computer Compatible Tape Data

I. L. Thomas

ABSTRACT

A feasibility study of the use of repetitive LANDSAT MSS CCT data for monitoring suspended sediment and siltation dynamics in a tidal basin is reported. Repetitive satellite coverage complements and extends available bathymetric and tidal data. Suspended sediment motions may be followed as progressions in both horizontal and vertical extent, using all four MSS bands. It is suggested that the difference between sediment motions and siltation accretion/depletion may be resolved by repeated satellite overpasses. Further work is necessary on the spectral influences of factors such as water turbidity and salinity upon the recorded radiances, as a function of water penetration depth. In this study penetration depths of 45-50 cm and 10-15 cm were found for MSS 5 and 6 respectively for such a sediment-laden tidal inlet.

12.1 INTRODUCTION

The spatial resolution required to monitor motions of suspended sediments or siltation changes within tidal basins is often compatible with that attainable using LANDSAT 2 MSS data. Such data have been used in many studies on the motions of sediment and the mapping of coastal currents, where the sediment plumes are used as the "tracer" (Carlson 1974; Klemas et al. 1974; Ritchie et al. 1976; Stortz and Sydor 1974, and others). However, little, if any, attention seems to have been directed at monitoring siltation accretion or depletion through the use of LANDSAT imagery.

The resolution in water depth necessary for siltation studies is often much finer than that attainable from published bathymetric charts and predicted tidal states; particularly if tidal lags are produced within a tidal basin by bottom topography. The various LANDSAT MSS bands penetrate water to different depths, yet little, if any, work using this instantaneous "snapshot" capability in the monitoring of sediment/siltation dynamics has been reported. An advantage of a platform such as LANDSAT over an aircraft is the small maximum off-vertical incidence angle possible with the resultant decrease in the refractive effects within the water target area. (In the case of the LANDSAT MSS system this angle is approximately 5.7°.)

Stortz and Sydor (1974) used single-band MSS 5 radiance data extracted from the Computer Compatible Tape (CCT) products in relating 600-700 nm reflectance to turbidity. Such CCT radiance data are superior to photographic densitometric data for sediment profile mapping, as they:

(a) are first generation data which may be directly related to scene radiance; and
(b) are free of the recorded radiance compression around the low intensity/low photographic negative density "toe" on the film response curve.

Another factor of importance in monitoring sediment profiles within a tidal basin is the saline/fresh water distribution. Stortz and Sydor (1974) found that such mixtures could lead to differing inferred penetration depths when using MSS sensing.

The objectives of the present study are:

i) To investigate the feasibility of using repeated satellite coverage to reduce the dependence on bathymetric charting over extended areas and thus to complement conventional techniques.
ii) To gauge the effectiveness of LANDSAT MSS four-band monitoring of suspended sediment motions as a function of depth.
iii) To ascertain if LANDSAT MSS dynamic range resolution could yield information on siltation accretion/depletion dynamics from repetitive satellite overpasses.
iv) To pose questions that should be answered in future similar studies on a tidal basin.

CCT data were thus used to monitor the motions and approximate structure of sediment patterns along a transect line for two stages in a tidal cycle within Pauatahanui Inlet, New Zealand (41° 06'S, 174° 54'E).

12.2 ANALYSIS

The scenes selected and the factors applicable to them are given in Table 12.1.

The tidal data were derived from material made available by Heath (1977). The tidal influence will obviously be modified within the basin, but similar tidal heights with dissimilar tidal states were chosen to aid in monitoring possible sediment pattern changes, although it is realised that some two months separated the available scenes.

Coded picture printouts were prepared on a line printer from the CCT data processed on an IBM 370/168 using the programs discussed by Thomas (1977).

TABLE 12.1

The LANDSAT Scenes Used in this Study and Factors Pertinent to the Conditions for Each Scene.

Scene No.	2281-21194	2334-21132
GMT Date	30 Oct 1975	22 Dec 1975
GMT Time	2120 GMT	2113 GMT
Predicted tidal parameters at inlet entrance		
Height	0.6 m	0.6 m
Previous tide to overpass time	High	Low
Time of previous tide	1730 GMT	1900 GMT
Time difference overpass/ tide turn	3 h 50 m	2 h 13 m
Tidal state	Ebbing	Flooding
Tidal range	1.1 m	1.1 m
Rainfall recorded at Porirua - adjacent to Pauatahanui		
During previous 4 days before overpass	0.0 mm	0.0 mm
During previous 5 to 8 days before overpass	43.4 mm	22.0 mm

As CCT products are not normally corrected for altitude/attitude variations between overpasses, the extracted transect profile data must be tied to recognisable ground control points. With water/land boundary monitoring this is easily accomplished. Better identification is usually achieved by using a sharp land protrusion into the water than a water incursion into the land mass. (The water line within a creek's entrance to such an inlet is more sensitive to tidal state. This degrades its usefulness as a reference over unknown and varying tidal conditions.) The transect for this study was taken between two land protrusions 2150 m apart (Moorehouse Point and the shoreline below the Ration Point Trigonometrical Site). The surveyed bathymetry chart (Irwin 1976) provided the topographic and bathymetric data for this investigation. Using the charted distance between the two transect control points, the topographic location of a particular picture element's data was readily established. Such identified ground control points overcome the problems of correcting for scale and orientation changes introduced by the different spacecraft altitude and attitude parameters - influences that are present in the raw CCT data. The positional accuracy of a particular element depends on the identification accuracy of the ground control points. In this study it is believed to be ± 1 picture element (pixel). (For LANDSAT 1 and 2 a picture element samples a ground area of approximately 56 m in the cross-track direction, by 79 m in the along-track direction, at a nominal satellite altitude of 920 km (Thomas 1973).)

The MSS 4, 5, 6 CCT data are expressed in the decompressed mode; those of MSS 7 are stored on the CCT in the linear mode. (See Thomas (1973) for a discussion on CCT data handling.) For this work this difference may be neglected, as MSS 7 has almost no water penetration capability and merely delineates the waterline. As the MSS 4, 5, and 6 channels all have similar maximum radiance levels in the low gain mode, it was deemed unnecessary here to convert the data from the decompressed CCT levels to absolute radiance levels.

After identification of the ground control points on the CCT printouts, CCT level profile plots for each MSS band were prepared for the two LANDSAT scenes under study. These are presented as Figs 12.1 and 12.2. From the data of Irwin (1976) the bathymetry profile for the same transect was prepared and used as the base for Figs 12.3 and 12.4. Each of these plots was prepared to the same horizontal distance scale to facilitate overlay comparisons.

Fundamental to the use of such CCT data for water penetration monitoring is the assumption that the four MSS bands penetrate water to different depths and that the minimum CCT level, within experimental uncertainty, marks that region of maximum penetration. The presence of suspended sediment, or shallower water, will lead to a higher radiance level being recorded. If such a trend in CCT levels for the same location is preserved over two or more scenes for different tidal states, the recorded feature is assumed to be a bottom feature. Any features which are variable from one scene to another are regarded as resulting from dissimilar amounts of suspended sediment. Of the four MSS bands it is further assumed that MSS 7 penetrates water the least (effectively zero penetration) and thus can be used to define the instantaneous waterline contour.

Each of the two scenes (2281-21194 and 2334-21132) was now considered independently. The first step in relating the CCT radiance level to suggested sediment patterns was to determine the location of the waterline on the topographic relief profile at the time of satellite overpass. The minimum radiance "plateau" of MSS 7 in each case was drawn on transparent material and overlaid on the bathymetry profile. The contour where this plateau intersected the bathymetric profile was regarded as the waterline at overpass time. This avoided any knowledge of tidal height or absolute bathymetric depth. Rather it relied on an accurate relative bathymetric profile. The position of the arbitrarily located horizontal reference line on the radiance overlay was now transcribed to the bathymetry profile figure. By moving the radiance profile up and down, with the above two reference lines retaining their superposition, the locations on the bathymetry profile where the minimum radiance plateaus for MSS 6 and 5 intersected that profile were located. These MSS 6 and 5 minimum radiance plateaus were sought within the limits of experimental uncertainty (± 60 m in distance along the transect and ± 2 CCT radiance levels in intensity). (MSS 4 exhibited no such plateau, thus confirming the greater water penetration possible in this band, exceeding the clear water depth of Pauatahanui Inlet.)

Following this determination of penetration depths a qualitative sediment profile was now sought. (Such a profile based on the reflected radiance from the sediment can obviously tell us nothing of sediment particle densities or distributions without further correlated ground/satellite studies. The profiles here advanced thus refer only to a qualitative sediment location that corresponds, in each MSS channel, to the maximum radiance recorded for that pixel.) In building up such a profile for each MSS band it is assumed that "a radiance level above that of the minimum radiance plateau is indicative of sediment being present between the maximum depth of penetration in that band and the surface." By considering the channels in the order MSS 6, 5, 4, a qualitative sediment profile was built up for both LANDSAT scenes under study. These profiles are plotted in Figs 12.3 and 12.4.

12.3 RESULTS AND DISCUSSION

On comparing Figs 12.1 and 12.3 (scene 2281-21194) and then Figs 12.2 and 12.4 (scene 2334-21132) it is evident that though the gross features show correlation between radiance bands, the fine structure is correlated only in part. Sediment is of varying composition, as is also the saline/fresh water distribution. An investigation into the wavelength dependence of the attenuation and scattering properties of this complex medium may resolve these non-sympathetic variations.

The sediment profiles portrayed in Figs 12.3 and 12.4 should not be taken as representing profiles of homogeneous sediment. The spectral studies suggested above would also add to the first-order analysis reported here.

It became rapidly apparent that if studies are being conducted in clear water, an accurate relative bathymetric profile at some location spanning the penetration depth range of the MSS sensors

is sufficient to allow the waterline and the other MSS band depths to be determined. This then quickly allows the bathymetric profile to be extended from the control location. If suspended sediment or varying saline/fresh water concentrations are believed to be present, repetitive satellite coverage at differing stages in the tidal cycle could aid in resolving the underlying bathymetry - within the limits of the spacecraft sensors.

The presence of suspended sediment may be differentiated from siltation changes by comparing two sediment-modified depth profiles at differing stages in the tidal cycle (cf. Figs 12.3 and 12.4).

On the ebbing tide (Fig. 12.3) sediment is concentrated near the surface between the 400 and 1000 m positions. (Distances taken from Moorehouse Point.) (The egress to this tidal inlet is, broadly, in the negative "x - axis" direction. Within such a tidal inlet any fill/empty cycle will be modified by bottom topography, and indeed wind patterns, leading to different circulation patterns for different tidal states.) With the flooding tide, Fig. 12.4, the surface sediment has apparently moved further into the inlet to between the 1300 and 1800 m positions. (This region samples the outlet from the Horokiwi Stream, one of the streams that feed the inlet. However, as no rainfall had fallen in its predominantly pastoral catchment during the previous four days, it would seem that the detected sediment had been placed between 1300 and 1800 m by tidal motions.) In the absence of simultaneous "water truth" data these motions must remain as suggestions only. However, inspection of later multi-spectral survey air photos and ground observations over differing tidal states confirm the general pattern advanced here.

From Figs 12.3 and 12.4 it would seem evident that no siltation accretion or depletion has occurred in the top half-metre of sensed depth over the period 30 October 1975 to 22 December 1975. Below this level it is suspected that denser sediments slowly follow tidal motions, but this is a one-band (MSS 4) area. "Water truth" can resolve this state of sediment motion or silt accretion/depletion. Future satellite equipment such as the Coastal Zone Color Scanner and/or narrower band, wider spectral range airborne studies would aid such siltation (and other) studies.

As a necessary byproduct of this investigation the penetration depths for such a sediment-laden coastal inlet in New Zealand waters have been determined for MSS 5 and 6 (45-50 cm and 10-15 cm respectively). MSS 7 is assumed to have no water penetration.

Further work on the spectral dependence of irradiance/radiance absorption within a varying salinity water medium subjected to a range of sediment particle sizes and overall densities is necessary for further development in this field. Coincident "water truth" profiling along a control transect and multi-spectral satellite/aircraft sensing are necessary first steps in this progression.

12.4 ACKNOWLEDGEMENTS

Helpful advice from Mr G. M. Allcock, Dr P. J. Ellis, and Dr R. Heath has greatly benefited this preliminary study. Assistance from Miss V. E. New and Mr G. J. Neale during the preparation

of the report is gratefully appreciated.

12.5 REFERENCES

Carlson, P. R. 1974: "Surface currents along the Californian coast observed on ERTS imagery". Proc. Ninth International Symposium on Remote Sensing of Environment, Environmental Research Institute of Michigan, USA p. 1279.

Heath, R. 1977: Private communication. DSIR Oceanographic Institute, New Zealand.

Irwin, J. 1976: "Pauatahanui Inlet Bathymetry 1:5,000" DSIR Oceanographic Institute Chart No. 47, New Zealand.

Klemas, V., Otley, M., Philpot, W., Wethe, C., Rogers, R., and Shah, N. 1974: "Correlation of coastal water turbidity and current circulation with ERTS 1 and Skylab imagery". Proc. Ninth International Symposium on Remote Sensing of Environment, Environmental Research Institute of Michigan, USA, p. 1289.

Ritchie, J. C., Schiebe, F. R., and McHenry, J. R. 1976: "Remote sensing of suspended sediments in surface waters", Photogram. Eng. and Rem. Sensing 42, p. 1539.

Stortz, K. and Sydor, M. 1974: "Remote sensing of Western Lake Superior" Proc. Ninth International Symposium on Remote Sensing of Environment, Environmental Research Institute, Michigan, USA p. 933.

Thomas, I. L. 1977: "Basic programs for accessing and utilising LANDSAT MSS CCT data using the PL/1 language on an IBM 370/168 computer". DSIR Physics & Engineering Laboratory Report No. 566.

Thomas, V. L. 1973: "Generation and physical characteristics of the ERTS MSS System corrected computer compatible tapes", NASA, GSFC, Maryland, USA, Document No. X-563-73-206.

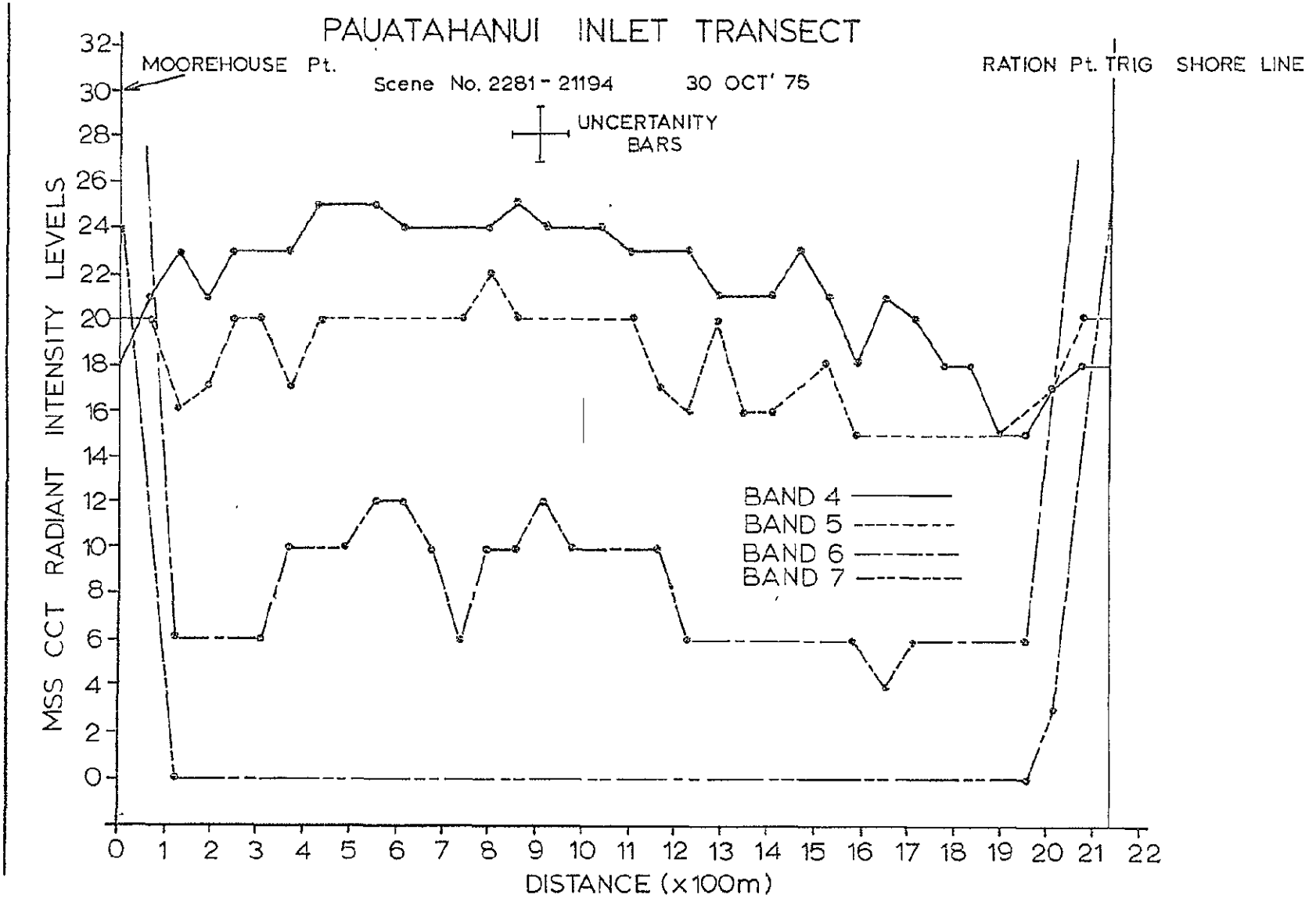

Fig. 12.1 Radiant intensity variations along the transect line for scene 2281-21194. (The vertical line beside the "y axis" is overlay reference line for Fig. 12.3.)

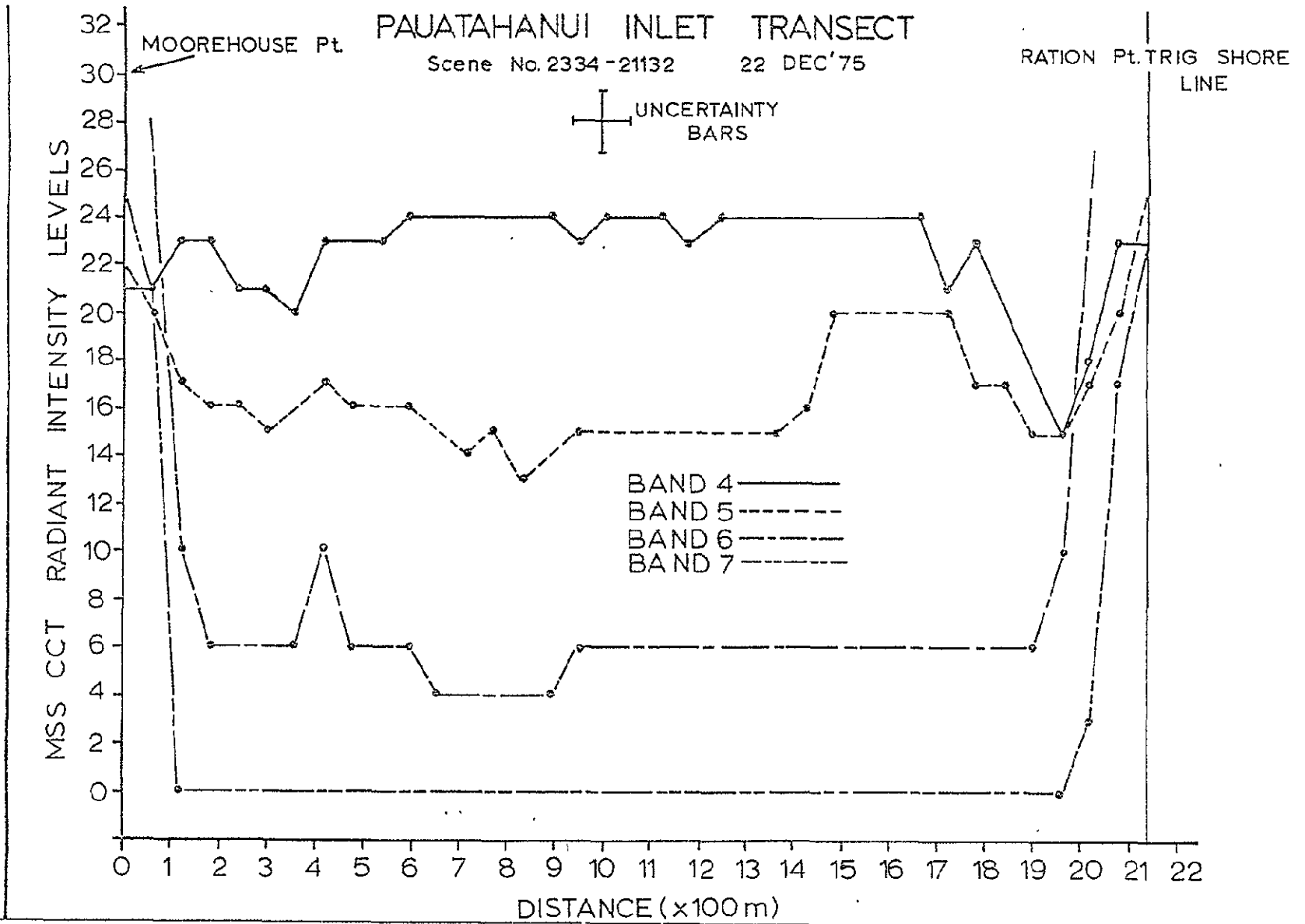

Fig. 12.2 Radiant intensity variations along the transect line for scene 2334-21132. (The vertical line beside the "y axis" is the overlay reference line for Fig. 12.4.)

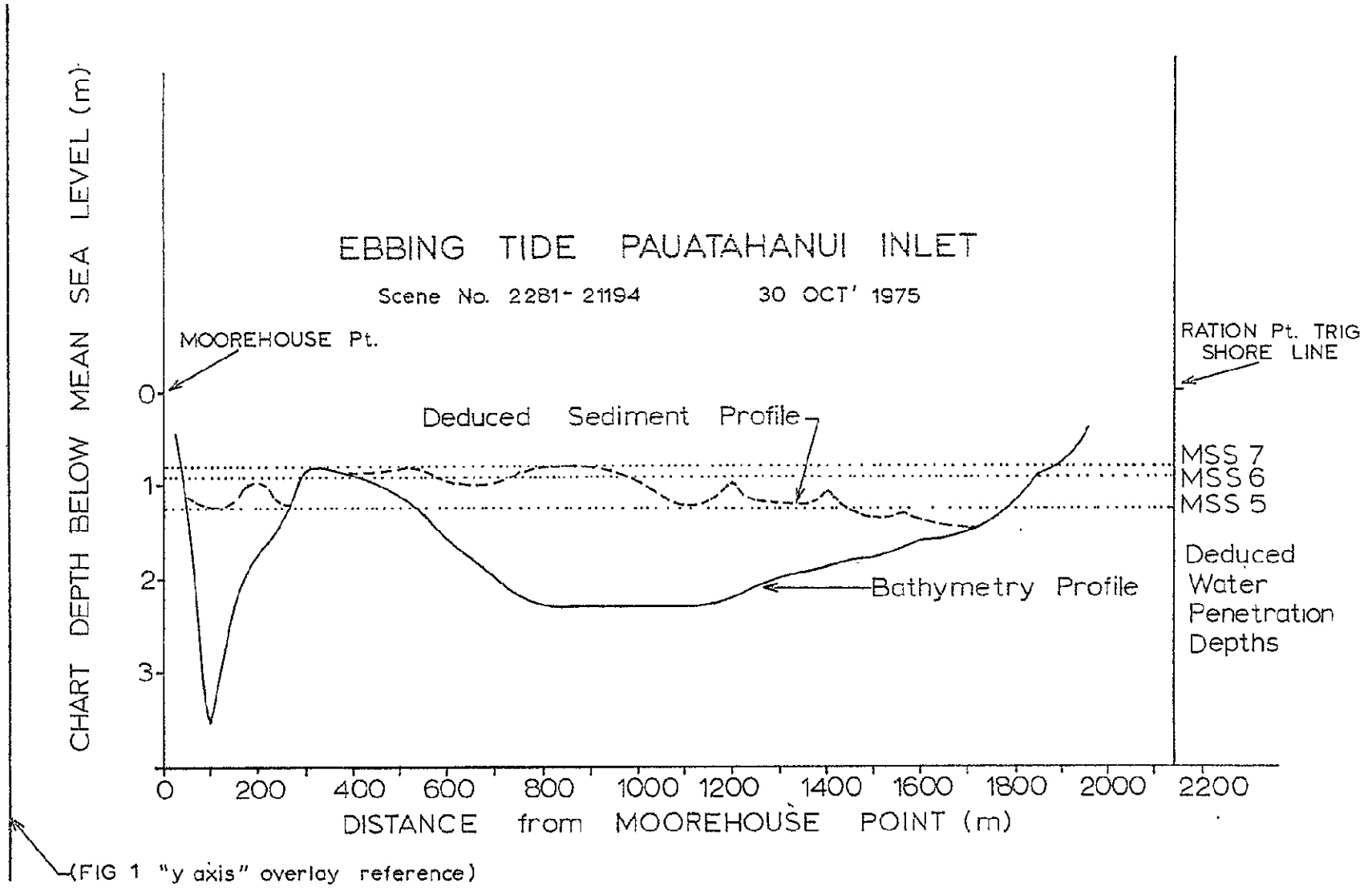

Fig. 12.3 Sediment profile deduced from Fig. 12.1 (bathymetry profile from Irwin, 1976) (Water penetration depth scale is identical to "Chart depth" scale.)

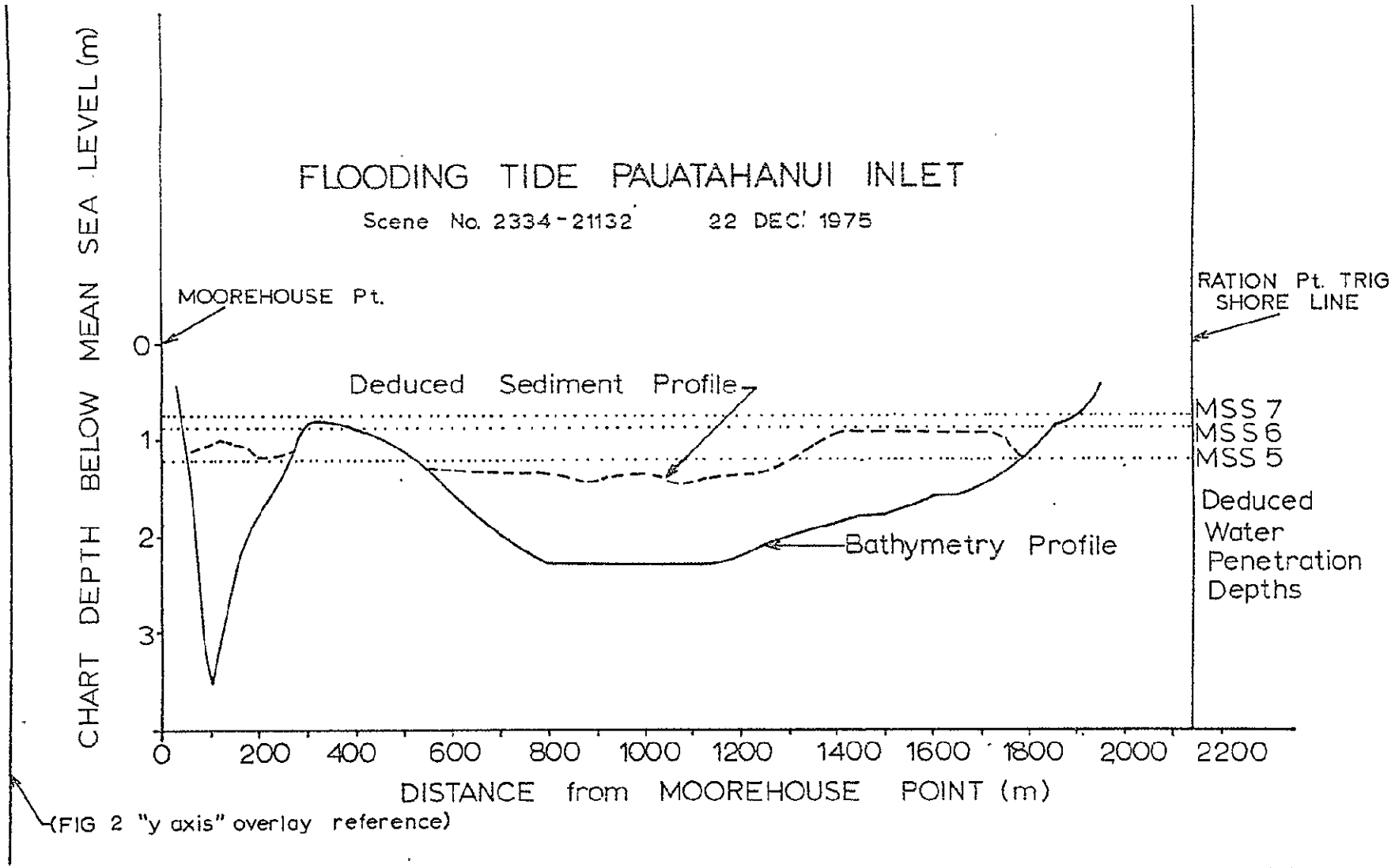

Fig. 12.4 Sediment profile deduced from Fig. 12.2 (bathymetry profile from Irwin, 1976) (Water penetration scale comment as for Fig. 12.3.)

CHAPTER 13

SOME CARTOGRAPHIC APPLICATIONS OF LANDSAT DATA

I L Thomas, R C Child, H A Jefferies,
D McK Scott, A D Fowler, and S R L Richards

ABSTRACT

One of the main cartographic benefits to accrue from the LANDSAT program is the ready ability of the system to monitor change. Updating cartographic data is quickly and economically possible with such almost orthographic imagery. Land use patterns, large man-made developments, and natural coastal changes lend themselves to LANDSAT monitoring. Examples of these are presented here.

As an aid to locating ground features on LANDSAT imagery, a solar reflector program, following on from Evans' (1974) work, is in operation and initial results from the 19 March 1977 overpass are discussed. Suggestions for future developments of this programme are advanced.

13.1 INTRODUCTION

The cartographic applications offered by LANDSAT imagery and the use the data can be put to in the New Zealand mapping programme are being considered and investigated. Tests on the accuracy that can be obtained have been conducted using the photogrammetric instruments of the Lands and Survey Department. In the tested areas the results are very encouraging, especially when compared with the data obtained by conventional methods (see chapter 14). As is usually the case, the aerial photography used for mapping is recorded several years before the map is finally produced. It is at the editing stage that LANDSAT has presented its best potential, when changes due to development can be incorporated.

Work on production cartography is reported in more detail in chapter 14. In this chapter investigations into the more experimental cartographic developments are reported. The results of these developments are then passed on to the relevant users in the cartographic production field for evaluation. Some such techniques have been adopted into the 'production line' and others need further development. It is expected that some of these supportive techniques will improve in quality with

improvements in the LANDSAT product. Here LANDSAT's general application to some of the usual cartographic problems is outlined and its potential commented upon.

Three current research areas, being pursued jointly by the Physics and Engineering Laboratory and the Lands and Survey Department, are then outlined. These are: the use of line overlays to locate features on LANDSAT imagery; the use of the zoom transferscope to compare LANDSAT imagery and maps with different scales, and the use of a solar reflector to identify ground features on the LANDSAT imagery.

13.2 LANDSAT AND SOME ROUTINE CARTOGRAPHIC APPLICATIONS

13.2.1 Point Location

LANDSAT's relatively coarse resolution compared with the accuracy of conventional survey methods (e.g. aerial photography and theodolite) for fixing location reduces its applicability for point fixing. However, the imagery can be useful at the initial planning stage for mapping a study area and to identify areas requiring more detailed and accurate surveys.

13.2.2 Monitoring Change

Using LANDSAT imagery, vegetation patterns, river deviations, new hydro-electric features, and coastal changes can all be edited at the colourproof stage for small scale mapping, (i.e. 1:100,000 scale and smaller) see fig. 13.1. Many New Zealand rivers have wide braided beds and although the water course changes from time to time an attempt is made to indicate the up-to-date position on the map. LANDSAT can be used to good effect as a cartographic guide for such updating.

13.2.3 Hill shading

LANDSAT has been used as an aid in depicting hill shading on topographic maps (see chapter 14)

13.2.4 Relative orientation of offshore features

This is also reported in chapter 14.

13.3 MAP OVERLAY ON LANDSAT IMAGERY

As mentioned in chapter 5, work has been carried out on combining the linework of topographic and resource maps with LANDSAT photographic products at various scales as an aid to the identification of position on the images. This product enables the user of enlarging viewing facilities (e.g. the zoom transferscope) to identify the location of the limited field of view on the image. This technique has been further investigated as a possible cartographic product (e.g. possible production of photomaps of Antarctica for updating the New Zealand mapping.)

Although LANDSAT products are not compatible with the projection used for our larger scale maps, we will soon have the capability and equipment to produce cartographically corrected images (see chapter 8). The combination of these images with line information will be produced as a base for standard resource thematic mapping of land tenure or land system cartography.

An example of the overlay technique used to identify and update the mapping of a new feature is shown in Fig. 13.1. This shows the actual route of a new canal for a hydro-electric scheme. It has been constructed since the time of the aerial photography that led to the map used in the overlay. The lake level has also changed since the time of preparation of the base map. Such monitoring of the fluctuating levels of hydro-electric lakes is an important task that an operational LANDSAT system could possibly perform. The braiding in New Zealand rivers often changes. LANDSAT imagery, such as portrayed in Fig. 13.1, can provide data on the "actual" situation at the time of satellite overpass.

13.4 MAPPING USING LANDSAT IMAGERY AND THE ZOOM TRANSFERSCOPE

13.4.1 Introduction

At the request of Mr J Brodie, Director of the Oceanographic Institute, DSIR (since retired), the Physics and Engineering Laboratory and the Department of Lands and Survey examined a LANDSAT I scene (1449-02355) recorded on 15 October 1973 (GMT), over the Sunda Strait. It contained the known Krakatau volcanic area (6.1°S, 105.5°E). The study had two objectives:

(i) to investigate the practicability of using LANDSAT MSS imagery to monitor potential growth and structural/vegetative changes of an active volcanic area; and

(ii) to establish the location and sea level outline contour of the Krakatau volcanic islets so that repetitive spacecraft coverage could monitor accretion/erosion effects.

LANDSAT I, II MSS areal resolution is generally compatible with the above requirements.

(A brief historical background to the activity of the Krakatau group is included as Appendix 13.1)

13.4.2 Methods

It rapidly became evident that the volcanic material that constituted Anak Krakatau had a very restricted MSS spectral signature. The material was only really evident on MSS 6 products. As a result, a colour composite was prepared where:

MSS 4 negative was printed through a red filter

MSS 6 positive was printed through a green filer

MSS 6 negative was printed through a blue filter

This combination allowed the water penetration properties of MSS 4 to be revealed in the final print and the "single band response" of Anak Krakatau to be accentuated.

To map the location and sea level outline contour of the Krakatau group, black and white enlargements of MSS 6 positive and negative transparencies were printed. These paper prints were viewed on the Department of Lands and Survey zoom transferscope and the outlines traced to a scale of approximately 1:78,000. In preparing this outline map, shown in Fig. 13.2, use was made of the best available (to us) map of the area. This was prepared by the Joint Operations group (1966). An outline of the islets obtained from this map is presented as the dotted contour in Fig. 13.2. By using this 1966 compilation as a mean three point control any slight distortions in the LANDSAT image were searched for. It was found that within the limits of the analysis the three islets in the satellite image surrounding Anak Krakatau were remarkably free of any systematic distortion within, or between, themselves.

MSS 6 negative yielded the print with the most distinct water/land boundary and was used to prepare the outline map.

13.4.3 Results and Conclusions

From the colour composite it was evident that the ground cover differs between Anak Krakatau and the three surrounding islets in the group. Active volcanism would restrict the growth of vegetative cover on Anak Krakatau. Repetitive satellite coverage could monitor the state of such activity. (By comparison with other neighbouring land areas the three islets surrounding Anak Krakatau are assumed to be vegetated rather than possessing different rock structure.)

Figure 13.2 portrays the water line contour for the four islets in the group prepared from the MSS 6 negative transparency at a scale of approximatley 1:78,000. Comparison with published map data (dotted contour) indicates areas of change. It remains for repetitive satellite coverage to reveal whether the minor outline and orientation differences were due to defects in the original survey or to accretion/depletion changes in the islets. Certainly the major changes could be expected to be due to growth/decay changes rather than inaccuracies in the original survey.

LANDSAT has here demonstrated its ability to monitor change on a shipping route. (Sunda Strait carried some 30 M tons of shipping during 1966 - Pergamon World Atlas (1968).) Confirmatory survey work would seem to be desirable.

13.5 LOCATING TOPOGRAPHIC FEATURES IN LANDSAT IMAGERY WITH A SOLAR REFLECTOR

LANDSAT uses passive sensors to record ground detail irradiated by the sun and sky. By increasing the reflected radiance from one picture element, that site can be made more evident in the recorded imagery.

Why mark LANDSAT imagery?

(i) An identified area can be used to distinguish it from similar areas in the surrounding region. (Predicted power level increases can be used to check that the returned signal is that of the reflector.) For rectification of images (see chapter 8) which include large featureless areas of agriculture, forest or snow, etc, a reflector can be used to highlight a known surveyed position.

(ii) Surveying in remote areas can be aided by a "leapfrog" type survey technique laying down the main grid points via LANDSAT imagery. This technique could be particularly useful in the climatically temperamental and logistically expensive Antarctic regions.

(iii) Test plots may be marked and thus located more easily on LANDSAT imagery using reflectors. An agricultural crop test area, or forest test plot etc, may be separated from like surrounding plots by this method. As reported in chapter 4, measurements of solar irradiance and some target radiance data are taken as part of our overall program. In order to relate such measurements, usually taken in the midst of a flat featureless plain, to simultaneous LANDSAT imagery, an identifier for the ground position is useful.

(iv) Monitoring the movement of glaciers (related to the heat budget of a region) is usually accomplished by repeated surveys of markers on the glacier with respect to the surrounding "trigs" on permanent features. LANDSAT imagery combined with suitably designed reflectors on large glaciers, or ice sheets, could allow this movement to be more routinely and economically monitored.

Evans (1974) used a 22 inch diameter mirror to mark imagery of the San Francisco Bay area in November 1972, and studies have continued in the U.S. since that time.

Here we report on the results of a similar program set up in New Zealand to evaluate the concept and to develop operational expertise.

Unhappily the calculations basic to the design and operation of the reflector program whilst not complicated are rather lengthy and must be omitted from this report. Rather, the interested reader is referred to a Physics and Engineering Laboratory Report currently in preparation as a joint project between the Physics and Engineering Laboratory and the Department of Lands and Survey. The fundamental steps in designing such a reflector and its operation are discussed briefly in Appendix 13.2.

The Physics and Engineering Laboratory reflector was operated at Burnt Hill in Canterbury for one overpass which was unfortunately completely cloud covered. Since June 1976, the reflector has been set up for every combination of favourable weather and LANDSAT overpass at the Physics and Engineering Laboratory Auroral Station (45.04°S, 169.68°E).

Of the two confirmed coincident LANDSAT 2 recording overpasses and reflector operation, data has been analysed from that of 19 March 1977 (GMT) only. At the time of writing, the Computer Compatible Tape (CCT) had still to arrive for the 6 April 1977 (GMT) overpass - scene number 2805-21163.

13.5.1 Design of the Physics and Engineering Laboratory Mk 1 reflector

The reflector in use at the Physics and Engineering Laboratory Auroral Station (PELAS) is the Mark 1 version. An improved design is currently being prepared for possible installation in late 1977 at both PELAS and at a site in Canterbury. (The calculations referenced here are for the Mk 1 unit. Those for the later design (Mk 2) are contained in the report under preparation referred to in 13.5.) These "Mk 1" results are presented in Appendix 13.2.

13.5.2 Operation of the solar reflector

The reflector was placed at the Physics and Engineering Laboratory Auroral Station to take advantage of the clear skies more typical of that area than other parts of New Zealand. The station is manned as a field station of the main laboratory. Station staff were trained in the operation of the reflector unit in middle 1976.

For scheduled LANDSAT overpass days the local weather and cloud cover forecast is usually discussed the day before between Physics and Engineering Laboratory, Wellington, and the New Zealand Meteorological Service. The forecasts are based on satellite imagery as well as local information. From this a probability suggestion is telexed to PELAS. On the day of the overpass the operator on the site makes the final decision.

13.5.3 Analysis of the 19 March 1977 overpass data

The reflector was difficult to see on the LANDSAT photographic product for scene 2787-21172, although a faint indication is present in channels MSS 4 and 5.

Table 13.1 Recorded signal increases (in CCT levels) obtained by subtracting the averaged level for the eight nearest neighbour pixels from that for the pixel under study. The search area is that part of scene 2787-21172 strip 2 bounded by scan lines 2263 to 2265 and pixels 18 to 21.

Scan line	Pixel 18	19	20	21
2263	-1	-2	-1	-2
2264	2	2	2	-1
2265	2	1	1	1

Table 13.1.1 Signal increases for MSS 4

Scan line	Pixel 18	19	20	21
2263	-1	-6	-4	-4
2264	1	6	2	-2
2265	3	6	4	4

Table 13.1.2 Signal increases for MSS 5

Scan line	Pixel 18	19	20	21
2263	-1	-2	-2	-2
2264	0	4	4	1
2265	0	4	3	1

Table 13.1.3 Signal increases for MSS 6

Scan line	Pixel 18	19	20	21
2263	0	-1	1	-1
2264	1	2	1	-1
2265	-1	1	1	1

Table 13.1.4 Signal increases for MSS 7

Accordingly, a combination of the photographic and CCT data were studied. (Thomas, 1973, discusses the CCT data product in detail.) Fifty-seven level coded print outs were prepared of the area using the IBM 370/168 (see chapter 6).

The general topography surrounding the reflector site was now identified on the coded print out of the CCT product by reference to the topographic map and the colour composite print. The latter was especially useful as it provided a three channel thematic map of the vegetation in the region. These changes in vegetation were most evident in the MSS 5 coded print-out.

Once the general topography had been outlined on the print-out five readily identifiable control points were located on the photographic colour composite, the coded computer print out, and the map. These five control points were selected to surround the mapped reflector position. They were all located within 5 km of this mapped position and thus removed the need to consider the influences of a changing mirror scan velocity profile in relating the recorded pixel to its location on the ground. (The reflector was sited close to one quarter of the distance along the scan line, a position where this effect approaches the positive maximum.)

Scan line and pixel numbers were allocated to each feature and the distance between features deduced from the difference in these values and the known pixel dimensions. (Allowance was made for scaling changes due to the departure of satellite altitude from the nominal value by comparing the predicted distance with that along a known baseline.)

Following the location of the control points on the print-out, likely areas of signal increase, shown on this print out, were examined. The distance to each of the control points, deduced from the above proposed reflector position's scan line and pixel number, was compared with that derived from the topographic map. In this way the area of signal increase bounded by scan lines 2264 to 2265 and pixel numbers 18 to 21 was advanced for further study.

A numerical print out of the radiance data, expressed in CCT level terms, was now prepared on the IBM 370/168 line printer. The average signal level obtained from the eight nearest neighbour pixels to the pixel under study was obtained and then subtracted from the signal level for that pixel. This yielded the observed signal increases for each pixel in the search area for each MSS channel in turn. These results are presented in table 13.1.

The reflector, if present, must increase the recorded radiance levels in all MSS channels above that of the surrounding terrain. The most consistent increases are seen in pixel 2264/19. These values (2 ± 2 CCT levels in MSS channel 4, 6 ± 2 in MSS 5, 4 ± 2 in MSS 6 and 2 ± 2 in MSS 7) are now compared with the predicted levels calculated in the following section. (Unfortunately, for the reasons outlined in

section 13.5.4, the MSS 6 result had to be used to determine the reflectivity of the unit.) These predicted levels were: MSS 4 - 3 levels, MSS 5 - 5 levels, MSS 6 - 5 levels, MSS 7 - 1 level. (Comment is made on the difference between the actual and predicted MSS 6 levels in section 13.5.5.) On comparing these predicted levels with those presented in Table 13.1 the trend shown in such predicted levels is most evident for pixel 2264/19. This pixel is therefore concluded to contain the reflector.

13.5.4 Calculation of predicted signal levels for the reflector

In section 5 of Appendix 13.2, expressions are advanced for the fractional increase in signal level Q_B and the related increase in number of CCT levels ΔL_B. Here these predicted values are evaluated for the Physics and Engineering Laboratory Mk 1 unit in operation for the 19 March 1977 overpass at the Physics and Engineering Laboratory Auroral Station.

Earlier (chapter 4 of this report) the following values for the mean solar irradiance at the top of the atmosphere for the nominal MSS passbands have been advanced as:

$$_4E_o = 17.70 \text{ mw cm}^{-2} \text{ (for MSS 4)}$$

$$_5E_o = 15.15 \text{ mw cm}^{-2} \text{ (for MSS 5)}$$

$$_6E_o = 12.37 \text{ mw cm}^{-2} \text{ (for MSS 6)}$$

$$_7E_o = 24.91 \text{ mw cm}^{-2} \text{ (for MSS 7)}$$

The atmospheric conditions at the Physics and Engineering Laboratory Auroral Station closely approximate those within a continental land mass (compare the meteorological figures for Alexandra - the closest major town - with those of other centres - chapter 10). In the absence then of simultaneous atmospheric extinction measurements at PELAS for the 19 March 1977 overpass we choose to use the averaged results from Menindee - Lake Tandou reported in chapter 4. Thus we take $\alpha_4 = 0.157$, $\alpha_5 = 0.116$, $\alpha_6 = 0.094$, and $\alpha_7 = 0.143$ - noting however that α_7 is based on only one acceptable result. (See chapter 4.)

The instantaneous field of view of the scanner at the nominal altitude of 900 km used here is 79 m. Hence the instantaneous angular field of view is $5.03 * 10^{-3}$ degrees. This leads to Ω_s having a value of $5.65 * 10^{-9}$ steradian (from the relation

$$\Omega_s = 2\pi \left[1 - \cos\left(\frac{5.03 * 10^{-3}}{2}\right)\right])$$

For the 19 March 1977 overpass the predicted apparent elevation to the satellite from the reflector site (ψ_t) is 87.3° and the apparent elevation to the sun (ψ_s) at 21 h 31 m 30 s is 27.70°.

The reflector is constructed of stainless steel of some 1.5 mm thickness. It rapidly became apparent that this test model, Mk 1, suffered from slight bows and surface variations. This led to a non-uniform spatial radiation pattern. Thus it was decided to evaluate R_B from the observed signal level increase in one band and use that value to predict the signal levels in the other three bands. This assumes that the reflectivity is constant over the MSS wavelength range. Measurements are necessary to evaluate this assumption. Of the available bands central in the MSS range the observed increase in MSS 6 was used to determine this reflectivity value. The relations used are presented in Appendix 13.2 and are repeated below. (Symbolism is discussed in Appendix 13.2.)

$$Q_B = \frac{A_R \, {}_B E_o \, R_B \exp\left[-\alpha_B(\operatorname{cosec} \psi_s + \operatorname{cosec} \psi_t)\right]}{\pi (h \tan \gamma/2)^2 \, N_B \, \Omega_s}$$

and

$$\Delta L_B = \frac{Q_B N_B - {}_o N_B}{N_B - {}_o N_B} * L_B$$

In addition to the values discussed already the following quantities from Appendix 13.2 are used here:

$h = 900 * 10^5$ cm

$\gamma = 5.1°$

$A_R = 1.167 * 10^4$ cm^2 (4 ft diameter)

Table 13.3 contains values for N_B, ${}_o N_B$ and L_B.

From an observed increase of 4 CCT levels in MSS 6 a reflectivity of $R_B = 0.3 \pm 0.1$ is deduced. (This value is "rounded" in line with the error calculation.)

Using the above values in these equations led to predicted signal increases of 3 ± 3 CCT levels for MSS channel 4, 5 ± 3 for MSS 5, 5 ± 3 for MSS 6 and 1 ± 3 for MSS 7.

13.5.5 Discussion of 19 March 1977 solar reflector results

Within the limits of experimental accuracy the reflector has been located and power levels matched between those predicted and actually recorded. These are presented below in table 13.2.

MSS Band	Recorded Radiance Increase (CCT levels)	Predicted Radiance Increase (CCT levels)
4	2 ± 2	3 ± 3
5	6 ± 2	5 ± 3
6	4 ± 2	5 ± 3*
7	2 ± 2	1 ± 3

Table 13.2. Comparison of the recorded and predicted radiance increases for pixel number 19 in strip 2 along scan line number 2264 of scene number 2787-21172 (* MSS band 6 was used to determine the experimental situation reflectivity.)

Obviously there are a number of largely unknown sources of possible disagreement pinpointed in the prediction equations. The major one that we have control over is the mirror reflectivity. The influence of this quantity is emphasised by comparing the actually measured value in MSS 6 and that predicted using the "rounded" reflectivity, rounded in obedience to the error calculation. Further, the requirement that CCT levels be integral necessitates a further "rounding". Before investigating other possible sources of disagreement the beam power diverging from the reflector must be made more uniform. This will be achieved in the PEL Mark II unit presently under design. Unhappily this variation in effective reflectivity demanded the use of the MSS 6 recorded radiance to evaluate the operational value.

Atmospheric extinction coefficients need to be measured too for the PEL Auroral Station.

However, it is interesting to note that the scene centre time for 19 March, 1977, overpass was 21 h 17 m 20-30 s (GMT). Previous imagery was used to determine a mean time for intersect and all alignment calculations were based on this time of 21 h 31 m 30 s (GMT). This wide variation meant that the satellite only caught the edge of the 5.1^{o} divergent beam. Such a variation may also contribute to the low observed power levels from the reflector.

The operational programme has since been modified to allow for similar timing variations but such along-track timing changes for essentially identical scene centres warrants further investigation.

With the above reservations the combined satellite and reflector programme of 19 March, 1977, has provided the encouragement to continue both equipmental and experimental development programmes in this field.

13.6 CONCLUSIONS

It is contended that the main application of LANDSAT imagery to cartographic tasks stems from its ability to quickly and economically monitor topographic change. Land use patterns, scrub/forest boundaries, urban and man-made development, river and coastal changes, etc., all lend themselves to rapid monitoring using currently available LANDSAT systems.

The production of LANDSAT photo maps down to a scale of 1:250 000 is currently possible using the imagery. Photo maps at larger scales can be produced using rectified imagery. Rectification, produced by techniques such as are described in chapter 8, is based on known ground control points. Well-defined natural features can be supplemented by positioned solar reflectors in featureless regions. The initial results from a trial reflector in operation at the PEL Auroral Station are encouraging. Further work using a glass reflector supplemented by ground atmospheric extinction coefficient results is necessary in this field.

The variation in along track timing for repetitive scenes having the same centre co-ordinates is a disturbing feature of the satellite programme and warrants further investigation by ourselves and NASA.

ACKNOWLEDGEMENTS

The work reported here has relied heavily upon the support of many people throughout New Zealand. Chief among these are Messrs. J. Hall and C. Couch of the Department of Lands and Survey, who performed the solar prediction calculations for the programme. The assistance of Dr. P. J. Ellis and Messrs. M. B. Forsyth and R. Eichelsheim of PEL in developing the alignment device, Messrs. D. S. Rowles, B. McNamara and J. G. Keys in the operation of the unit at the PEL Auroral Station and the support of the Chief Surveyors in Christchurch and Dunedin, has been greatly appreciated.

The duty forecasting staff of the New Zealand Meteorological Service in Wellington have continued to furnish the forecasts upon which the operation is based and we are grateful for their help.

Thanks are due also to Mr. J. W. Brodie and Dr. R. Heath of the Oceanographic Institute for framing the Krakatau mapping request to highlight another application of LANDSAT imagery.

During the preparation of this report the work has profited greatly from the suggestions of Messrs. G. M. Allcock and A. B. Trotter of PEL.

122

REFERENCES

Encyclopaedia Britannica (1976) vol. 5, published by Hemingway, London.

Evans, W. E. (1974) "Marking ERTS images with a small mirror reflector", Photogram. Eng. and Rem. Sens. XL p.665.

Furneaux R. (1965) "Krakatoa" published by Secker and Warburg, London, 224 p.

Joint Operations Graphic Ground (1966) 1:250 000 map of East Indies, Series 1501(G), Sheet SB 48-11, Edition 2-GSGS, Compiled 1966, published by U.K. Ministry of Defence 1969.

NASA (1976) "LANDSAT Data Users Handbook" Goddard Space Flight Center, Maryland, U.S.A. Doc. No. 76SDS4258, Sept., 1976.

NASA (1977) "LANDSAT Newsletter" No. 15, Goddard Space Flight Center, Maryland, U.S.A., June 1977.

"Pergamon World Atlas" (1968) published by PWN-Poland, Warsaw, 525 p.

Symons, C. J. (1888) "The eruption of Krakatoa" published by Trübner and Co., London, 494 p.

Thomas V.L. (1973) "Generation and physical characteristics of the ERTS MSS system corrected computer compatible tapes" Goddard Space Flight Center, Document No. X-563-73-206, July, 1973.

Appendix 13.1 History and Activity of Krakatoa (Indonesian KRAKATAU)

May	1680	First known eruptions destroyed all vegetation on Krakatoa. Explosions described as moderate.
Sept	1880	Frequent earthquakes, felt as far away as North Australia. Eruptions seriously damaged Java's First Point Lighthouse.
May 20	1883	Krakatoa erupted again, ash laden clouds reached a height of six miles. Explosions heard in Djakarta, one hundred miles away.
June 19	1883	More violent eruptions occured and continued spasmodically until August 26.
Aug 27	1883	Major eruption takes place as Krakatoa reaches a climax at 10.00 am. Explosions heard 2,200 miles away in Australia.
Aug 28	1883	Activity dies. Minor eruptions occur in the following months and then all becomes quiet.
Dec 29	1927	Renewed activity recorded on seabed where old Krakatoa split and sank.
Jan 24	1928	More eruptions brought a new cone up to sea level. New cone named Anak (child of) Krakatau.
	1929	Further movements bring the islet up to two hundred feet above mean sea level.
Jan	1960	Latest known eruption, lifted Anak Krakatau up to a height of 433 feet AMSL. New cone's rim is some three hundred feet in diameter.

Resulting activity from August 27 1883 Eruption

The immediate area for fifty miles was plunged into fifty-seven hours of total darkness and areas one hundred and thirty miles away saw twenty-four hours of blackness, due to falling ash.

The discharge of Krakatoa sent five cubic miles of rock fragments into the air. Out of the original eighteen square miles of Island, eleven remained, as Krakatoa split and collapsed in on the now empty volcanic core. The resulting submergence created one hundred foot tidal waves that swamped nearby coastal villages and took 36,000 lives. Fine dust, blasted into the upper atmosphere, drifted around for several years, causing spectacular sunsets all over the world.

The fine dust also blocked out solar radiation, dropping the earth's temperature by 0.27°C. One hundred feet of ash and pumice accumulated on Verlaten and Lang Islands. (These developments are discussed further by Symons (1888), Furneaux (1965) and the Encyclopaedia Britannica (1976).)

Fig. 13.4 compares the "before" and "after" outlines of the Krakatoa group.

Appendix 13.2 Design parameters for the Physics and Engineering Laboratory Mark 1 solar reflector

Appendix 13.2.1 Determination of the apex angle of the emission cone

LANDSAT operates to an orbital cross track tolerance of some ±20 km (LANDSAT Data Users Handbook). As currently the only orbital track information available to us are the scene centre nadir locations, a variation of ±40 km must be allowed for in setting up a radiation field at a nominal satellite altitude of 900 km. (Allowance has been made for the proximity of the reflector site to the geolatitude of perigee.) To achieve the 80 km diameter radiation field an apex cone angle of 5.1° was thus found to be necessary. A beam width of 5.1° also allows variations of some ±15 min in along-track timing to be accommodated.

Appendix 13.2.2 Determination of apparent elevation and azimuth of the satellite at the average time of intersect

The ray from the reflector should intersect the mean orbital path at right angles to produce the maximum response in the multispectral scanner.

By analyzing previous imagery an average nadir track was constructed past the reflector site. Spherical trigonometry then readily yielded the nadir location of intersection and the geographic elevation and azimuth from the site to the spacecraft. This data, when combined with the averaged scene centre times, gave the predicted time of intersect. From the imagery available prior to 19 March 1977 the best estimates of the apparent elevation and azimuth from PELAS to the spacecraft at intersect time were 87.3° and 106.2° E of N respectively. The best estimate of the average intersect time was 21 h 31 m 30 s. (All times and dates throughout chapter 13 are expressed in GMT.) The scene studied here (2787-21172) was apparently recorded around 21 h 17 m 20 s. A variation in time in satellite along-track position repeatability thus seems to be present in the March/April 1977 imagery.

Appendix 13.2.3 Determination of apparent elevation and azimuth of the sun at time of intersect

The Computing Branch of the Lands and Survey Department have routinely evaluated the solar elevation and azimuth from the reflector site for the scheduled satellite overpass times and dates. The standard techniques, based on the tabulated ephemeris values and spherical trigonometry, were used in these evaluations.

Appendix 13.2.4 Determination of the apparent elevation and azimuth of the reflector axis to achieve contact with the satellite

This orientation problem is most easily handled by three dimensional vector geometry, with the station at the origin. The reflector axis vector is midway between the vectors to the sun and to the intersection point. This vector must lie in the plane defined by the other two vectors.

Obviously this reflector axis orientation direction will change bweteen overpasses. To aid in these calculations a computer programme in the BASIC language has been written and performs the somewhat tedious calculations to the required accuracy. (At least 8 significant figures must be used in these calculations.)

Appendix 13.2.5 Determination of a relation between irradiance satellite, reflector; parameters and the fractional increase in signal level recorded by LANDSAT 2.

Let the reflector have area A_R cm^2, with reflectivity R_B in the MSS band B under consideration, and be irradiated by a solar flux of value ${}_BE_o$ mw cm^2 at the top of the atmosphere, after passing through the atmosphere, which has an extinction coefficient α_B in band B, at an apparent elevation angle from the reflector site of ψ_s. The fraction of full scale signal level increase Q_B is then given by:

$$Q_B = \frac{A_R \; {}_BE_o R_B \exp[-\alpha_B(\operatorname{cosec} \psi_s + \operatorname{cosec} \psi_t)]}{\pi(h \tan \gamma/2)^2 \quad N_B \quad \Omega_s}$$

where ψ_t is the apparent elevation angle from the site to the satellite,

h is the height of the spacecraft in cm

γ is the apex cone angle

N_B is the full scale satellite radiance level in band B

and Ω_s is the acceptance solid angle of the multispectral scanner optics. (Again a complete discussion is presented in the report under preparation, referenced in 13.5.)

We must now relate this fraction of the maximum signal level Q_B to the expected number of levels ΔL_B on the CCT product. The LANDSAT Newsletter No 15 carried the revised calibration levels for LANDSAT 2 effective from 15 July 1975 (GMT). The radiance values for a zero CCT level are given as ${}_oN_B$ and those for full scale are listed under N_B in table 13.3. The number of CCT levels per band L_B is also presented in table 13.3. The relation between Q_B and ΔL_B is

$$\Delta L_B = \frac{Q_B N_B - {}_oN_B}{N_B - {}_oN_B} * L_B$$

(For our application the base level for the surrounding terrain is subtracted from the level for the pixel suggested as containing the reflector, before deriving the actual Q_B produced by the unit.)

MSS Band (B)	Radiance (mw ster^{-1}cm^{-2})		Number of CCT levels per band (L_B)
	for a zero CCT level ($_oN_B$)	for full scale (N_B)	
4	0.08	2.63	127
5	0.06	1.76	127
6	0.06	1.52	127
7	0.11	3.91	63

Table 13.3 Relation between zero and full scale CCT levels and recorded radiance aboard LANDSAT 2 from 15 July 1975 (GMT). The number of CCT levels in each band is also listed (see chapter 6 for discussion on this point).

Appendix 13.2.6 Design of the reflector and alignment device

In section 1 of this appendix the apex angle for the cone of emission (γ) was determined. To produce such a diverging reflected beam a convex circular reflector is required. For a reflector of diameter d cm this means bowing plane material into the form of a spherical cap. The "height" of the centre above the plane of the edge is x_1 cm. Subsidiary spacers can be located at distances from the centre dependent upon the practically available thicknesses of spacer material. Plane geometry leads to both the relation between d, γ, and x_1 and to the determination of the radial locations for the subsidiary spacers. The central spacer height is thus related to reflector diameter and desired beam divergence by

$$x_1 = \frac{2d}{\gamma^*} (1 - \cos \frac{\gamma}{4})$$

where γ^* is in radian.

Practical considerations limit the size of the reflector and the attainable power levels.

For the Physics and Engin. Lab. Mk 1 reflector a stainless steel sheet was cut to form a circular reflector of diameter 1.22 m (4 feet). As determined previously γ was found to be 5.1° and hence the central spacer height x_1 was deduced to be 6.8 mm. This four foot diameter reflector was placed over concentric rings of 1 mm thick cardboard glued in pyramidal form to the central height of 6.8 mm upon a hardboard baseboard. Operationally this baseboard can be set to the desired elevation using a bubble inclinometer and to the required azimuth by aligning it on surveyed topographic horizon features.

A ready check on the reflector alignment makes use of sunlight reflected off a plane mirror affixed to the baseboard, intercepting a suspended ball, and casting a shadow upon a horizontal screen. The radial distance from the ball's suspension point can be related to the elevation angle to the satellite and once coincidence of the ball's shadow and the predicted position is achieved, the beam is correctly oriented in elevation. A similar technique is to be shortly incorporated to check azimuthal alignment. This alignment device was conceived and developed by P.J. Ellis of Physics and Engineering Laboratory.

In fig. 13.3 the reflector can be seen in operation at PELAS. The circular reflector is evident and the usual operator, Mr H A Jefferies, is adjusting the reflection alignment device.

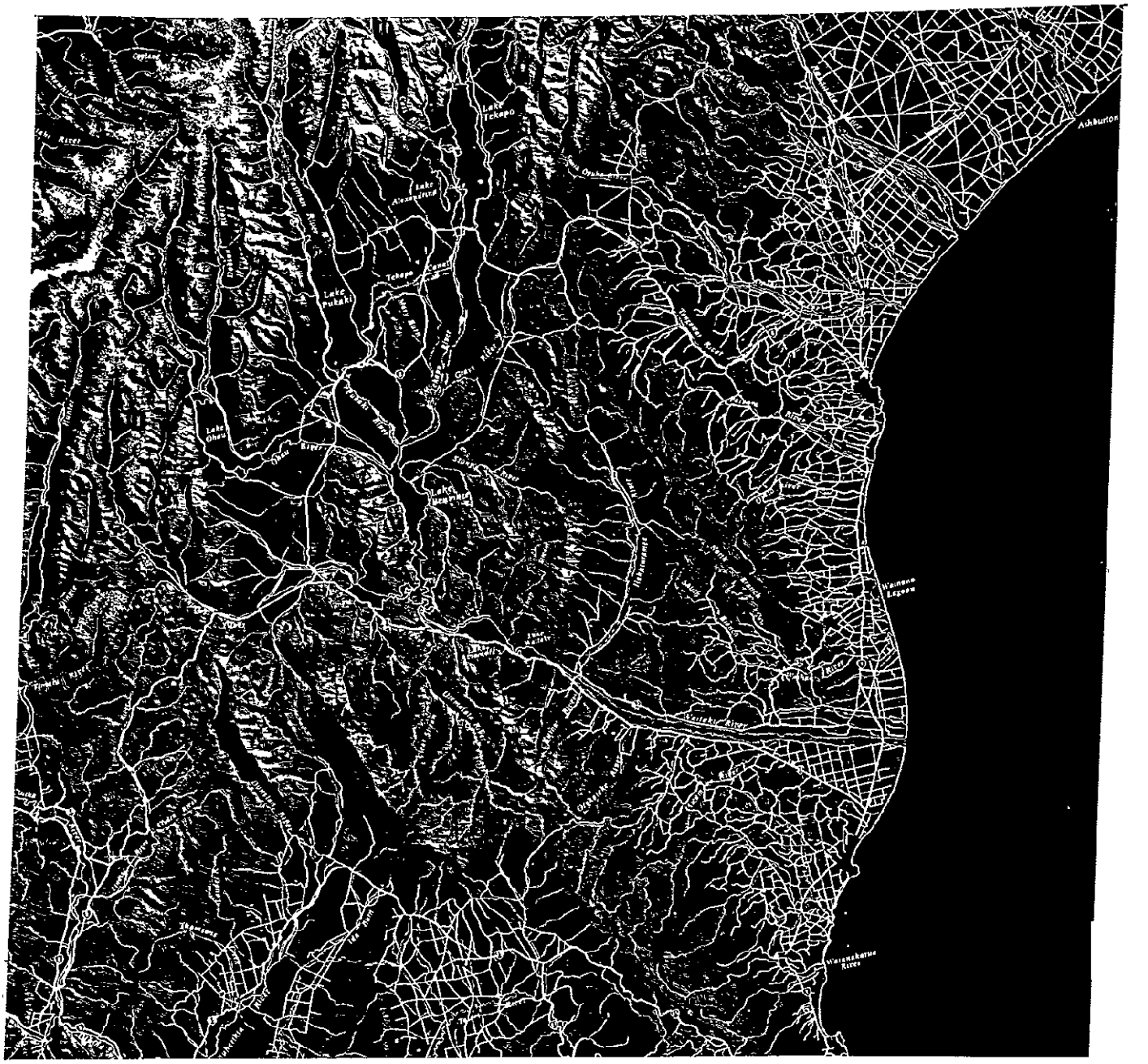

Fig. 13.1 Topographic compilation data at 1:1,000,000 scale combined with LANDSAT scene E-2805-21163 MSS channel 5 indicating changes in hydroelectric lake levels and 'actual' position of Tekapo Canal.

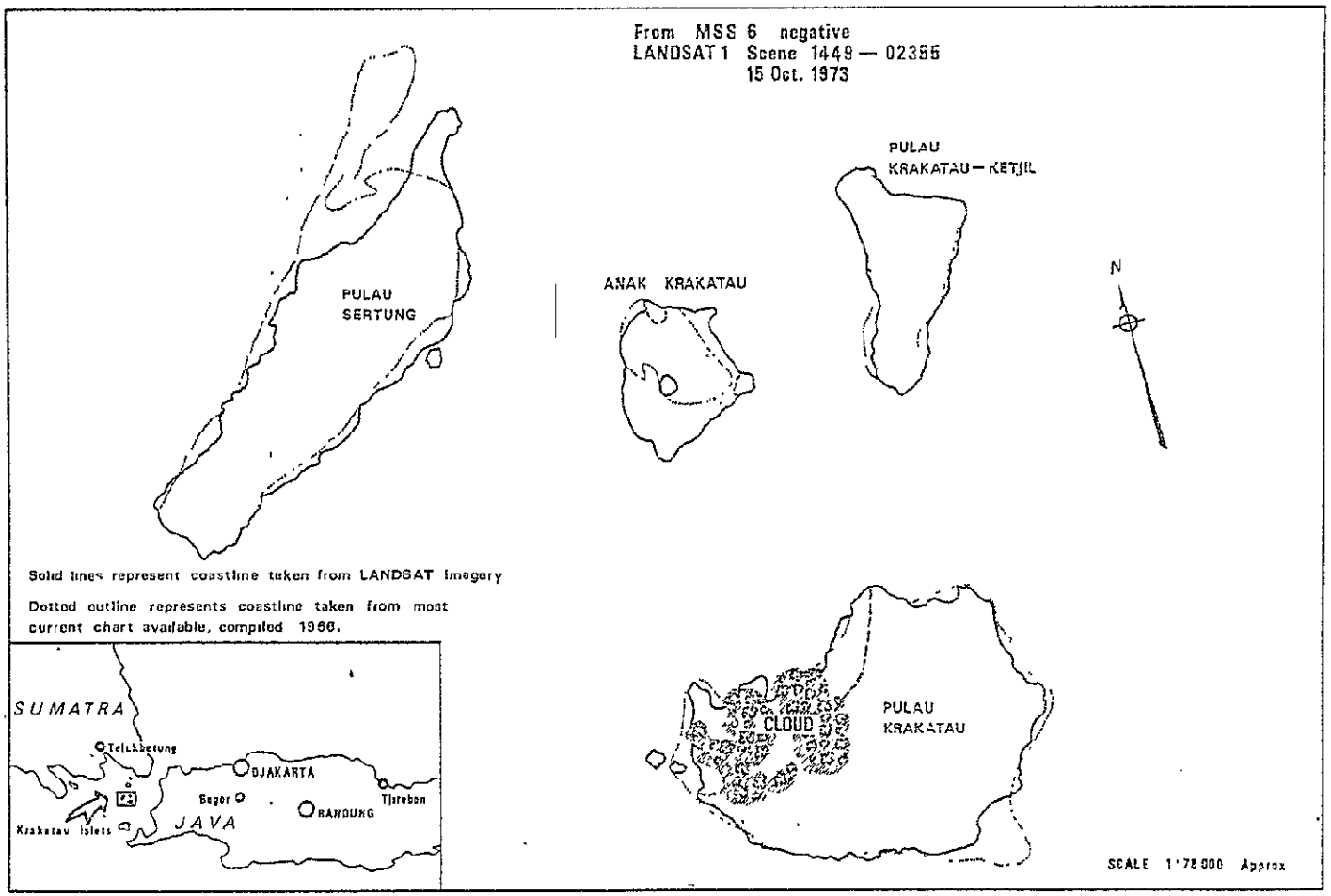

Fig. 13.2 1:78 000 outline map of the Krakatau group prepared from the MSS 6 negative of LANDSAT scene 1449-02355 recorded on 15 October 1973, with a 1966 compilation map contour overlaid in dots.

Fig. 13.3 The solar reflector in operation at the Physics and Engineering Laboratory Auroral Station with the usual operator, Mr H A Jefferies adjusting the reflector alignment device.

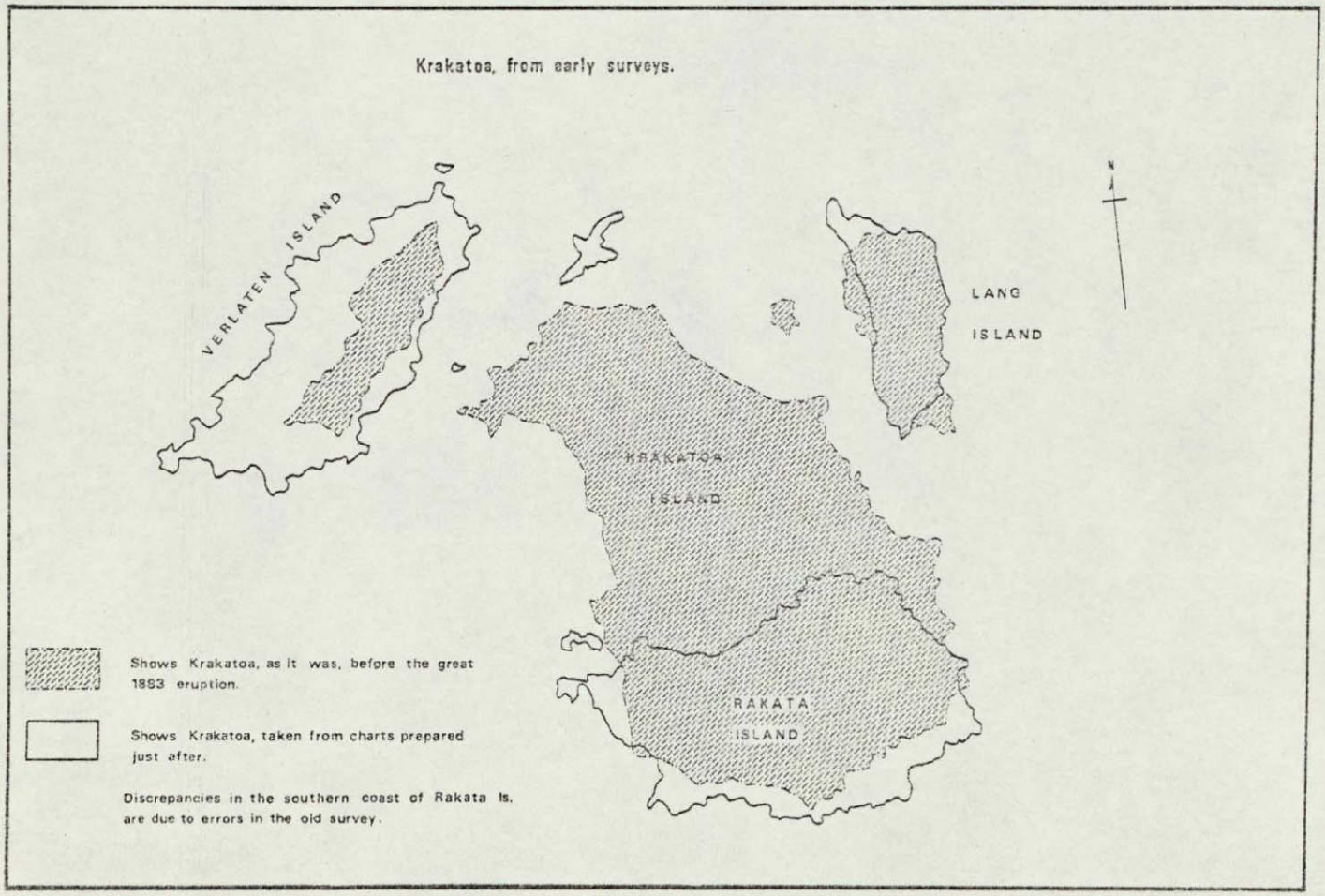

Fig. 13.4 Sketch map of the Krakatau group prepared from early survey charts before and after the 1883 eruption.